[American Journal of Science, Vol. 311, November, 2011, P. 719–772, DOI 10.2475/09.2011.01]

American Journal of Science

NOVEMBER 2011

ZIRCON U-Pb ISOTOPE, $\delta^{18}O$ AND TRACE ELEMENT RESPONSE TO 80 m.y. OF HIGH TEMPERATURE METAMORPHISM IN THE LOWER CRUST: SLUGGISH DIFFUSION AND NEW RECORDS OF ARCHEAN CRATON FORMATION

JOHN R. BOWMAN*, DESMOND E. MOSER**, JOHN W. VALLEY***, JOSEPH L. WOODEN§, NORIKO T. KITA***, and FRANK K. MAZDAB§§

ABSTRACT. **Coordinated cathodoluminescence (CL) imaging and ion microprobe (SHRIMP and CAMECA 1280) analysis document micron-scale U-Pb-O isotope and trace element zoning in zircons from deep crust exposed to 80 m.y. of high temperature and pressure metamorphism. Three, along-strike paragneiss samples across the amphibolite to granulite facies transition in the Kapuskasing Uplift crustal cross-section in the Archean Superior province yield detrital, originally igneous zircon cores overgrown by progressively larger volumes of metamorphic zircon with increasing grade. The cores generally retain primary age (2.85±0.03 to 2.67±0.02 Ga), oxygen isotope (5.1 to 7.0‰) and trace element compositions similar to those reported for magmatic arc sources. Dark CL, metamorphic zircon rims record nearly continuous overgrowth events for ~80 m.y. from 2.66±0.01 to 2.58±0.01 Ga during uppermost amphibolite to granulite facies regional metamorphism. These rims have significantly higher $\delta^{18}O$ values (8.4 to 10.4‰) and trace element compositions quite distinct from those of the cores; these differences indicate that their $\delta^{18}O$ and trace element compositions were not inherited from the igneous cores, consistent with extensive textural evidence for rim formation as metamorphic overgrowths. Multi-spot traverses record steep oxygen isotope discontinuities (4‰ over <10 μm) at core-rim boundaries, confirming the extremely sluggish rates of volume diffusion of O in non-metamict zircon during extended (~80 m.y.) granulite-grade metamorphism (peak T=750-800 °C) at substantial $f(H_2O)$ but water-undersaturated (fluid-absent) conditions. Likewise no evidence of significant diffusive exchange of $\delta^{18}O$ could be detected along deformation microstructures such as annealed fractures in cores infilled with high $\delta^{18}O$ zircon. Application of simple diffusion models to detailed $\delta^{18}O$ profiles in a large number of zircon grains constrain maximum values of the diffusivity of oxygen in zircon ($\log D^{Zrc}_{ox}$) to the range −27.5 to −26.4 m^2/s. For the estimated 80 m.y. and 700 to 800 °C time-T window of rim formation, these maximum values are similar to or slower than values reported by Page and others (2007, 2010) and the experimentally-determined "dry" diffusivity of oxygen in zircon (Watson and Cherniak, 1997), but are markedly slower than the experimentally-determined "wet" diffusivity of oxygen in zircon (Watson and Cherniak, 1997). Fast diffusion of oxygen in zircon predicted by hydrothermal experiments may, in nature, require the presence of a hydrous fluid**

* Department of Geology and Geophysics, Frederick A. Sutton Building, 115 South 1460 East, Room 383, University of Utah, Salt Lake City, Utah, 84112, USA; 801-581-7250, john.bowman@utah.edu

** Department of Earth Sciences, University of Western Ontario, London, Ontario, Canada N6A 5B7; 519-661-4214, desmond.moser@uwo.ca

*** WiscSIMS, Department of Geoscience, University of Wisconsin, Madison, Wisconsin, 53706, USA; 608-263-5659, valley@geology.wisc.edu; 608-262-7118, noriko@geology.wisc.edu

§ USGS-Stanford Ion Microprobe Facility, Stanford, California 94305, USA; 650-725-6536, jwooden@stanford.edu

§§ Department of Geosciences, University of Arizona, Tucson, Arizona, 85721, USA; 520-626-5275, fmazdab@email.arizona.edu

rather than a threshold value of $f(H_2O)$. Our test demonstrates that unrecrystallized metamorphosed igneous zircons and metamorphic zircons will retain the geochemical (U-Pb age, trace element and $\delta^{18}O$) record of their origin and evolution despite prolonged, high-grade metamorphism at significant $f(H_2O)$ but water under-saturated (fluid-absent) conditions. Such zircons, particularly those that exhibit $\delta^{18}O$ zoning, are micron-scale records for the T-time-fluid interaction history of deep crustal rocks. Such records will not be preserved in less refractory phases and promise new insights into the processes of continent formation and evolution.

Key words: zircon, oxygen isotopes, oxygen diffusion, ion microprobe, Kapuskasing, U-Pb, Archean or Archean craton, granulite facies.

INTRODUCTION

The integration of U-Pb and O isotope data for igneous zircons is a powerful methodology for providing new insights into global-scale processes such as early planetary cooling, rates of crustal recycling over time, and the history of continental lithosphere/hydrosphere interaction (for example, Valley and others, 1994, 2005; Peck and others, 2000; Mojzsis and others, 2001; Wilde and others, 2001; Rumble and others, 2002; Valley, 2003; Hawkesworth and Kemp, 2006; Cavosie and others, 2007; Moser and others, 2008; Harrison and others, 2008; Harrison, 2009). The oxygen and trace element compositions of metamorphosed and metamorphic zircon from the deep crust have equal potential for revealing new aspects of the nature and timing of crust-hydrosphere and crust-mantle interaction during continent evolution. However a rigorous assessment of oxygen mobility in zircon during prolonged regional metamorphism is required before we can confidently discriminate primary from secondary (for example, diffusion and/or replacement altered) oxygen values in grains with high temperature histories. Experimental studies suggest that the diffusion of oxygen in zircon is much faster under water-saturated conditions down to $P(H_2O)$ as low as 7 MPa—"wet" diffusion—than under water-absent conditions—"dry" diffusion (Watson and Cherniak, 1997; Cherniak and Watson, 2003). More rapid, "wet" volume diffusion would cause exchange of primary oxygen isotopic compositions of zircon during high-grade metamorphic episodes of sufficient duration, without affecting U-Pb ratios (Watson and Cherniak, 1997); however this view has been challenged (Peck and others, 2003; Page and others, 2007; Moser and others, 2008). In addition, the impact of replacement/recrystallization processes during high grade metamorphism on the mobility of oxygen and trace elements in zircon is not yet clear (Martin and others, 2006, 2008; Harley and Kelly, 2007).

In an attempt to improve the accuracy and scope in applications of zircon geochemistry, including oxygen isotope analysis, to the deep lithosphere, we have used spatially correlated SIMS analysis to evaluate oxygen and lead isotope, and trace element mobility in detrital and metamorphic zircons along a transect across an exposed middle to lower crust transition. The zircons occur in a paragneiss unit exposed in the Kapuskasing crustal cross-section, and have a thermal history that produced granulite-grade temperatures at P=1.0 to 1.1 GPa less than 10 Ma after deposition of the originally igneous zircon as detrital grains in siliciclastic sediments (Krogh, 1993; this study). The results have implications for the interpretation of oxygen isotope ratios in zircon generally, and reveal new aspects of the geochemical and thermal evolution of early crust.

Oxygen Isotope Behavior in Metamorphosed and Metamorphic Zircon

Several studies have documented that zircons with primary magmatic $\delta^{18}O$ values have survived regional metamorphism, partial melting, and hydrothermal alteration (Valley and others, 1994; Peck and others, 2003; Valley, 2003; Valley and others, 2005). Modern ion microprobe techniques now allow high precision analysis of U-Pb age,

trace elements, and oxygen isotope composition on areas of <20 to 30 μm diameter in zircon crystals (Ireland and Williams, 2003; Kita and others, 2009; Valley and Kita, 2009). Correlating cathodoluminescence (CL) zoning in zircon crystals with ion microprobe analysis, Cavosie and others (2006) demonstrated that magmatic domains are preserved in individual detrital zircon crystals from the Jack Hills, Australia, as these domains are distinct in U-Pb age, trace element compositions and $\delta^{18}O$ value from domains produced by metamorphic or hydrothermal processes.

Using this same approach, Page and others (2007) made very careful traverses across the boundary between a bright CL-zoned igneous (low $\delta^{18}O$) core and dark CL (higher $\delta^{18}O$) metamorphic/anatectic rim using <1 μm ion microprobe spots in a zircon from the high-grade metamorphic terrain in the SE Adirondacks, New York. Page and others (2007) were able to resolve that oxygen isotope exchange was limited to within 2 μm to either side of this contact, indicating slow diffusion of oxygen and consistent with a maximum oxygen diffusion coefficient of $10^{-27.5\pm1}$ m^2/s. For this analysis, these authors estimated a timescale for high-grade metamorphism of ~50 Ma and assumed slow cooling based on regional geochronology studies in the Adirondacks. Recent analysis of zoning in garnets suggests that the duration of peak metamorphism was shorter (~5 Ma), such that $\leq 10^{-26.5\pm1}$ m^2/s is a better estimate (Page and others, 2010). Based on the preservation of this sharp profile in $\delta^{18}O$, Page and others (2007) predicted that domains with primary $\delta^{18}O$ values should be preserved in zircons from high-grade metamorphic terrains. Following on this prediction, Lancaster and others (2009) measured oxygen isotope compositions of metamorphosed and metamorphic zircons and coexisting garnet in migmatitic paragneiss from mid-crustal paleodepths (0.7-0.8 GPa) in the Adirondacks Mountains. Differences in $\delta^{18}O$ between detrital cores and metamorphic overgrowths are preserved following intense regional metamorphism and zircon cores are out of $\delta^{18}O$ equilibrium with whole rock $\delta^{18}O$ composition.

Zircon is known to form by replacement of pre-existing zircon in low-medium T hydrothermal environments (Geisler and others, 2007). Chiarenzelli and McLelland (1993) and Martin and others (2008) present textural evidence for the formation of metamorphic zircons or zircon rims both by replacement/recrystallization of pre-existing magmatic zircon and as overgrowths on these magmatic zircons in high-grade metamorphic rocks from the Adirondacks and Naxos, Greece, respectively. Using ion microprobe analysis, Martin and others (2008) document that Pb is reset (open system) during both replacement and overgrowth, but argue that O and REE can be inherited from the pre-existing zircon and hence act as a closed system during replacement.

Correlating cathodoluminescence (CL) zoning in zircon crystals with an initial set of ion microprobe analyses, Moser and others (2008) documented that the great majority of zircon grains from a granulite-grade paragneiss in the Kapuskasing uplift have older, low $\delta^{18}O$ (5.1-7.0‰, VSMOW) magmatic cores and younger, higher $\delta^{18}O$ (8.8-10.4‰) metamorphic rims. In addition, steep discontinuities in $\delta^{18}O$ are preserved at the micron scale at the core-rim boundary in the two composite zircon grains that were analyzed in detail. These data indicate that these cores and rims retain their original oxygen and lead isotopic compositions throughout protracted regional high-grade metamorphism, also demonstrating the slow diffusion of oxygen in non-metamict zircon. The U-Pb age and oxygen isotope zoning preserved in the zircons from this granulite grade paragneiss allowed Moser and others (2008) to document a >150 m.y. high fidelity record of the formation, evolution, and rifting of Archean continental lithosphere in North America. Rare zircon grains in the granulite facies sample of paragneiss, however, were also noted to have experienced patchy oxygen isotopic exchange with the whole rock. The trace element, $\delta^{18}O$ and U-Pb isotopic

compositions of the granulite-facies zircons and those in broadly correlative metasediment structurally higher in the crustal section were not discussed, and links between chemical composition, microtextures and microstructures remained to be explored.

The Borden Lake Belt as a Natural Laboratory for Evaluating Element Mobility in Zircon

The Moser and others (2008) study demonstrates that the Borden Lake Belt of the Kapuskasing crustal cross-section offers an unusually well-constrained geological setting for assessing the extent of oxygen and trace element mobility in zircon during extended high grade metamorphism. No studies have yet examined in detail the oxygen behavior of zircon in the context of a well understood crustal cross-section through the amphibolite to granulite facies transition, nor explored the underlying mechanisms and trace element changes that are potentially associated with oxygen isotope exchange in non-metamict zircon at high temperatures. Here we present analyses of zircon from three sites representing a range of paleodepths where metasedimentary units can be traced from middle amphibolite facies grade (P=~0.5 GPa) to granulite-grade (P=~1.0 GPa) along strike within the Borden Lake belt (Moser, ms 1993, 1994) representing a paleodepth range of ~15 km across the mid- to lower crustal transition. Magmatic zircons with near-mantle $\delta^{18}O$ values (5.1-6.5‰) are incorporated as detrital zircons into the $^{18}O/^{16}O$-enriched sedimentary rock hosts at all three sites. These magmatic zircons—which were initially out of oxygen isotope exchange equilibrium with their high $\delta^{18}O$ sedimentary host rock by up to 4 permil—have been subjected to prolonged high-grade metamorphism at water-undersaturated conditions (Mäder and others, 1994), during which $^{18}O/^{16}O$-enriched metamorphic rims form.

The compositions and textures of the lower grade zircons provide critical comparative baselines for the zircons at granulite-grade that allow assessment of replacement versus overgrowth mechanisms for formation of metamorphic zircon rims. At the high grade site we have performed diffusion tests with multi-spot $\delta^{18}O$ core-rim traverses in a large number (13) of composite zircon grains as well as detailed oxygen and trace element analyses in rare zircon cores that exhibit elevated $\delta^{18}O$ values suggestive of exchange with the bulk rock. These data, and particularly the core-rim $\delta^{18}O$ profiles at the granulite site, in conjunction with Pb age and Ti(Zrc) geothermometry data on a large number (>50) of zircon grains that have experienced the same T-time history, permit the most comprehensive suite of diffusion tests, to date, for evaluating the mobility of oxygen and trace elements in zircon that experienced extended, high T regional metamorphism common in the deep levels of orogenic belts. Our interpretations are aided by the rich geologic, geochronologic and geophysical knowledge of the study area, a classic site for the study of early crustal evolution and crustal-scale fluid flow (for example, Krogh, 1993).

TECTONICS AND REGIONAL METAMORPHISM

The Superior Province of the Canadian Shield is the largest Archean tectosphere fragment, and peneplenation after the Paleoproterozoic Kapuskasing Uplift event has exposed an oblique crustal cross-section through its southern subduction-accretion margin (fig. 1) (Percival and West, 1994). The Abitibi-Wawa terrain in the southern Superior Province (fig. 1) was among the last to be accreted during northward subduction in a series of discrete orogenies (2750 Ma to 2670 Ma; Corfu and Davis, 1992; Percival and others, 2006; Percival, 2007a, 2007b) that we will collectively refer to for simplicity as the Kenoran orogeny. Evidence for this subduction is preserved as north-dipping upper mantle reflectors to the north of the Abitibi belt (Calvert and others, 1995). At the south end of the 500 km-long zone of the Kapuskasing Uplift, structural modification of the hanging wall is at a minimum, and a more or less continuous metamorphic and structural gradient representing a 15 km thick section of

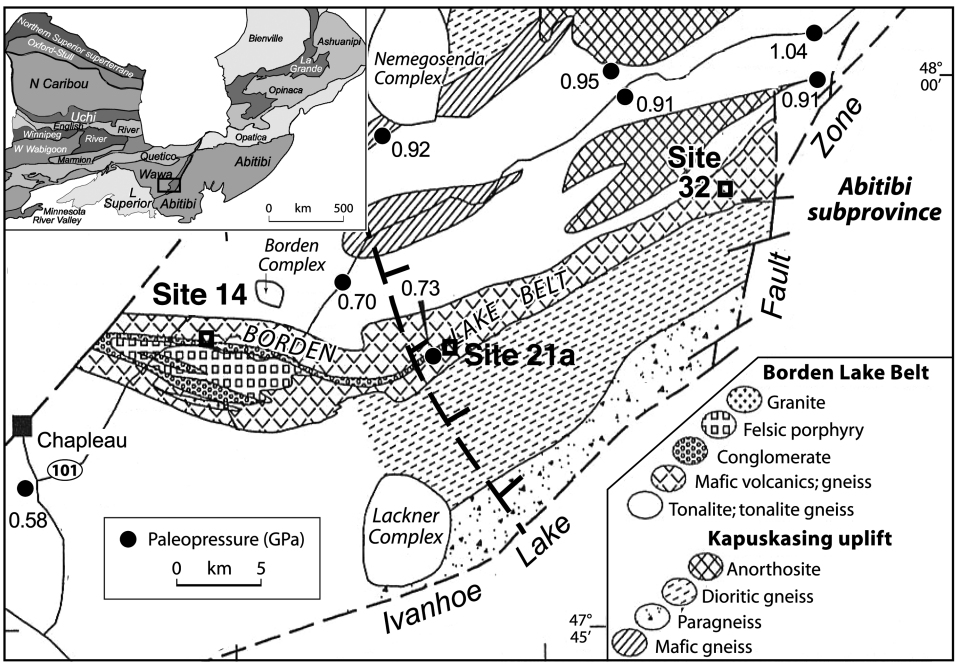

Fig. 1. Geology and tectonic framework of southern Superior province of the Canadian shield, with location of the Kapuskasing Uplift indicated (inset). Bedrock geology map of the Borden Lake belt in the southern Kapuskasing Uplift is modified after Percival and West, 1994, and shows the amphibolite-granulite transition (dashed line), paleopressures (solid circles, in GPa), and the locations of the three sites (14, 21A and 32; open squares) from which zircons were separated for this study.

Abitibi-Wawa crust is exposed, which consists of a series of metaplutonic and metasupracrustal layers and/or belts. The largest and most extensive of these is the Borden Lake belt (Moser, 1994; Bursnall and others, 1994), a 5 km by 25 km, east-striking, steep to moderately north-dipping synformal structure (figs. 1 and 2) consisting mostly of multiply deformed metabasalts (now mafic gneiss) locally cross-cut by foliated felsic porphyry and interlayered with narrow, discontinuous units of garnetiferous paragneiss (metawacke and metaconglomerate). The Borden Lake Belt strikes at a high angle across the amphibolite-granulite transition and has a maximum age of 2667±2 Ma for conglomerate deposition (Krogh, 1993) making it one of the youngest supracrustal units recognized in the Superior province and comparable in age to the 2672 to 2673 Ma Timiskaming Group in the Abitibi region (Davis, 2002).

Peak metamorphism of surrounding gneisses has been estimated at ~2.66 Ga based on the oldest widespread age of zircon growth in granulite-facies metabasalts (Krogh and Moser, 1994). More recent analyses of zircons from mafic granulites identify much older 3 Ga zircons that may represent "pre-Abitibi" crust (Benn and Kamber, 2009). Deep crustal metamorphism followed polyphase compressional folding at all levels, and is broadly coeval with orogen parallel ductile flow in the middle and lower crust between 2660 Ma and 2630 Ma. The metamorphism and compressional folding are Superior province–wide events that, in the Kapuskasing cross-section, appear to young with depth (Krogh, 1993; Moser and others, 1996). Paleopressures gradually increase to the east from ~0.5 GPa in the middle amphibolite facies to maximum values in the granulite-facies domain of 1.1 GPa and peak temperatures of 750 to 800 °C (Percival, 1990; Mäder and others, 1994; Pattison, 2003; Pattison and

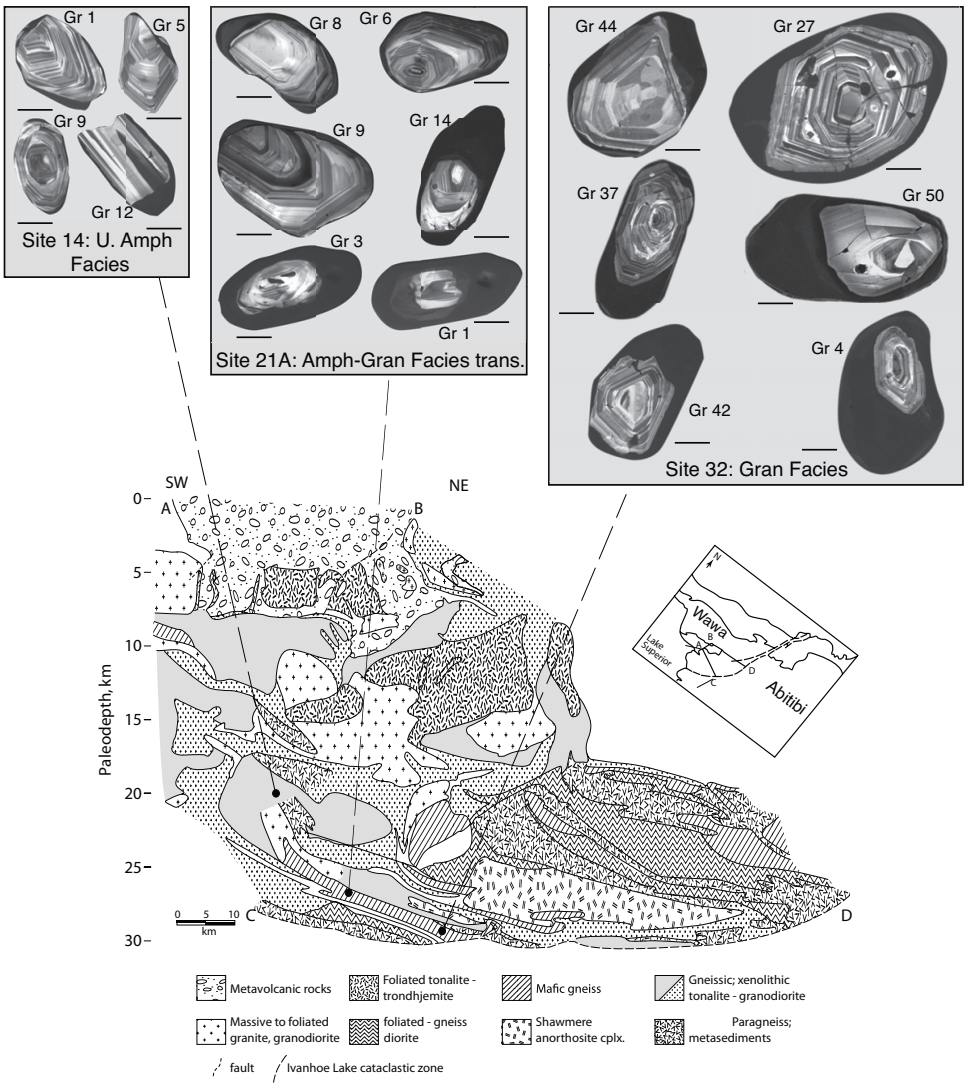

Fig. 2. Down plunge projection (constant, 17 degrees to East, 2:1 vertical exaggeration) of bedrock geology of the southern Kapuskasing Uplift modified after Percival and Card (1985) and paleodepths based on regional geobarometry (Mäder and others, 1994). See tilted inset for geographic tie points (A, B, C, D) for this projection and for location of the Uplift (dashed lines) with respect to the Abitibi and Wawa subprovinces (see also inset, fig. 1). SEM-CL images of representative zircons from the three sites sampled in paragneiss on the margin of the mafic gneiss limb of the Borden Lake belt are shown above. These three sites represent three different paleodepths and metamorphic grades (see text). All grain images are at the same scale so that their sizes (bright CL core and total size) can be compared; the black scale bar in each image is 50 microns in length. Note the progressive increase in width of the dark CL, U-rich zircon overgrowths with paleodepth and metamorphic grade (that is, from site 14 to 21A to 32). Note also that the sizes of the bright CL (detrital, originally igneous) zircon cores do not decrease with increasing paleodepth and metamorphic grade.

others, 2003). These geothermobarometry and geochronology results suggest that the Borden Lake Belt has undergone rapid burial (up to ~35 km/10 Ma) followed by a single, albeit unusually prolonged (~80 Ma), stage of regional metamorphism. Water

activity in mafic gneisses during metamorphism has been estimated at between 0.1 and 0.5 (Mäder and others, 1994), so regionally, fluid (water) paleopressure was likely 1000 to 5000 bars. Granulite facies gneisses are retrograded (hydrated) at contacts with meter-scale tonalitic boudins and granitic (pegmatite) dikes dated at 2640±2, 2630±2 and 2584±2 Ma (Krogh, 1993).

SAMPLE SITES AND ZIRCON SEPARATES

Zircons were separated from paragneiss samples at three sites within the Borden Lake Belt (fig. 1): site 14 in the middle amphibolite facies; site 21A in the amphibolite-granulite transition zone; and site 32 in the granulite zone. At each site, a representative (~15 Kg) sample of paragneiss was collected, and zircons were separated by standard heavy liquid and magnetic separation techniques. Based on the regional metamorphic gradient (fig. 1) from Mäder and others (1994), P-T conditions were ~0.5 GPa and ~600 to 650 °C at site 14, ~0.7 GPa and ~650 to 700 °C at the amphibolite-granulite facies transition, and ~1 GPa and 750 to 800 °C at site 32. Appendix A provides further information on the geology of these sites, the petrology of the paragneiss samples, and on the optical characteristics of the zircon sample populations.

ANALYTICAL METHODS

Methods for the oxygen isotope analysis of garnet (laser fluorination) and the procedures for ion microprobe (SIMS) analyses of U-Pb age, trace elements and oxygen isotope compositions of zircons are presented in Appendix B.

RESULTS

Cathodoluminescence (CL) Imaging of Zircon Internal Textures

Prior to ion microprobe analysis, each zircon grain was ground and polished to its mid-plane and imaged in secondary electron (SE) and cathodoluminescence (CL) to identify internal domains within grains, to map targets for ion microprobe analysis (for example, detrital cores and metamorphic rims) and to identify features to avoid during analysis (pits, cracks, inclusions).

At the lower grade site 14, zircon grains are characterized by oscillatory CL zoning consistent with the development of concentric planar growth bands during crystallization from magma (fig. 2). The rounded edges of these grains often cut across this primary CL zoning, consistent with a detrital origin. Narrow dark CL rims are developed on a few of these detrital cores. In the two higher grade sites 21A and 32, the great majority of grains consist of similarly bright, zoned CL cores surrounded by dark CL rims. The abundance of these composite grains, the width of the dark CL rim, and hence the overall size of these composite grains, increase with metamorphic grade (fig. 2). Consequently, at the granulite grade site 32, the presence of thick rims cause these composite zircon grains to be up to four times larger than the detrital grains at the lower grade sites where rims are scarce and thin (fig. 2).

At all three sites, many detrital cores have eu- or subhedral outlines, but rounded tips (for example, grains 4 and 37, site 32; fig. 2). Internally, the core-rim boundary can locally crosscut oscillatory zoning in the core along curvilinear surfaces or along irregular, jagged boundaries that appear to be fracture surfaces on the detrital grains. These features support rounding by mechanical abrasion as the dominant process, but the occasional presence of lobate re-entrants in the core-rim boundary crosscutting oscillatory zoning in the core (grain 42, site 32; fig. 2) suggests localized dissolution. These observations will be returned to in the interpretation of oxygen isotope profiles across core-rim boundaries in light of metamorphic epitactic growth vs. replacement/recrystallization models.

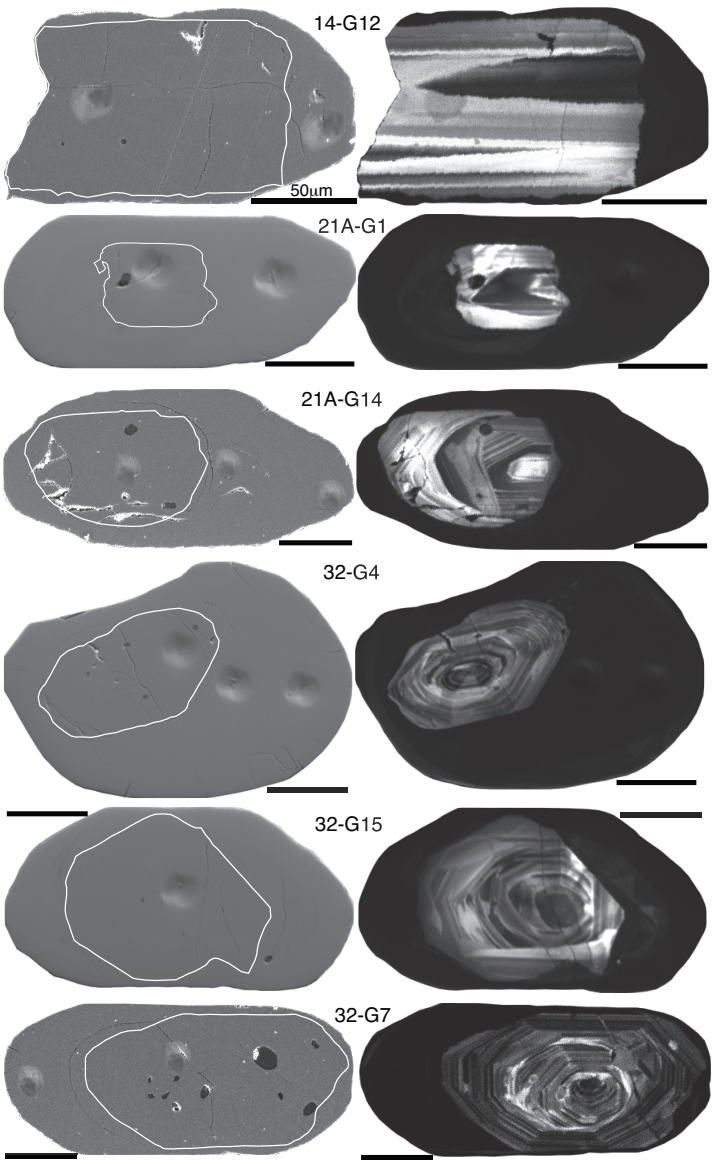

Fig. 3. Paired CL (right) and secondary electron (SE) (left) images of some representative zircon grains from sites 14, 21A and 32. Pits from secondary ion mass spectrometry (SIMS) are visible in the SE images. The black scale bar in each image is 50 microns in length. Paired images of each grain are at the same scale for direct comparison. The white outline superimposed on the paired SE image for each grain shows the location of the core-rim boundary defined in CL in each grain. These images show that there are no poorly-polished (porous) transition zones in the dark CL rims at core-rim boundaries and that rims do not contain thorite or coffinite inclusions; such features have been attributed to formation of metamorphic zircon rims by replacement processes (Geisler and others, 2007; Martin and others, 2008).

At all three sites, metamorphic rims are well polished (non-porous) throughout, including areas near the core-rim boundary (fig. 3). There are no poorly-polished (porous) transition zones at core-rim boundaries and the rims do not contain thorite or coffinite inclusions, features observed in metamorphic zircon rims by Martin and

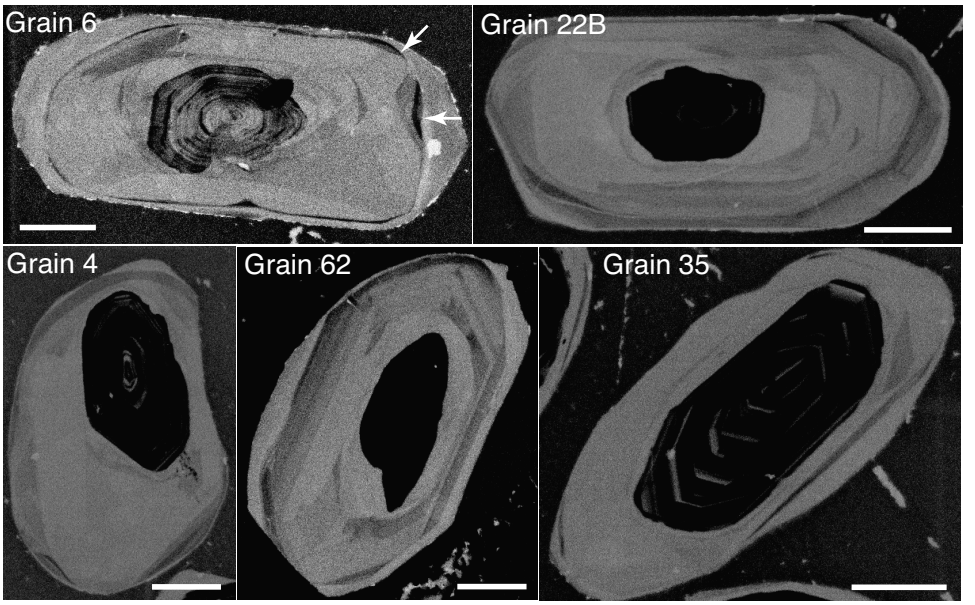

Fig. 4. Inverted grayscale CL images of five zircon grains from site 32, illustrating the ~concentric CL banding often developed within the metamorphic rims. White scale bar in all images is 50 μm in length. At the right end of grain 6, white arrows point to where the outer growth tip on this grain truncates CL zoning within the main rim.

others (2008). The dark CL, metamorphic rims exhibit concentric but discontinuous and weak internal CL banding better illustrated in inverse CL images (fig. 4). This banding is mostly concentric to the core-rim boundary but in some grains is truncated at low angles by outer, younger growth zones (for example, the outer growth tip on the right end of grain 6; refer to caption, fig. 4).

Two types of cores, normal and disturbed, are recognized based on their CL characteristics and associated isotopic compositions as reported in Moser and others (2008). "Normal" cores are dominant and exhibit bright CL signals and planar growth banding consistent with a magmatic origin. A small subset of cores at site 32 exhibit patchily distributed domains of anomalously low CL signal intensity associated with elevated oxygen isotope values and $^{207}Pb/^{206}Pb$ ages falling within the time of metamorphism. These are interpreted to be due to recrystallization during the early stages of metamorphism (see Discussion), and are referred to below as "disturbed" cores.

Oxygen Isotope Composition of Bulk Garnet and Bulk Zircon

Bulk garnet.—The $\delta^{18}O$ values of bulk garnet separates from the paragneisses at the three sites studied were measured by laser fluorination (Sharp, 1990; Crowe and others, 1990) and range from 7.7 to 9.9 ±0.1 permil (2 SD) (table 1). The $\delta^{18}O$ value of garnet is somewhat lower at the amphibolite-granulite transition site 21A compared to the other two sites. Even though these units are all part of the same sedimentary/volcanic rock package, m-scale variations in bulk composition—and $\delta^{18}O$ values—exist across strike within the belt (Longstaffe and Schwarcz, 1977; Li and others, 1991; Puris and Wickham, 1994). The lower $\delta^{18}O$ value of paragneiss at site 21A is reflected in its lower biotite and higher hornblende contents relative to paragneiss at the other two sites. Garnet from cm-width leucosome bands (9.2‰) in the granulite-grade parag-

TABLE 1

Oxygen isotope compositions ($\delta^{18}O$ VSMOW) of bulk garnet, bulk zircon, and zircon rims from three sites within the Borden Lake paragneiss

Sample	garnet[a]	bulk zircon[a]	zircon rims[b,c]	Δ(Gn-blk Zrc)[d]	Δ(Gn-Zrc rim)[d]
K05-14	8.85	6.35	8.7 (1)	2.50	0.15
K05-21A	7.75, 7.65	7.40	7.8 (10)	0.30	-0.10
K05-32 matrix	10.0, 9.75	8.85	9.3 (26)	1.05	0.60
K05-32 leucos.	9.40, 8.95			0.35	-0.10

[a] Garnet and bulk zircon analyzed by laser fluorination procedure.
[b] Zircon rims analyzed by SIMS; value listed is average of rim analyses in this sample.
[c] No. of zircon rims analyzed in parentheses.
[d] Average of multiple analyses of garnet used to determine Δ(Gn-blk Zrc) and Δ(Gn-Zrc rim).

neiss at site 32 is 0.7 permil lower in $\delta^{18}O$ than the garnets taken from a bulk sample of the surrounding paragneiss matrix (9.9‰). Because these two domains were separated on a cm-scale (by diamond saw), the two bulk garnet separates may be cross-contaminated to some extent by each other [they may be imperfectly separated by the planar saw cut]. Hence the $\delta^{18}O$ values of these bulk garnet samples probably record the minimum difference in $\delta^{18}O$ between the leucosome and matrix domains within the paragneiss at site 32. At all three sites (including garnet in leucosome at site 32), garnet has $\delta^{18}O$ values significantly higher than would be in equilibrium with magmatic zircons derived from Abitibi-Wawa arc magmatism (avg. 5.7‰; range 5 to 7‰; King and others, 1998). These results indicate that detrital igneous zircons will be out of oxygen isotope exchange equilibrium by several permil with their $^{18}O/^{16}O$-enriched paragneiss host rock at the outset of metamorphism, as confirmed by our detailed analyses.

Bulk zircon.—The $\delta^{18}O$ values of bulk (n=hundreds of grains per analysis) composite (cores plus rims if present) zircon aliquots from the paragneiss non-magnetic fractions, determined by laser fluorination, increase progressively with metamorphic grade from 6.4 permil (site 14) to 7.4 permil (site 21A) to 8.9 permil (site 32) (table 1). At the lower grade site 14, bulk zircon has a significantly lower $\delta^{18}O$ value than bulk garnet; at the higher grade site 32, bulk garnet and bulk zircon approach oxygen isotope exchange equilibrium. This progressive increase in $\delta^{18}O$ of bulk zircon and its approach to exchange equilibrium with garnet (and the host paragneiss) reflect the progressive increase in the proportion of the composite zircon grains occupied by the $^{18}O/^{16}O$-enriched metamorphic rims in progressively higher metamorphic grade samples.

Age and Oxygen SIMS Analysis of Zircon Cores and Rims

A single, spatially correlated, set of core and rim analyses of U-Pb isotope, trace element and oxygen isotope composition was first made to characterize the zircon population. Then, multi-spot SIMS analyses and/or transects were conducted in grains exhibiting large areas of core and rim material, in order to evaluate isotope and trace element systematics with higher sampling density and spatial control. These multi-spot data are reported separately below.

"Normal" (magmatic) core populations.—The age and $\delta^{18}O$ values of the magmatic cores from all three sites sampled (this study; Moser and others, 2008) are plotted in figure 5 and compiled in table 2. All measurement uncertainties are given at 2 standard deviations with age ranges given below based on the most precise data. At site 14, the sixteen analyzed cores range in $^{207}Pb/^{206}Pb$ age from 2760±17 to 2682±18 Ma, and

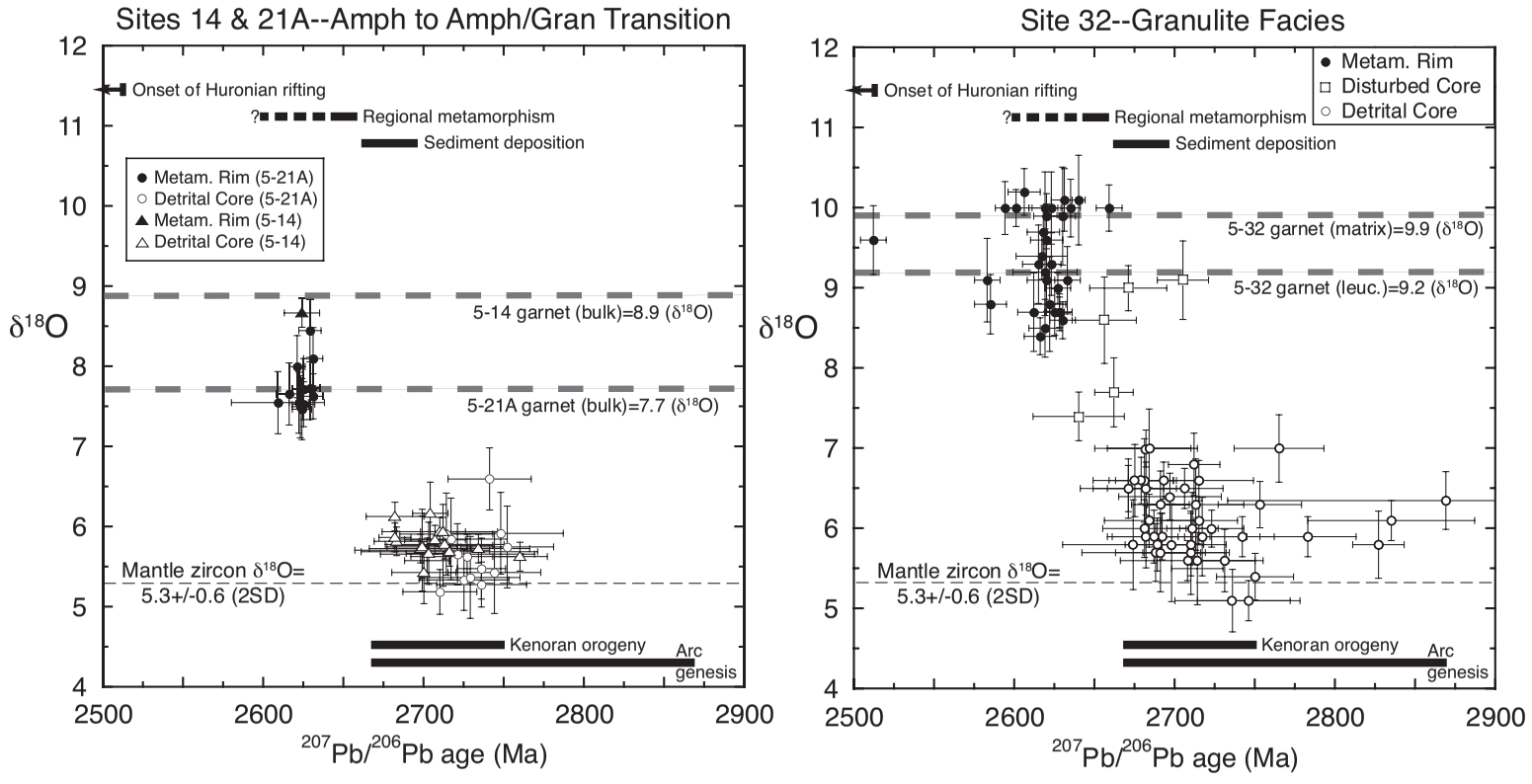

Fig. 5. Comparison of spatially correlated $^{207}Pb/^{206}Pb$ age and $\delta^{18}O$ SIMS measurements (with 2 SD uncertainty bars) for detrital (igneous) cores and metamorphic rims in zircons from the granulite zone site 32 (this study; Moser and others, 2008) with analogous measurements for detrital cores and metamorphic rims in zircons from the lower grade sites 14 and 21A (see table 2 and table A1 for analytical details http://earth.geology.yale.edu/~ajs/SupplementaryData/2011/08BowmanTableA1.xls). Gray dashed lines indicate the $\delta^{18}O$ values of bulk garnet (laser fluorination) from the host paragneiss rocks at the three sites. Age ranges for events depicted by solid black bars are based on regional geochronology studies using TIMS analysis of single zircon crystals (Corfu and Davis, 1992; Krogh, 1993; Krogh and Moser, 1994; also see text for further discussion). Note the small time gap between the end of sedimentation in the Borden Lake belt and the onset of lower crustal metamorphism of the same sediments. Average $\delta^{18}O$ of mantle zircon from Valley and others (2005). Previous laser fluorination analyses of Superior province magmatic zircon give regional avg. $\delta^{18}O$ of 5.7 ± 0.6‰ and values as high as 6.5 ± 0.4‰ for late sanukitoid magmas (King and others, 1998).

TABLE 2

Summary of $\delta^{18}O$, U-Pb age, and U and Th concentrations in igneous cores and metamorphic rims of Kapuskasing zircons

##Sample No.	$\delta^{18}O$*,**	2sd error***	207/206 age	2sd error	Conc (%)	Pb204corr 207r/206r	% err	Pb204corr 207r/235	% err	Pb204corr 206r/238	% err	err corr	U (ppm)	Th (ppm)	Th/U
IGNEOUS CORES															
(A) Site 14															
K05-14 G1	5.7	0.18	2698	32	5	0.1850	1.0	12.56	1.8	0.4925	1.6	0.848	46	20	0.43
K05-14 G2	5.7	0.18	2734	32	-1	0.1891	1.0	13.90	1.6	0.5332	1.3	0.803	48	17	0.35
K05-14 G3	5.8	0.18	2683	14	3	0.1833	0.4	12.62	0.7	0.4995	0.6	0.795	263	352	1.34
K05-14 G4	5.9	0.18	2682	10	1	0.1832	0.3	12.85	0.5	0.5087	0.4	0.807	434	59	0.14
K05-14 G5	5.8	0.18	2713	37	2	0.1867	1.1	13.20	2.0	0.5128	1.6	0.819	29	11	0.38
K05-14 G6	6.1	0.18	2682	18	-1	0.1832	0.5	13.11	0.9	0.5193	0.8	0.817	136	98	0.72
K05-14 G7	6.2	0.39	2704	11	4	0.1856	0.3	12.77	0.6	0.4990	0.5	0.801	361	275	0.76
K05-14 G8	5.7	0.18	2716	55	6	0.1871	1.7	12.66	2.2	0.4908	1.5	0.660	29	14	0.48
K05-14 G9	5.8	0.18	2707	19	-1	0.1859	0.6	13.51	0.9	0.5270	0.7	0.773	92	38	0.41
K05-14 G10	5.4	0.39	2700	20	3	0.1852	0.6	12.80	1.0	0.5013	0.8	0.801	67	22	0.33
K05-14 G11	5.8	0.39	2699	22	0	0.1851	0.7	13.29	1.1	0.5207	0.9	0.812	53	40	0.76
K05-14 G12	5.9	0.18	2710	36	5	0.1864	1.1	12.61	1.6	0.4907	1.1	0.722	41	19	0.47
K05-14 G13	5.9	0.18	2712	14	2	0.1865	0.4	13.17	0.8	0.5120	0.6	0.824	141	96	0.69
K05-14 G14	5.6	0.18	2760	17	-1	0.1921	0.5	14.37	0.9	0.5426	0.7	0.825	102	83	0.82
K05-14 G15	5.7	0.39	2703	14	3	0.1856	0.4	12.91	0.7	0.5047	0.6	0.815	154	167	1.09
K05-14 G53	5.6	0.28	2702	14	4	0.1854	0.4	12.72	0.7	0.4976	0.6	0.811	167	64	0.38
AVERAGE	**5.8**	**0.24**	**2707**	**23**	**2.1**								**135**	**86**	**0.60**
(B) Site 21A															
K05-21A G1	5.9	0.39	2738	20	6	0.1896	0.6	12.88	1.1	0.4926	0.9	0.812	64	49	0.76
#K05-21A G2	7.0	0.39	2696	24	6	0.1848	0.7	12.27	1.2	0.4814	0.9	0.786	55	39	0.71
K05-21A G3	6.6	0.39	2741	26	0	0.1898	0.8	13.90	1.4	0.5310	1.2	0.832	35	20	0.56
K05-21A G4	5.9	0.51	2748	39	3	0.1907	1.2	13.46	2.0	0.5119	1.6	0.806	19	9	0.45
K05-21A G5	5.7	0.51	2752	29	0	0.1911	0.9	14.02	1.6	0.5318	1.3	0.830	30	15	0.48
K05-21A G6	5.9	0.51	2714	29	2	0.1868	0.9	13.24	1.5	0.5139	1.3	0.820	31	17	0.56
K05-21A G7	5.4	0.51	2729	31	0	0.1885	0.9	13.62	1.6	0.5240	1.4	0.825	27	12	0.46
K05-21A G8	5.7	0.51	2699	42	1	0.1852	1.3	13.13	2.6	0.5145	2.2	0.866	24	12	0.50
K05-21A G9	5.8	0.51	2712	31	2	0.1865	0.9	13.14	1.6	0.5110	1.3	0.814	29	14	0.49
K05-21A G10	5.4	0.51	2744	29	2	0.1903	0.9	13.59	1.6	0.5180	1.3	0.828	29	11	0.39
K05-21A G13	5.9	0.51	2717	35	3	0.1871	1.0	13.09	1.8	0.5073	1.5	0.820	21	9	0.44
K05-21A G14	5.2	0.28	2710	23	-2	0.1863	0.7	13.71	1.2	0.5337	1.0	0.818	57	27	0.48
K05-21A G15	5.6	0.28	2727	35	1	0.1882	1.1	13.46	1.8	0.5187	1.5	0.811	26	12	0.45

TABLE 2
(continued)

##Sample No.	$\delta^{18}O$*,**	2sd error***	207/206 age	2sd error	Conc (%)	Pb204corr 207r/206r	% err	Pb204corr 207r/235	% err	Pb204corr 206r/238	% err	err corr	U (ppm)	Th (ppm)	Th/U
IGNEOUS CORES															
(B) Site 21A															
K05-21A G17	5.3	0.28	2736	28	1	0.1893	0.8	13.67	1.5	0.5235	1.2	0.820	39	19	0.49
K05-21A G19	5.7	0.38	2721	48	-1	0.1876	1.5	13.70	2.2	0.5295	1.6	0.738	23	8	0.37
K05-21A G20	5.3	0.38	2725	28	1	0.1880	0.9	13.50	1.5	0.5210	1.2	0.810	50	26	0.53
K05-21A G21	5.5	0.38	2736	15	1	0.1893	0.5	13.59	0.8	0.5209	0.7	0.817	121	127	1.05
$K05-21A G22	5.9	0.38	2636	22	-6	0.1782	0.7	13.45	1.1	0.5475	0.8	0.782	88	21	0.24
AVERAGE	**5.7**	**0.43**	**2726**	**30**	**1.5**								**40**	**25**	**0.54**
(C) Site 32															
K05-32 G1mc	5.4 (2)	0.29	2750	24	4	0.1909	0.7	13.27	1.2	0.5042	1.0	0.810	56	20	0.36
K05-32 G4ic	5.8 (7)	0.60	2699	28	8	0.1850	0.9	12.10	1.2	0.4744	0.8	0.696	86	82	0.95
K05-32 G4oc	5.4 (7)	0.33	2687	26	4	0.1838	0.8	12.40	1.2	0.4895	0.9	0.759	68	49	0.72
K05-32 G7	6.0	0.23	2723	20	2	0.1878	0.6	13.27	1.0	0.5123	0.8	0.793	74	45	0.61
#K05-32 G8	6.6	0.23	2693	22	7	0.1845	0.6	12.15	1.1	0.4776	0.9	0.806	66	58	0.88
K05-32 G11	6.3	0.29	2753	26	9	0.1913	0.8	12.65	1.4	0.4797	1.2	0.821	42	20	0.48
$KO5-32 G12ic	6.2	0.19	2672	20	1	0.1821	0.6	12.69	1.0	0.5054	0.8	0.795	80	50	0.62
K05-32 G13ic	5.7 (12)	0.52	2710	22	2	0.1863	0.7	13.15	1.1	0.5119	0.9	0.816	56	14	0.25
K05-32 G14	6.5	0.33	2682	24	3	0.1831	0.7	12.59	1.3	0.4984	1.0	0.817	45	43	0.97
K05-32 G15oc	5.8 (3)	0.56	2674	44	1	0.1824	1.4	12.75	2.2	0.5071	1.7	0.786	29	18	0.62
K05-32 G15ic	5.6 (3)	0.23	2702	24	5	0.1854	0.8	12.50	1.2	0.4890	1.0	0.796	58	36	0.62
K05-32 G16moc	5.1 (3)	0.25	2746	32	-3	0.1904	1.0	14.44	1.7	0.5499	1.4	0.823	55	19	0.33
K05-32 G16mc1	5.7 (3)	0.54	2705	36	-3	0.1858	1.1	13.90	1.9	0.5427	1.5	0.812	41	15	0.37
K05-32 G16oc	5.4 (3)	0.25	2696	23	5	0.1848	0.7	12.49	1.2	0.4903	0.9	0.793	94	36	0.38
^K05-32 G16mc2	7.4 (3)	0.54	2606	56	-5	0.1750	1.7	12.81	2.1	0.5309	1.3	0.608	54	10	0.19
K05-32 G16ic1	6.0 (3)	0.59	2721	26	1	0.1876	0.8	13.48	1.3	0.5212	1.1	0.804	122	66	0.54
^K05-32 G16ic2	7.2 (4)	0.59	2679	40	8	0.1829	1.2	11.81	1.5	0.4684	0.9	0.607	69	39	0.57
K05-32 G17ic	5.9	0.25	2742	20	7	0.1900	0.6	12.83	1.0	0.4896	0.8	0.818	78	43	0.56
K05-32 G18mc	6.6	0.25	2715	34	4	0.1869	1.0	12.89	1.6	0.5003	1.3	0.778	30	13	0.44
K05-32 G19mc	5.9	0.25	2783	30	0	0.1948	0.9	14.47	1.6	0.5389	1.3	0.814	30	12	0.40
K05-32 G19oc	6.2	0.25	2690	28	4	0.1841	0.8	12.56	1.2	0.4951	0.9	0.744	51	15	0.29
K05-32 G19ic	6.1	0.25	2835	52	2	0.2011	1.6	14.96	2.7	0.5396	2.2	0.805	33	15	0.45
K05-32 G20	6.4 (2)	0.29	2697	32	2	0.1849	1.0	12.90	1.6	0.5060	1.2	0.774	33	14	0.42
KO5-32 G21	5.9	0.29	2692	10	4	0.1843	0.3	12.53	0.7	0.4932	0.6	0.871	298	244	0.82

TABLE 2
(continued)

##Sample No.	$\delta^{18}O$*,**	2sd error***	207/206 age	2sd error	Conc (%)	Pb204corr 207r/206r	% err	Pb204corr 207r/235	% err	Pb204corr 206r/238	% err	err corr	U (ppm)	Th (ppm)	Th/U
IGNEOUS CORES															
(C) Site 32															
K05-32 G22	6.1 (2)	0.33	2684	28	0	0.1834	0.8	12.99	1.4	0.5137	1.2	0.819	50	24	0.49
KO5-32 G23	7.0	0.23	2682	32	0	0.1832	0.9	12.98	1.7	0.5140	1.4	0.823	36	17	0.47
K05-32 G24	6.0 (5)	0.45	2711	16	0	0.1864	0.5	13.44	0.8	0.5229	0.7	0.826	142	71	0.50
#K05-32 G26oc	6.5	0.25	2706	24	2	0.1859	0.8	13.09	1.3	0.5109	1.0	0.803	57	35	0.62
K05-32 G27mc	6.5 (5)	0.42	2765	28	6	0.1927	0.8	13.26	1.3	0.4991	1.0	0.782	65	20	0.30
K05-32 G27oc	5.8 (5)	0.42	2827	16	5	0.2001	0.5	14.29	0.9	0.5177	0.8	0.823	111	51	0.46
K05 32 G28oc	5.8	0.33	2689	20	-1	0.1840	0.6	13.20	1.1	0.5204	0.9	0.809	75	53	0.71
K05-32 G29	5.6	0.25	2708	42	3	0.1861	1.3	13.00	1.9	0.5064	1.5	0.763	30	12	0.40
K05-32 G30			2697	28	-1	0.1849	0.8	13.43	1.4	0.5268	1.1	0.805	44	18	0.41
K05-32 G32ic	5.8	0.49	2691	28	-1	0.1842	0.9	13.38	1.5	0.5268	1.2	0.824	60	67	1.12
K05-32 G32oc	5.4	0.49	2695	14	5	0.1847	0.4	12.43	0.6	0.4881	0.5	0.794	287	238	0.83
K05-32 G34	5.9	0.49	2717	28	-1	0.1871	0.9	13.68	1.5	0.5301	1.3	0.823	54	23	0.43
K05-32 G35ic	7.0	0.49	2684	26	2	0.1835	0.8	12.82	1.2	0.5069	0.9	0.762	107	46	0.43
K05-32 G37ic	6.1 (3)	0.39	2731	24	4	0.1888	0.7	13.12	1.3	0.5041	1.0	0.806	90	58	0.65
K05-32 G37oc	6.0 (2)	0.44	2701	16	1	0.1853	0.5	13.09	0.8	0.5126	0.7	0.818	187	156	0.83
K05-32 G38oc	5.9	0.39	2682	24	-4	0.1832	0.7	13.62	1.4	0.5390	1.2	0.855	70	45	0.64
K05-32 G39	5.8	0.39	2710	22	7	0.1863	0.6	12.40	1.1	0.4828	0.8	0.793	124	63	0.51
K05-32 G41ic	6.8	0.39	2712	16	-1	0.1866	0.5	13.61	0.7	0.5290	0.6	0.784	264	135	0.51
K05-32 G42ic	5.7 (7)	0.61	2698	18	1	0.1850	0.5	13.07	0.9	0.5123	0.7	0.815	165	119	0.72
K05-32 G43	5.1	0.39	2736	36	0	0.1893	1.1	13.79	2.0	0.5285	1.7	0.830	33	20	0.60
K05-32 G44c	6.4 (10)	0.57	2713	30	6	0.1867	0.9	12.50	1.5	0.4857	1.2	0.811	58	57	0.97
K05-32 G45ic	5.7	0.36	2688	46	0	0.1838	1.4	13.12	1.8	0.5176	1.0	0.590	82	40	0.48
K05-32 G46	6.3 (5)	0.36	2869	136	2	0.2053	4.2	15.52	6.1	0.5483	4.5	0.730	72	90	1.25
$K05-32 G47	6.3	0.36	2662	26	7	0.1810	0.8	11.82	1.3	0.4737	1.0	0.798	63	21	0.33
K05-32 G50ic	6.0	0.36	2681	26	3	0.1830	0.8	12.52	1.3	0.4962	1.1	0.812	58	21	0.37
K05-32 G51	5.5	0.45	2714	16	-4	0.1868	0.5	14.17	0.8	0.5501	0.7	0.803	170	63	0.37
K05-32 G53	6.6	0.45	2675	26	0	0.1824	0.8	12.97	1.3	0.5154	1.1	0.814	53	32	0.61
K05-32 G57oc	6.1	0.29	2715	24	-1	0.1868	0.7	13.66	1.2	0.5302	1.0	0.818	66	23	0.35
K05-32 G59	6.6	0.29	2679	20	2	0.1829	0.6	12.68	1.1	0.5026	0.8	0.800	95	176	1.86
K05-32 G61	6.5	0.29	2671	30	1	0.1820	0.9	12.67	1.6	0.5047	1.2	0.801	47	34	0.72
K05-32 G71	6.6	0.33	2728	30	11	0.1883	0.9	12.02	1.5	0.4628	1.2	0.797	41	13	0.32
K05-32 G73	6.6 (12)	0.52	2681	18	1	0.1831	0.6	12.82	1.0	0.5078	0.8	0.816	81	41	0.51

TABLE 2
(continued)

##Sample No.	$\delta^{18}O$*,**	2sd error***	207/206 age	2sd error	Conc (%)	Pb204corr 207r/206r	% err	Pb204corr 207r/235	% err	Pb204corr 206r/238	% err	err corr	U (ppm)	Th (ppm)	Th/U
IGNEOUS CORES															
(C) Site 32															
K05-32 G77	6.5 (10)	0.37	2671	22	3	0.1820	0.6	12.49	1.1	0.4979	0.9	0.818	65	35	0.54
K05-32 G78	6.3 (9)	0.42	2691	18	5	0.1842	0.5	12.43	0.9	0.4895	0.7	0.815	97	33	0.34
AVERAGE	**6.0**	**0.36**	**2713**	**29**	**2.3**								**82**	**50**	**0.62**
METAMORPHIC RIMS															
(A) Site 14															
K05-14 G12	8.7	0.18	2624	11	1	0.1769	0.3	12.07	0.5	0.4951	0.4	0.782	315	2	0.01
(B) Site 21A															
K05-21A G1	8.0	0.39	2621	5	3	0.1766	0.2	11.84	0.4	0.4861	0.4	0.936	1003	11	0.01
K05-21A G2	8.1	0.39	2631	6	-1	0.1776	0.2	12.54	0.3	0.5119	0.3	0.808	716	10	0.01
K05-21A G3	8.5	0.39	2629	7	3	0.1774	0.2	11.90	0.7	0.4866	0.7	0.957	651	12	0.02
K05-21A G11or	7.7	0.39	2629	6	0	0.1775	0.2	12.29	0.3	0.5024	0.2	0.825	991	14	0.01
K05-21A G12	7.7	0.39	2616	8	2	0.1760	0.2	11.79	0.4	0.4858	0.3	0.797	461	7	0.01
K05-21A G14	7.5	0.28	2625	7	3	0.1770	0.2	11.85	0.3	0.4854	0.3	0.808	729	15	0.02
K05-21A G17	7.6	0.28	2631	6	3	0.1776	0.2	11.96	0.3	0.4885	0.2	0.802	1171	14	0.01
K05-21A G20	7.5	0.38	2624	6	3	0.1769	0.2	11.81	0.3	0.4843	0.2	0.802	1196	15	0.01
K05-21A G21	7.7	0.38	2625	7	2	0.1770	0.2	12.03	0.4	0.4930	0.3	0.809	631	11	0.02
K05-21A G22	7.6	0.38	2622	6	0	0.1767	0.2	12.17	0.3	0.4993	0.2	0.768	1060	14	0.01
AVERAGE	**7.8**	**0.36**	**2625**	**6**	**1.8**								**861**	**12**	**0.01**
(C) Site 32															
K05-32 G2	8.7	0.29	2625	6	2	0.1770	0.2	11.85	0.4	0.4858	0.3	0.838	633	57	0.09
K05-32 G3.5or	9.2 (3)	0.54	2626	8	0	0.1771	0.2	12.32	0.4	0.5046	0.4	0.838	496	36	0.07
K05-32 G3.7or	9.2 (2)	0.33	2632	10	4	0.1778	0.3	11.78	0.5	0.4804	0.4	0.794	500	42	0.08
K05-32 G3mor	8.8 (3)	0.54	2611	8	0	0.1755	0.2	12.15	0.4	0.5019	0.3	0.808	490	46	0.09
K05-32 G3ir	8.9	0.54	2608	8	1	0.1752	0.3	11.85	0.4	0.4906	0.3	0.802	437	16	0.04
K05-32 G4ir	8.7 (8)	0.19	2628	8	-1	0.1773	0.2	12.43	0.4	0.5084	0.3	0.814	515	43	0.08
K05-32 G4mr	8.8 (3)	0.19	2628	8	1	0.1773	0.2	12.20	0.4	0.4989	0.3	0.842	524	55	0.10
K05-32 G4or	9.0 (3)	0.19	2623	8	0	0.1767	0.2	12.22	0.4	0.5015	0.3	0.819	563	64	0.11
K05-32 G5ir	9.8	0.19	2639	8	11	0.1784	0.2	10.94	0.6	0.4448	0.5	0.918	604	67	0.11
K05-32 G5or	9.0	0.19	2627	8	4	0.1772	0.2	11.73	0.4	0.4800	0.3	0.808	569	66	0.12

TABLE 2
(continued)

##Sample No.	$\delta^{18}O$*,**	2sd error***	207/206 age	2sd error	Conc (%)	Pb204corr 207r/206r	% err	Pb204corr 207r/235	% err	Pb204corr 206r/238	% err	err corr	U (ppm)	Th (ppm)	Th/U
METAMORPHIC RIMS															
(C) Site 32															
K05-32 G6ir	10.0 (3)	0.59	2617	8	8	0.1761	0.3	11.07	0.4	0.4558	0.3	0.807	476	18	0.04
K05-32 G6or	8.8 (15)	0.59	2622	10	0	0.1767	0.3	12.30	0.4	0.5048	0.3	0.685	595	54	0.09
K05-32 G6tip	9.6 (3)	0.43	2512	8	0	0.1654	0.2	10.82	0.4	0.4746	0.3	0.794	558	16	0.03
K05-32 G7ir	8.4	0.23	2616	10	7	0.1760	0.3	11.16	0.5	0.4598	0.4	0.755	466	47	0.10
K05-32 G8ir	8.6	0.23	2627	8	7	0.1772	0.3	11.34	0.5	0.4642	0.4	0.827	461	41	0.09
K05-32 G8or	8.6	0.23	2630	8	4	0.1777	0.2	12.01	0.4	0.4902	0.3	0.798	485	45	0.09
K05-32 G9ir	8.7 (2)	0.23	2628	8	3	0.1773	0.3	11.85	0.4	0.4846	0.3	0.790	652	72	0.11
K05-32 G9or	10.0 (2)	0.23	2601	8	5	0.1744	0.2	11.24	0.4	0.4675	0.3	0.751	666	24	0.04
K05-32 G10ir	8.5	0.33	2590	8	8	0.1734	0.3	10.56	0.4	0.4419	0.3	0.783	546	53	0.10
K05-32 G10mr	8.5	0.33	2590	8	8	0.1734	0.3	10.56	0.4	0.4419	0.3	0.783	610	54	0.09
K05-32 G10or	10.0	0.33	2594	6	0	0.1738	0.2	11.91	0.3	0.4970	0.3	0.805	805	24	0.03
K05-32 G15	10.1 (4)	0.56	2640	4	3	0.1786	0.1	11.97	0.3	0.4859	0.2	0.806	1460	32	0.02
K05-32 G16	10.4	0.52	2615	12	13	0.1759	0.4	10.51	0.5	0.4331	0.4	0.735	531	18	0.03
K05-32 G27	10.0 (13)	0.45	2619	8	3	0.1763	0.2	11.81	0.4	0.4857	0.3	0.803	721	16	0.02
K05-32 G34	9.3	0.49	2615	10	-1	0.1760	0.3	12.33	0.5	0.5080	0.4	0.813	448	38	0.09
K05-32 G35	8.7	0.49	2612	10	1	0.1756	0.3	11.95	0.5	0.4937	0.4	0.813	609	51	0.08
K05-32 G37	10.1	0.39	2631	8	-1	0.1776	0.3	12.46	0.4	0.5087	0.3	0.780	800	15	0.02
K05-32 G39ir	9.1	0.39	2620	12	0	0.1765	0.4	12.15	0.6	0.4994	0.4	0.741	516	49	0.09
K05-32 G39or	8.6	0.39	2620	10	3	0.1765	0.3	11.81	0.5	0.4852	0.4	0.789	551	49	0.09
K05-32 G42	9.7 (7)	0.61	2630	8	9	0.1775	0.2	11.05	0.3	0.4517	0.2	0.731	1538	67	0.04
K05-32 G43	9.3	0.39	2623	6	1	0.1768	0.2	12.06	0.3	0.4946	0.2	0.712	1833	25	0.01
K05-32 G44	10.0 (10)	0.5	2644	8	13	0.1791	0.3	10.84	0.4	0.4392	0.3	0.771	934	13	0.01
K05-32 G46	10.0 (6)	0.36	2635	6	1	0.1781	0.2	12.19	0.3	0.4965	0.2	0.808	1165	14	0.01
K05-32 G50	8.5	0.36	2619	10	2	0.1763	0.3	11.90	0.5	0.4896	0.4	0.809	489	39	0.08
K05-32 G53	9.6	0.45	2620	10	1	0.1764	0.3	12.05	0.4	0.4954	0.3	0.721	751	12	0.02
K05-32 G56	10.0 (6)	0.45	2623	14	5	0.1768	0.4	11.59	0.6	0.4757	0.4	0.639	506	15	0.03
K05-32 G57	10.0	0.29	2659	8	5	0.1807	0.3	11.97	0.4	0.4803	0.3	0.779	640	16	0.02
K05-32 G59	10.2	0.29	2606	10	5	0.1750	0.3	11.30	0.5	0.4684	0.4	0.799	647	16	0.02
K05-32 G61	9.4	0.29	2617	16	0	0.1761	0.5	12.22	0.6	0.5034	0.3	0.546	613	74	0.12
K05-32 G63	9.9	0.28	2620	8	3	0.1764	0.3	11.75	0.4	0.4829	0.4	0.805	544	45	0.08
K05-32 G70			2630	10	13	0.1776	0.3	10.67	0.5	0.4359	0.4	0.796	475	33	0.07
K05-32 G71	8.7 (2)	0.33	2618	10	5	0.1763	0.3	11.46	0.5	0.4715	0.4	0.812	427	33	0.08

TABLE 2
(continued)

##Sample No.	$\delta^{18}O$*,**	2sd error***	207/206 age	2sd error	Conc (%)	Pb204corr 207r/206r	% err	Pb204corr 207r/235	% err	Pb204corr 206r/238	% err	err corr	U (ppm)	Th (ppm)	Th/U
(C) Site 32															
K05-32 G73	9.5 (10)	0.52	2583	8	3	0.1726	0.2	11.35	0.4	0.4767	0.3	0.800	601	19	0.03
K05-32 G76			2596	8	3	0.1740	0.3	11.46	0.4	0.4779	0.3	0.766	652	15	0.02
K05-32 G77or	9.0 (16)	0.37	2585	10	3	0.1728	0.3	11.29	0.5	0.4739	0.4	0.805	439	33	0.08
K05-32 G78or	9.1 (15)	0.42	2633	8	5	0.1779	0.2	11.63	0.4	0.4743	0.3	0.805	526	37	0.07
AVERAGE	**9.3**	**0.38**	**2619**	**9**	**3.7**								**654**	**37**	**0.06**
MEDIAN			**2620**		**3.0**										
DISTURBED CORES															
K05-32 G3.2ic	8.5	0.54	2668	18	2	0.1817	0.6	12.49	0.7	0.4988	0.5	0.658	209	172	0.82
K05-32 G3.5mc	8.7	0.54	2644	20	1	0.1791	0.6	12.38	0.9	0.5015	0.7	0.767	176	92	0.52
K05-32 G3.6oc	6.6 (2)	0.44	2694	32	-2	0.1846	1.0	13.49	1.3	0.5302	0.8	0.625	139	83	0.60
K05-32 G3 ave	8.6 (2)	0.54	2668	23									175	116	0.66
K05-32 G5	7.4	0.19	2641	28	4	0.1787	0.8	11.85	1.2	0.4808	0.8	0.702	78	34	0.44
K05-32 G6.1ic	8.9 (3)	0.54	2645	12	6	0.1792	0.4	11.60	0.6	0.4694	0.4	0.757	315	206	0.65
K05-32 G6.5moc	8.1 (2)	0.33	2661	10	3	0.1809	0.3	12.29	0.5	0.4928	0.4	0.799	484	459	0.95
K05-32 G6.6oc	6.6 (2)	0.33	2677	12	6	0.1826	0.4	12.04	0.6	0.4784	0.5	0.802	360	262	0.73
K05-32 G6.7oc	7.6 (3)	0.43	2666	12	-1	0.1814	0.4	12.96	0.6	0.5180	0.5	0.815	397	297	0.75
K05-32 G6 ave	7.7 (12)	0.43	2661	12									389	306	0.79
K05-32 G16ic	7.2 (4)	0.59	2678	30	-1	0.1828	0.9	13.15	1.5	0.5217	1.2	0.791	95	51	0.54
K05-32 G31	9.1	0.49	2705	16	-1	0.1857	0.5	13.47	0.9	0.5261	0.7	0.818	166	82	0.49
K05-32 G63	9.0	0.28	2671	24	8	0.1820	0.7	11.78	1.1	0.4697	0.9	0.767	100	33	0.33

16

Oxygen isotope (#) or age analysis ($) or both (^) overlap inclusion, core-rim boundary, metamorphic vein (in cores), "disturbed" core, or has an anomalous ^{16}O yield (oxygen isotope analysis); these analyses are not plotted nor used in computing ranges and averages.

Locations of analytical spots within grains denoted by: c=core, r=rim, i=inner, o=outer, m=middle.

* Oxygen isotope analyses corrected with respect to measured $\delta^{18}O$ values of bracketing standards, and reported in permil relative to VSMOW (refer to table A1, http://earth.geology.yale.edu/~ajs/SupplementaryData/2011/08BowmanTableA1.xls).

** $\delta^{18}O$ values reported for rims or cores with multi-spot analyses are averages of these analyses; the number of these analyses are in parentheses.

*** 2 SD errors assigned for single $\delta^{18}O$ analyses are reproducibility of bracketing standard; those for multiple analyses are the largest of the 2 SD errors from multiple sets of bracketing standards.

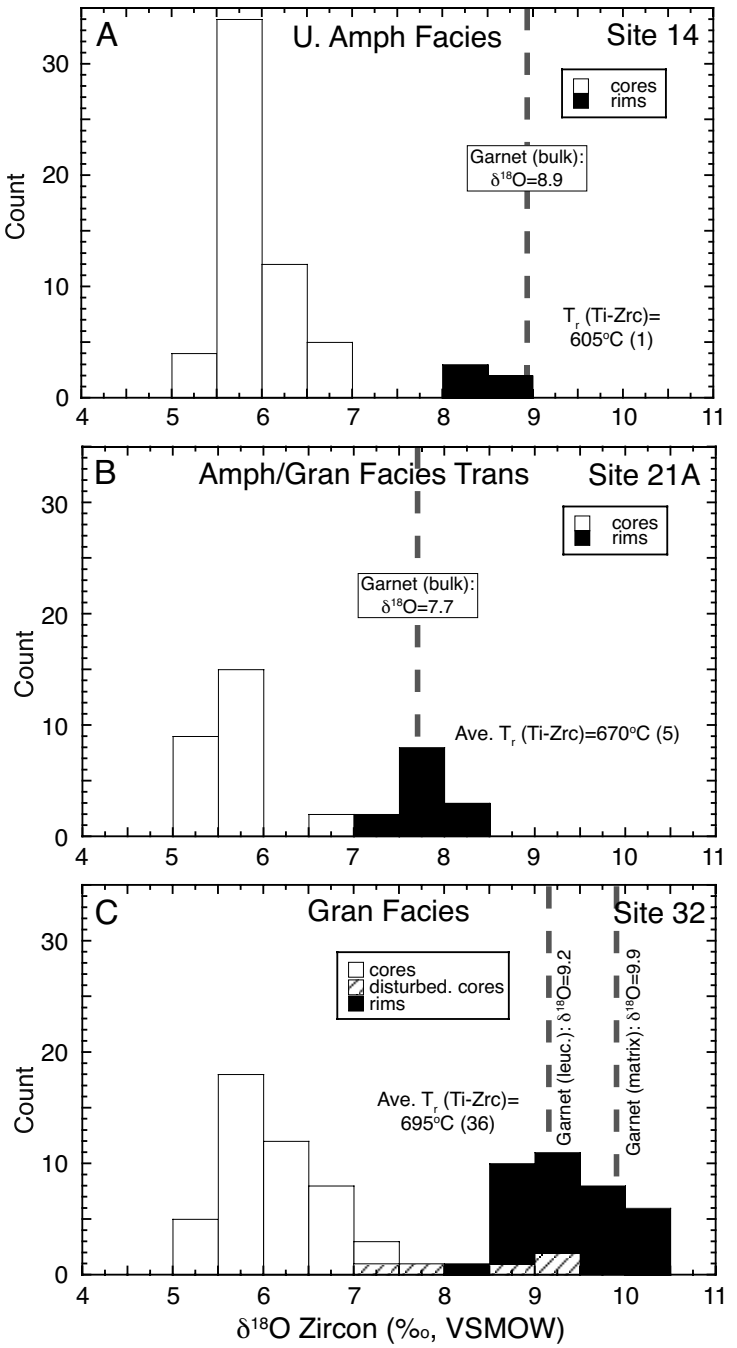

Fig. 6. Histograms of SIMS $\delta^{18}O$ values of zircon cores and rims from sites 14, 21A and 32. The histograms for all three sites include the analyses from table 2 plus additional $\delta^{18}O$ analyses from table A1 http://earth.geology.yale.edu/~ajs/SupplementaryData/2011/08BowmanTableA1.xls [additional cores and rims with no available age analyses and rims (sites 14 and 21A) too small for age analyses]. Vertical dashed lines indicate $\delta^{18}O$ values of bulk garnet (laser fluorination analysis) from the host rock paragneiss at each site. There is a significant (0.7‰) difference in $\delta^{18}O$ of garnet from matrix and leucosome at site 32. This heterogeneity is reflected in the greater range of $\delta^{18}O$ values of metamorphic rims at site 32 (see text for further discussion). There are differences in $\delta^{18}O$ value of garnet (and therefore host rock) among the three

have $\delta^{18}O$ values from 5.4 to 6.2 permil [up to 6.6‰ including all grains with $\delta^{18}O$ analyses but no age analyses; see fig. 6 and table A1 http://earth.geology.yale.edu/~ajs/SupplementaryData/2011/08BowmanTableA1.xls]. At site 21A, the cores range in $^{207}Pb/^{206}Pb$ age from 2752±29 to 2696±24 Ma and have $\delta^{18}O$ values from 5.2 to 6.6 permil. At the granulite-grade site 32, the overwhelming majority of the zircon cores (n = 45 of 51) range in $^{207}Pb/^{206}Pb$ age from 2827 ± 16 to 2671 ± 30 Ma. The $\delta^{18}O$ values of these cores range from 5.1 to 7.0 permil.

The $^{207}Pb/^{206}Pb$ ages and $\delta^{18}O$ values of the detrital cores at all three sites are similar (figs. 5 and 6) although there are a greater proportion of cores with $\delta^{18}O$ values of 6 to 7 permil at the granulite site 32. All but four of the age analyses in cores have low discordance of ≤7 percent (average ~2.3% for site 32; table 2) and have lower intercepts of discordant arrays near 0 Ma; thus there is no evidence of ancient (that is, Precambrian) Pb-loss. These ages correspond to known ages of crust formation preceding and during the Kenoran orogeny from prior ID-TIMS studies in the region (Corfu and Davis, 1992) as illustrated by black bars in figure 5. Hence we treat these $^{207}Pb/^{206}Pb$ ion microprobe ages as close approximations of true U-Pb isotopic age. The $\delta^{18}O$ values of zircon cores at all three sites range from 5.1 to 7.0 permil (figs. 5 and 6) regardless of size, and are similar to the range of laser fluorination data for zircons from plutonic rocks throughout much of the Superior province (King and others, 1998), and partially overlap mantle or primitive zircon values of 5.3 ± 0.6 permil (Valley and others, 2005).

Metamorphic rims.—Dark CL (metamorphic) rims at all three sites have younger U-Pb and $^{207}Pb/^{206}Pb$ ages, and are enriched significantly in $^{18}O/^{16}O$ compared to the "normal" igneous cores (table 2; figs. 5 and 6). At the lowest grade, amphibolite facies site 14, only one grain had a rim with sufficient width for a SHRIMP analysis. Its $^{207}Pb/^{206}Pb$ age is 2624±11 Ma and its $\delta^{18}O$ value is 8.7 permil. Oxygen isotope compositions of four more rims could be measured at site 14. Their $\delta^{18}O$ values range from 8.2 to 8.7 permil (table A1 http://earth.geology.yale.edu/~ajs/SupplementaryData/2011/08BowmanTableA1.xls) and are similar to the measured $\delta^{18}O$ value of garnet (8.9‰, laser fluorination) from the paragneiss host rock (fig. 6A). At the amphibolite/granulite transition site 21A, the ten analyzed rims range in $^{207}Pb/^{206}Pb$ age from 2631±6 to 2616±8 Ma (fig. 5). The average $\delta^{18}O$ value of these rims (7.8‰) is very close to the measured $\delta^{18}O$ value of garnet (7.7‰) from the paragneiss host rock (fig. 6B). The 33 rims analyzed at the granulite-grade site 32 have $^{207}Pb/^{206}Pb$ ages ranging from 2659 ± 8 Ma to 2583 ± 8 Ma with an average of 2619 Ma (table 2). One rim tip (grain 6, fig. 4) has a much younger $^{207}Pb/^{206}Pb$ age of 2512 ± 8 Ma and is concordant.

All metamorphic rims at site 32 are significantly enriched in $^{18}O/^{16}O$ compared to detrital cores, but have a significant range of $\delta^{18}O$ values from 8.4 permil to 10.4 permil. This range in $\delta^{18}O$ values encompasses the smaller but still significant difference in $\delta^{18}O$ values of bulk garnet separates from leucosome (9.2‰) and matrix (9.9‰) in the paragneiss rock host. The $\delta^{18}O$ value of garnet from the leucosome (9.2‰) coincides with the mode (the 9.0-9.5‰ interval) of the $\delta^{18}O$ values of the zircon rims, and the $\delta^{18}O$ value of garnet from the matrix (9.9‰) falls in the middle of

sites. Despite these differences, the measured fractionations between bulk garnet and average zircon rim at the two lower grade sites are small, and the $\delta^{18}O$ values of leucosome and matrix garnet at the granulite grade site are close to the mode of the rim analyses and to the abundant number of rims with higher $\delta^{18}O$ values (9.4 to 10.4‰), respectively. These similarities are consistent with the growth of the zircon rims in a close approach to oxygen isotope exchange equilibrium with garnet and their rock hosts at all three metamorphic grades. The average value of temperature calculated from the measured Ti content of zircon rims, based on the calibration of Ferry and Watson (2007), and the number of rims analyzed in parentheses, are also shown for each site.

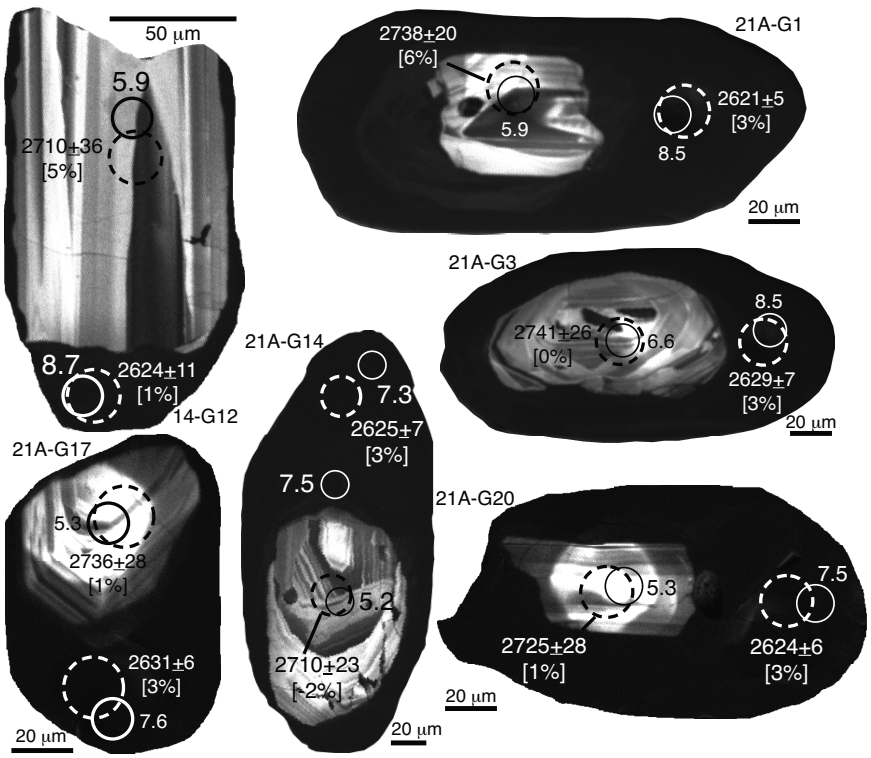

Fig. 7. CL images of six grains from sites 14 and 21A, superimposed with spot $^{207}Pb/^{206}Pb$ age (dashed white or black circles) and $\delta^{18}O$ (solid white or black circles) analyses. Circles are in black or white only to maximize contrast with the background CL image. The $^{207}Pb/^{206}Pb$ ages (Ma) include analytical uncertainty (2 SD) and [% discordance]. The CL images of grains from 21A are post-trace element analysis and contain bright spots produced by the presence of gold-coated SHRIMP analytical pits (particularly noticeable in cores of grains 17 and 20). The image of grain 3 at site 21A (the only grain with a core $\delta^{18}O$ value >6.0‰ out of 15 grain cores analyzed to date) is included. All cores analyzed to date at these two lower grade sites have low $\delta^{18}O$ values equivalent to those of the cores at site 32 (figs. 5 and 6). Many of the analytical spots in cores are ≤30 μm from the core-rim boundary yet show no sign of $^{18}O/^{16}O$ enrichment from exchange with high $\delta^{18}O$ rims.

the higher range (9.4 to 10.4‰) of $\delta^{18}O$ values of zircon rims (fig. 6C). These correlations are consistent with a close approach to oxygen isotope exchange equilibrium between garnet and zircon rims within two isotopically distinct domains in the paragneiss at site 32; leucosome and host rock matrix. Thin section observations indicate that zircons occur in both leucosome and matrix domains within the paragneiss. Even though the host rocks at the three sites have different $\delta^{18}O$ values, the $\delta^{18}O$ values of zircon rims and garnet from the rock host at each site are similar or have overlapping ranges (site 32), indicating that the zircon rims grew in oxygen isotope exchange equilibrium with their rock hosts at the time of metamorphism at all three sites (fig. 6).

The $^{207}Pb/^{206}Pb$ ages of the dark CL rims at all three sites are similar, although the much greater number and volume of rims at site 32 record the greatest range of age. These rims record ~80 Ma of nearly continuous zircon overgrowth events, with the greatest frequency at ~2.62 Ga (table 2, fig. 5), that constitutes the main phase of rim growth.

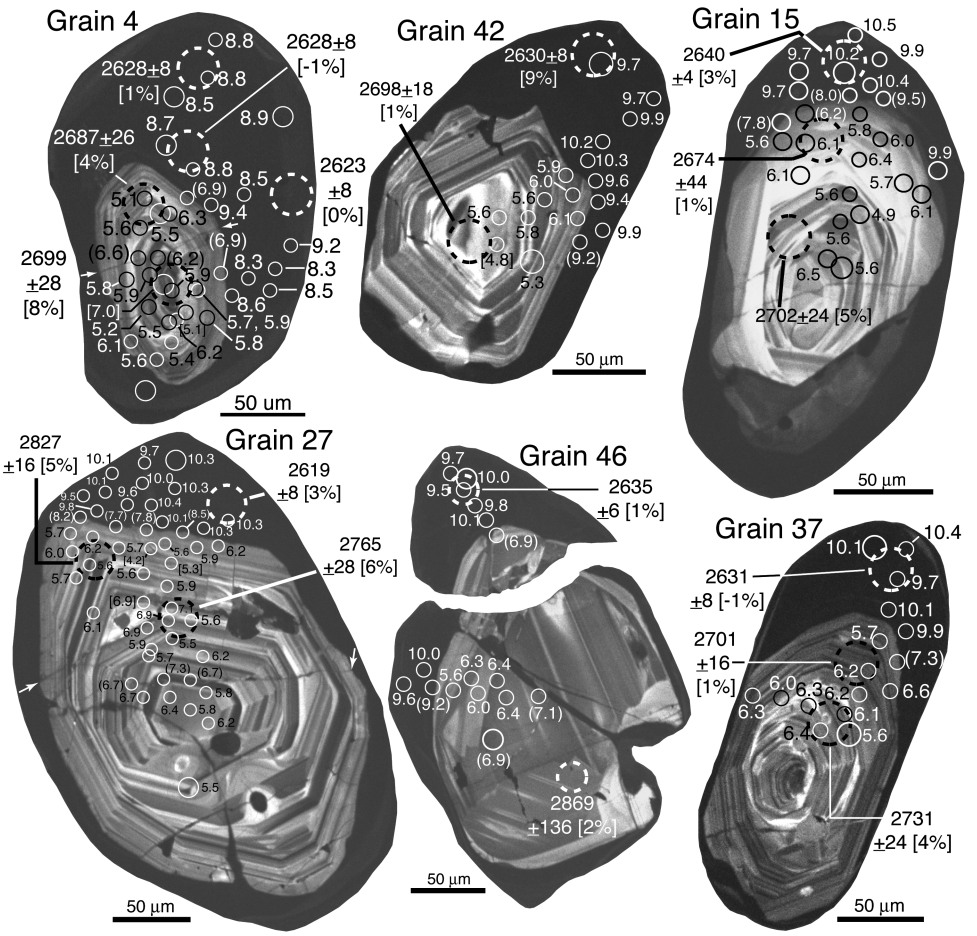

Fig. 8. CL images of six zircon grains with normal CL (igneous) cores from the granulite-grade site 32, superimposed with the locations and results of spot $\delta^{18}O$ (solid white or black circles) and $^{207}Pb/^{206}Pb$ age (dashed white or black circles) analyses. The $^{207}Pb/^{206}Pb$ ages (Ma) include analytical uncertainty (2 SD) and [% discordance]. Spot $\delta^{18}O$ analyses that straddle the core-rim boundary or metamorphic zircon veinlets are in parentheses; spot $\delta^{18}O$ analyses that fall on fractures and have low ^{16}O yields are in brackets. Circles are in black or white only to maximize contrast with the background CL image. In all grains, bright CL cores are significantly older, and have significantly lower $\delta^{18}O$ values, than dark CL rims. There is a steep discontinuity in $\delta^{18}O$ value that corresponds spatially with the core-rim boundary defined by CL in each grain (see text for further discussion).

Multispot Age and $\delta^{18}O$ Analyses of Individual Grains

Detailed ion microprobe $\delta^{18}O$ traverses were measured across the core-rim boundaries of 13 grains with "normal" CL cores from site 32 (table A1 http://earth.geology.yale.edu/~ajs/SupplementaryData/2011/08BowmanTableA1.xls) in order to test for: a) evidence for diffusion of oxygen between these cores and their enclosing, $^{18}O/^{16}O$-enriched rims; or b) diffusion adjacent to deformation microstructures created during high-temperature metamorphism (grain 16). Multiple spot analyses of both $\delta^{18}O$ and age were also made in two grains from site 32 exhibiting "disturbed" cores with uncommon intermediate to low CL intensity and variable $^{18}O/^{16}O$-enrichment, to gain insight into the mechanisms responsible for these changes (table A1 http://earth.geology.yale.edu/~ajs/SupplementaryData/2011/

08BowmanTableA1.xls). Although our detailed analyzes are focused on the highest T granulite zone site 32, all cores analyzed to date at the two lower grade sites also have low $\delta^{18}O$ values equivalent to those of the cores at site 32 (fig. 6, table 2). Locations of analyses in low $\delta^{18}O$ cores and high $\delta^{18}O$ rims in zircons from sites 14 and 21A are often within 30 to 50 μm of each other and ≤30 μm from the core-rim boundary (fig. 7). Even though the regional metamorphism at site 21A likely occurred under significant $f(H_2O)$ up to 4000 or 5000 bars and T≥650 °C (Percival, 1983; Mäder and others, 1994), there is no evidence for $^{18}O/^{16}O$ enrichment of the zircon cores at site 21A at a scale as small as 30 μm from $^{18}O/^{16}O$-enriched metamorphic rims (fig. 7).

Multi spot analysis of grains with "normal" cores.—The locations and results of $\delta^{18}O$ and age analyses are superimposed on CL images in figure 8 for six of the grains with normal CL cores from the granulite zone site 32 that were analyzed in detail. The values for ion microprobe pits that, in post-analysis SEM analyses, were revealed to straddle the core-rim boundary or metamorphic veinlets are in parentheses in figure 8. Excluding these data, the core domains of grains 4, 15, 27, 37, 42 and 46 have average values in the range 5.8 to 6.1 permil. In grains 15 and 27, there are significantly higher $\delta^{18}O$ domains in the core interior that correspond to a specific CL band or group of bands (fig. 8). The higher $\delta^{18}O$ domain in grain 27 has a pre-metamorphic age (fig. 8, table 2) and is interpreted to be primary, representing a xenocrystic domain or temporal variation in magma chemistry.

$\delta^{18}O$-distance profiles across boundaries between normal igneous cores and metamorphic rims.—The $\delta^{18}O$ values from the spot analyses are plotted versus distance from the core-rim boundary in figure 9 for 12 of the grains with "normal" CL cores that were analyzed in detail. Distances were measured on enlarged, composite SE&CL SEM single-grain images in which the core-rim boundary from the CL image is superimposed on the SE image that illustrates the locations of the ion microprobe pits. Distances were measured perpendicular to the local orientation of the nearest core-rim boundary in these images. In all of these grains, there is a sharp discontinuity in $\delta^{18}O$ values between the low $\delta^{18}O$ igneous core and high $\delta^{18}O$ metamorphic rim that corresponds spatially with the core-rim boundary defined in CL. The only $\delta^{18}O$ values intermediate between core and rim $\delta^{18}O$ values are spots that physically straddle the core-rim boundary. These detailed traverses indicate that the width of any oxygen isotopic gradient between the core and rim, which could have formed by volume diffusion, is <7 μm (the diameter of the ion beam pits).

$\delta^{18}O$-distance profiles across normal igneous cores adjacent to deformation microstructures.—Grain 16 (fig. 10) is one of several grains in which the bright CL igneous core is crosscut by dark CL, $^{18}O/^{16}O$-enriched veins (filled fractures) that connect seamlessly with the dark CL rim overgrowth (figs. 10A and 10B). In addition, there are a number of fine/thin, irregular dark CL lines between and parallel to the two larger veins, and these crosscut the midsection of the grain. Secondary electron (SE) imaging shows that neither the veins nor these dark CL lines are current fractures except locally (fig. 10A). Both the veins and these irregular dark CL lines are reasonably interpreted either to be fracture infilling or micro-veins of zircon or recrystallized igneous zircon along these fractures formed contemporaneously with the metamorphic zircon rim. Detailed multispot oxygen isotope analyses show that the dark CL rim and thick fracture infilling are significantly enriched in $^{18}O/^{16}O$ (fig. 10B). Most of the core has $\delta^{18}O$ values ranging from 4.9 to 6.1 permil, similar to values of the main population of "normal" cores. However, the area containing abundant micro-veins (curvilinear, dark CL features) has significantly higher $\delta^{18}O$ values. Many of the analytical spots with high $\delta^{18}O$ values in this area overlap the dark CL micro-veins (figs. 10C and 10D); their elevated $\delta^{18}O$ values can be interpreted in a straightforward way in terms of contributions of $^{18}O/^{16}O$-enriched, metamorphic zircon from these micro-veins. Three analy-

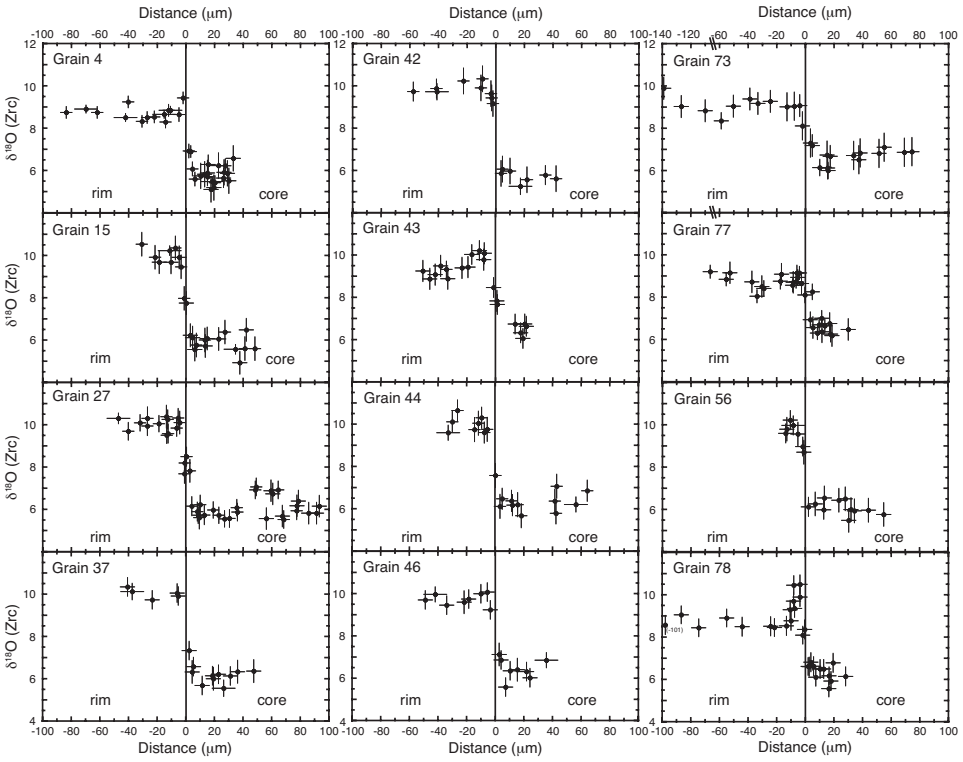

Fig. 9. Plots of the $\delta^{18}O$ values of spot ion microprobe analyses (with 2 SD analytical error bars) vs. distance (in μm's) of the spot from the core-rim boundary (solid vertical line at 0 distance) for 12 of the zircon grains with normal CL cores from the granulite facies site 32 that were analyzed in detail. Distances were measured perpendicular to the core-rim boundary defined in CL. In this and later figures, individual analyses are plotted with spatial uncertainty of ±5 or ±8 μm to account for both analytical spot size (≤7 or 15 μm) and some uncertainty in locating the spot relative to the core-rim boundary. Note that the scales for the rims in grains 73 and 77 extend to −140 μm, and are discontinuous. One spot in the rim of grain 78 is −101 μm from the core-rim boundary. In all grains, there is a steep discontinuity in $\delta^{18}O$ value at the core-rim boundary between low $\delta^{18}O$ cores and higher $\delta^{18}O$ rims. If any change in $^{18}O/^{16}O$ in these two domains resulted from volume diffusion across this boundary, the scale of exchange is limited to a distance from this boundary of less than the diameter of the ion microprobe analysis (7 μm).

ses with $\delta^{18}O$ values ≥7.4 permil (black squares, fig. 10D) do not overlap any visible dark CL micro-veins. These analyses are located in dark, unbanded and somewhat blurred CL material at the center of the core where the two $^{207}Pb/^{206}Pb$ ages are also younger (figs. 10B and 10C). This central area may be a "disturbed" core (see below). It is unlikely that this $^{18}O/^{16}O$ enrichment in the core center is the result of diffusion from the high $\delta^{18}O$ veins; the spot with the highest $\delta^{18}O$ value within this dark CL domain is the farthest of the three analyses from dark CL micro-veins (figs. 10C and 10D).

A plot of the $\delta^{18}O$ values of the spot analyses of the core vs. their distance from metamorphic rim or veins (fig. 10D) shows that there is no systematic enrichment in $^{18}O/^{16}O$ of core with proximity to these veins that might result from diffusion of oxygen, at the scale of the diameter of the ion microprobe spots (7 μm). These results provide no evidence for deformation-enhanced diffusion of oxygen in this core.

The several pieces of the core within grain 16 do not appear to be moved/rotated with respect to one another. However, the fracture walls do not precisely line up,

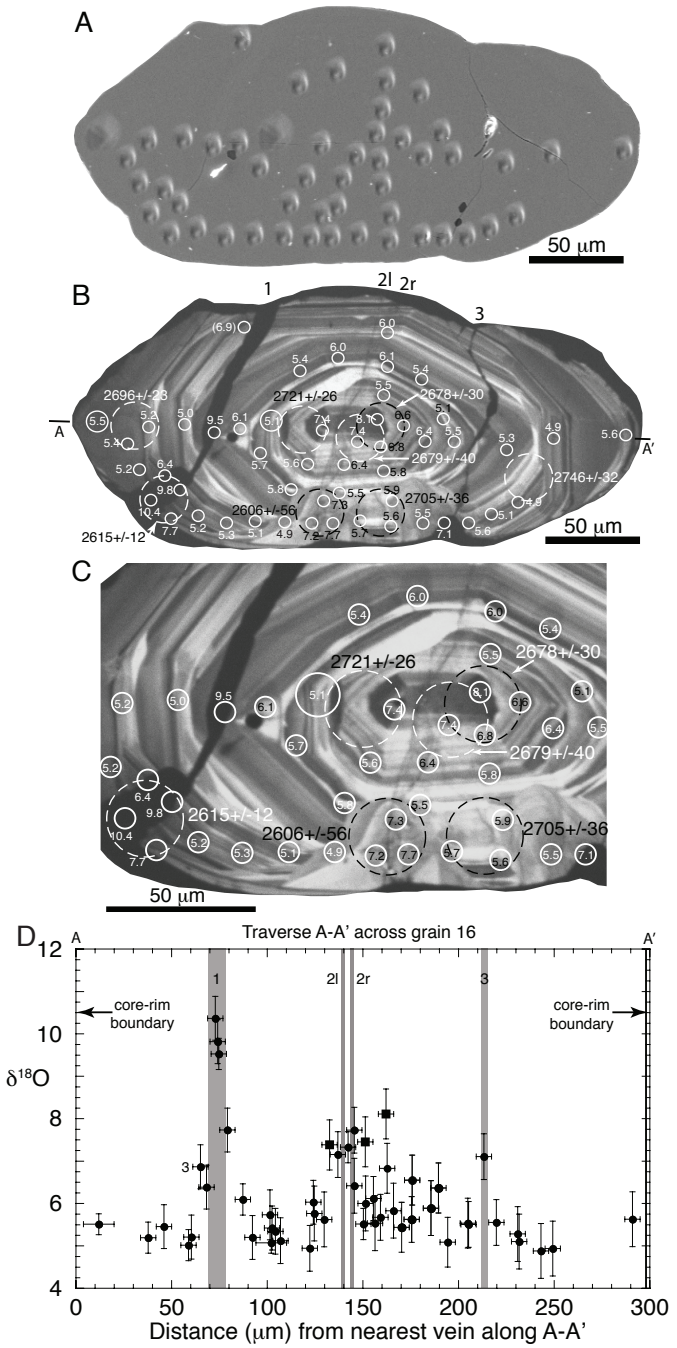

Fig. 10. (A) SE image of grain 16 showing locations of analytical pits from Wisc-SIMS oxygen isotope analysis, July 2006. (B) CL image of grain 16 (same scale as A) showing metamorphic (dark CL) zircon forming a thin rim and filling several fractures cross-cutting the igneous (bright CL) core. The SE image (A) shows that these dark CL veins/fractures are not current fractures; current fractures coincide only locally with these dark CL veins. Also included on this CL image are the locations and results of $\delta^{18}O$ (solid white or black circles) and age (dashed white or black circles) analyses. Traverse A-A′ used to construct the $\delta^{18}O$-distance plot in panel D.

suggesting that either motion has occurred at a high angle to the plane of section or that some chemical dissolution of the detrital zircon may have occurred prior to precipitation of the metamorphic zircon within the fractures.

Grains with "disturbed" CL cores.—A small group (5 of 51 grains measured for both $^{207}Pb/^{206}Pb$ age and $\delta^{18}O$) of zircon cores at site 32 have muted CL intensity and blurred to locally disrupted planar growth banding quite distinct (fig. 11) from the CL characteristics of the main population of cores at all three sites (figs. 2, 3, and 8). These types of cores (labeled as "disturbed" in fig. 5) have higher but variable $\delta^{18}O$ values relative to those of normal cores, and three of the five yield lower $^{207}Pb/^{206}Pb$ spot ages coeval with regional metamorphism. Multiple analyses were made on two of these cores; these analyses reveal significant age and $\delta^{18}O$ heterogeneity that correlate with the degree of disruption of the CL (fig. 11).

The entire core of grain 6 (fig. 11) is muted in CL compared to isotopically normal cores, but also contains patchy areas near the center where the CL banding is more blurred and even destroyed (for example, dark unbanded CL domains). This core is heterogeneous with respect to $\delta^{18}O$ (6.3 to 9.1‰), and all four age spots are equivalent to, or approach, ages of regional metamorphism. The bottom-most section of the core nearest the rim (fig. 11) has lower $\delta^{18}O$ values (6.3-7.0‰) within the upper end of the range typical for the main population of cores; this section also contains the oldest of the four core $^{207}Pb/^{206}Pb$ ages (2677±12 Ma). Darker, more disrupted looking CL domains within the core have anomalous, higher $\delta^{18}O$ values (up to 9.1‰) and younger $^{207}Pb/^{206}Pb$ ages overlapping those of the metamorphic overgrowths (rims). The youngest age (2645±12 Ma) is recorded in the center of the core, which has the highest $\delta^{18}O$ values (8.8, 9.0, 9.1‰) and the darkest, least-banded CL signal. Thus, there is no systematic spatial correlation within the core of higher $\delta^{18}O$ values and younger $^{207}Pb/^{206}Pb$ ages with proximity to the core-rim boundary. These spatial relationships with respect to the core-rim boundary are inconsistent (at least within the 2-D plane of this CL image) with resetting of $\delta^{18}O$ and age values in this core by volume diffusion of O and Pb. Grain 3 exhibits analogous correlations in CL signal, age and $\delta^{18}O$ changes within its disturbed core, and in the spatial relationships of these parameters with respect to the core-rim boundary (fig. 11). Within the disturbed cores of both grains there is an approximate correlation of the extent of blurring and darkening of CL banding, higher $\delta^{18}O$ values, and younger $^{207}Pb/^{206}Pb$ ages.

Isotopic zonation within metamorphic rims.—Some individual zircon rims exhibit zonation in $\delta^{18}O$ well beyond analytical error (±0.38‰ ave 2 SD). In grains 43 and 78 (fig. 9) and in grains 64 and 71 (table A1 http://earth.geology.yale.edu/~ajs/SupplementaryData/2011/08BowmanTableA1.xls), the $\delta^{18}O$ values are highest (>10‰) at the core-rim boundary, and decrease to 8.5 to 9 permil into the outer part of the rims. In grain 6 (fig. 11), $\delta^{18}O$ values are ~10 permil nearest the core-rim boundary. From this boundary out to the boundary with the young (2512 Ma) tip, $\delta^{18}O$

Fig. 10 (continued). (C) Higher magnification CL image of the lower central section of grain 16, showing more clearly the spatial relationships between age, $\delta^{18}O$ analyses and a series of thin, dark CL microfractures. Note that the only high (>6.0‰) $\delta^{18}O$ analyses in the core are of pits that either overlap these thin dark CL microfractures or are the three analyses ($\delta^{18}O$>7.0‰) from the central, dark CL core of the grain (see text for further discussion). (D) Plot of the $\delta^{18}O$ values of the spot analyses within the core with respect to their distance from the nearest dark CL vein, superimposed at the same scale on the longitudinal traverse across the grain, A-A′ (from B). The three analyses ($\delta^{18}O$>7.0‰) from the central, dark CL core of the grain are plotted as squares. Veins are numbered in sequence from left to right across the grain (B), and are plotted as gray bands where they intersect the traverse A-A′. All analytical spots are plotted accurately along this profile with respect to their distance (perpendicular to the vein trend) from the nearest vein (the critical information). However the veins are not linear nor at right angle to the long direction of the grain, and some analyses are located well above and below the traverse A-A′. Hence not all analyses are located accurately with respect to each other.

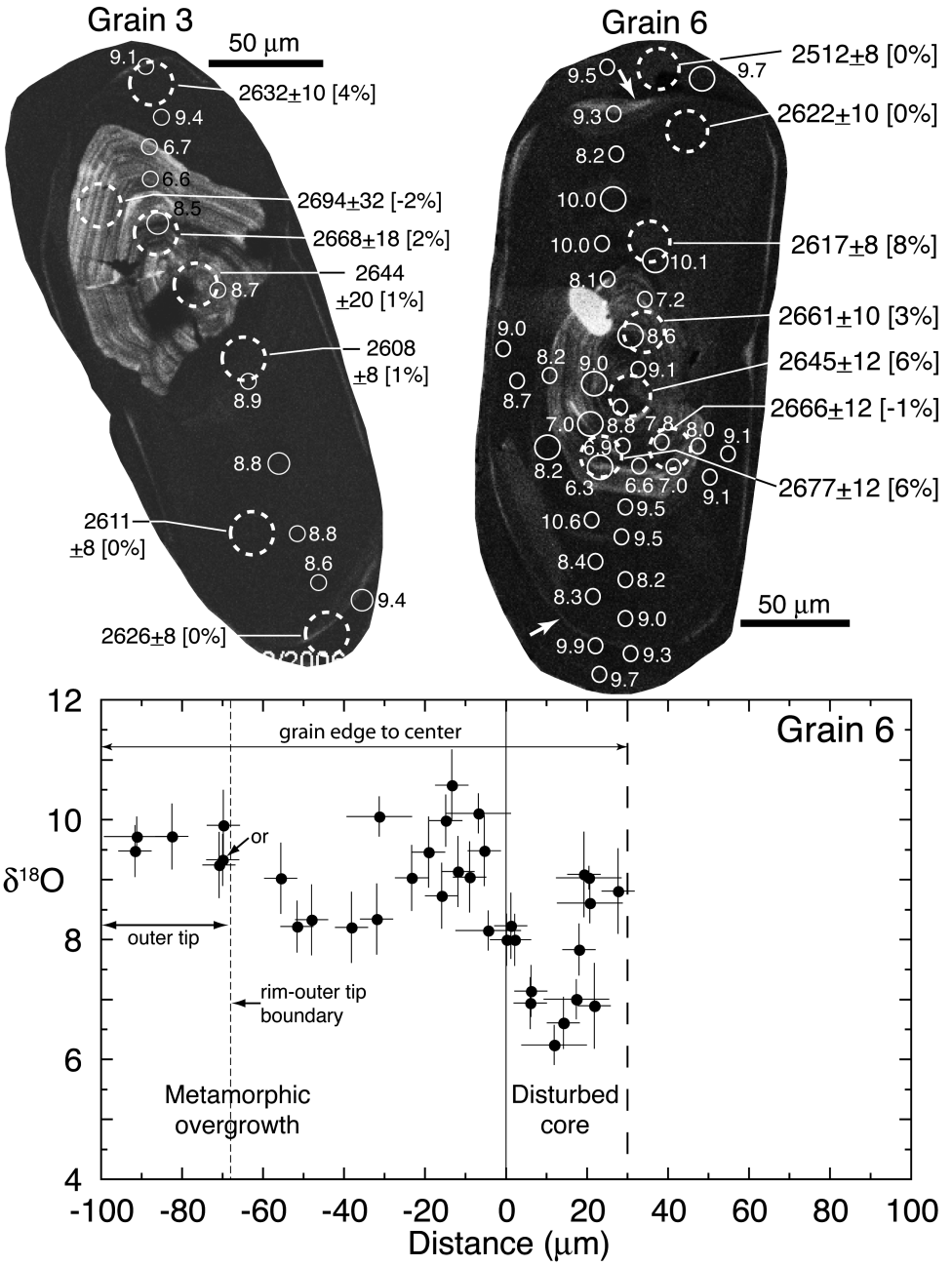

Fig. 11. CL images of two composite grains (grains 3 and 6) with disturbed (faded and/or blurred) CL cores from the granulite-grade site 32, with the locations and results of spot $\delta^{18}O$ (solid white or black circles) and $^{207}Pb/^{206}Pb$ age (dashed white circles) analyses superimposed. Circles are in black or white only to maximize contrast with the background CL image. The CL response of both cores is blurred and muted compared to isotopically normal igneous cores; these images were recorded at significantly higher photomultiplier collector setting than used with normal cores in order to produce contrast between these muted CL cores and rim. The patchy area of dark, unbanded CL that appears to disrupt CL banding in the inner core of grain 3 is a pitted area. In grain 6 white arrows at the top and bottom of the grain point out the boundary, visible in CL, between the main-stage metamorphic rim in this grain and the much younger (2512 Ma) outer rim tip. Below the two CL images is a plot of the $\delta^{18}O$ values of spot ion microprobe analyses (with 2 SD

values decrease to as low as 8.2 permil, and then increase again to just over 9 permil (fig. 11). The isotopic zonation pattern is similar at both ends of the rim overgrowth in grain 6, suggesting that it is approximately concentric within the rim overgrowth.

Trace Element Compositions

After polishing to remove the ~1 μm deep SHRIMP U-Pb analysis pits, a suite of trace elements was measured on the SHRIMP-RG at or very near the same locations of the previous SHRIMP age pits within cores and rims of these composite zircons from site 32 as confirmed with post-analysis CL imaging. Results are summarized here and in table 3; further details are presented in Appendix C and full analytical results are compiled in table A2 http://earth.geology.yale.edu/~ajs/SupplementaryData/2011/09BowmanTableA2.xls.

Trace element composition of cores and rims.—The trace element composition of the igneous cores is quite distinct from that of the metamorphic rims (fig. 12, table 3). Igneous cores have lower U, Th and Li contents (figs. 12A, 12B, and 12D), and on average higher Y and Yb contents (figs. 12C and 12E), than metamorphic rims. As a consequence, cores also have lower U/Yb ratios than rims (fig. 12E). In general, the U, Th Th/U, Y and Yb values of the igneous cores (fig. 12) are similar to values for magmatic arc sources (Grimes and others, 2007, 2009, 2011; unpublished SUMAC SHRIMP-RG data library). These trace element compositions are consistent with an origin of these cores as igneous grains prior to deposition in the sedimentary protolith of the Borden Lake belt paragneisses. Because of their significant enrichment in U, metamorphic rims (figs. 12C and 12D) have significantly lower Th/U ratios (0.01-0.14; 0.07 ave.) that are typically characteristic of metamorphic zircons (for example, Hoskin and Black, 2000; Rubatto, 2002; Hoskin and Schaltegger, 2003). Principally resulting from their higher U contents, rims have significantly higher U/Yb ratios than cores. The trace element compositions of these metamorphic rims, particularly U, Th Th/U, Y, Yb and U/Yb (fig. 12), are similar to trace element compositions of zircons from continental sources (Grimes and others, 2007, 2009) and distinct from zircons in modern ocean crust (Grimes and others, 2007, 2011). Large differences in Li concentration are preserved between magmatic cores (10-51 ppm) and metamorphic rims (86-252) despite prolonged high-T regional metamorphism.

The small number (5 of 51 grains analyzed, fig. 5) of "disturbed" cores showing patchy $\delta^{18}O$ variation (fig. 11) have trace element compositions quite distinct from metamorphic rims (fig. 12). Many of the trace element compositions of the disturbed cores are similar to, to somewhat higher than, those of normal detrital cores, which results in many disturbed cores plotting within and as extensions of the fields defined by normal cores (for example, Th vs. U, U/Yb vs. Y; figs. 12A and 12E). Disturbed cores are enriched in both U and Th up to five-fold compared to average U and Th concentrations in normal cores. In contrast, metamorphic rims are enriched in U at similar to somewhat lower Th contents (fig. 12A). Hence the Th/U ratios in these disturbed cores, including in the most U-enriched portions, remain high, similar to those of normal cores and much higher than those of metamorphic rims (fig. 12D).

Ti results and Ti-in-zircon thermometry.—At the granulite-grade site 32, Ti concentrations in zircon rims range from 2.3 to 9.9 ppm. The Ti-in-zircon [Ti (Zrc)] geothermometer depends additionally on the $a(TiO_2)$ and $a(SiO_2)$ in the rock host to zircon

analytical error bars) vs. distance of the spot from the core-rim boundary (solid vertical line at 0 μm) for grain 6. The short-dashed line in the diagram shows the location of the boundary between the metamorphic rim and the much younger outer rim tip. There is no systematic spatial correlation within the core between higher $\delta^{18}O$ value and proximity to the core-rim boundary that might be expected if these $\delta^{18}O$ values were reset by diffusion of oxygen from the $^{18}O/^{16}O$-enriched rim.

TABLE 3

Summary of trace element concentrations, U-Pb age, and $\delta^{18}O$ in igneous cores and metamorphic rims of Kapuskasing zircons

*Sample No.	Ti(48) ppm	Ti(49) ppm	***T°C Ti (Zrc)	Y ppm	Yb ppm	Hf ppm	$U ppm	$Th ppm	Li ppm	Th/U	U/Yb	^Age (Ma)	^$\delta^{18}O$
CORES													
K05-32-G1.1mc	4.0	4.0	695	472	221.8	9218	50	18		0.37	0.23	2750	5.4
K05-32-G4.1oc	5.3	5.3	720	517	166.3	10228	82	69	26	0.84	0.49	2687	5.4
K05-32-G4.5ic					171.5	8588	80	77		0.96	0.47	2699	5.8
K05-32-G7.1c	3.4	3.3	680	551	191.1	9952	54	31		0.58	0.28	2724	6.0
K05-32-G8.1c	6.1	5.9	735	259	78.6	9077	58	58		1.00	0.73	2693	6.6
K05-32-G12.1ic	4.3	4.4	700	521	220.2	9150	59	27		0.46	0.27	2672	6.2
K05-32-G13.1ic	2.6	2.7	660	176	75.9	12148	46	10	32	0.23	0.60	2710	5.7
K05-32-G15.2oc					66.4	9252	26	16		0.61	0.40	2674	5.8
K05-32-G15.1ic	4.5	4.7	705	790	206.5	9055	61	48	11	0.80	0.29	2702	5.6
K05-32-G17.1ic	5.2	5.1	720	484	174.3	9219	50	25		0.51	0.28	2742	5.9
K05-32-G18.1c	4.0	4.1	695	342	152.7	9896	33	15		0.45	0.22	2715	6.6
K05-32-G19.1mc	4.9	5.1	715	365	170.3	9387	30	12	14	0.38	0.18	2783	5.9
K05-32-G19.2oc	3.1	3.3	675	254	91.9	12044	51	15	30	0.30	0.56	2690	6.2
K05-32-G19.3ic	4.6	4.7	710	270	98.9	9043	33	15	38	0.46	0.34	2835	6.1
K05-32-G20.1c	4.9	5.0	715	352	134.7	8458	29	13		0.44	0.22	2697	6.4
K05-32-G21.1c	4.8	4.9	710	312	115.9	11226	372	330		0.89	3.21	2692	5.9
K05-32-G27.2mc					119.4	11008	60	18		0.29	0.50	2765	6.5
K05-32-G27.4oc					247.8	9862	101	46		0.45	0.41	2827	5.8
K05-32-G32.1ic					94.9	9025	56	61		1.10	0.59	2691	5.8
K05-32-G34.1c					163.1	9267	51	21		0.41	0.31	2717	5.9
K05-32-G35.1ic	3.9	4.0	695	839	264.7	11571	106	49	25	0.46	0.40	2684	7.0
K05-32-G35.3oc					171.9	10664	104	59		0.56	0.60	2698	
K05-32-G37.1ic	4.9	4.9	715	247	101.6	9351	74	47	51	0.63	0.73	2731	6.1
K05-32-G37.2oc					116.9	10812	174	141		0.81	1.49	2701	6.0
K05-32-G38.1c					228.0	9840	64	40		0.62	0.28	2682	5.9
K05-32-G39.1c					187.3	8739	116	58		0.50	0.62	2710	5.8
K05-32-G41.1ic					184.8	11294	249	125		0.50	1.35	2712	6.8
K05-32-G42.1ic	4.1	4.1	700	414	151.2	10639	68	27	16	0.40	0.45	2698	5.7
K05-32-G43.1c	3.9	3.8	695	347	131.6	9043	20	10	10	0.51	0.15	2736	5.1
K05-32-G44.1oc	10.5	11.5	785	307	79.3	8175	58	57	40	0.98	0.73	2713	6.4
K05-32-G45.1ic					239.4	7663	76	36		0.47	0.32	2688	5.7
K05-32-G46.1ic					120.1	9004	65	80		1.22	0.54	2869	6.3
#K05-32-G47.1oc					142.2	9645	58	19		0.32	0.41	2662	6.3

TABLE 3
(continued)

*Sample No.	Ti(48) ppm	Ti(49) ppm	***T°C Ti (Zrc)	Y ppm	Yb ppm	Hf ppm	$U ppm	$Th ppm	Li ppm	Th/U	U/Yb	^Age (Ma)	^$\delta^{18}O$
CORES													
K05-32-G50.1ic	6.5	6.8	740	669	238.9	8908	53	20	17	0.38	0.22	2681	6.0
K05-32-G50.2oc					146.1	9488	39	13		0.35	0.26	2705	
K05-32-G51.1c					170.3	10065	152	56		0.37	0.89	2714	5.5
K05-32-G53.1ic					125.5	9381	49	29		0.60	0.39	2675	6.6
#K05-32-G56.1oc	4.3	3.9	700	432	173.0	10153	63	29	23	0.46	0.36	2659	
K05-32-G57.3oc	4.6	4.8	710	651	228.8	10589	77	30	13	0.39	0.34	2715	6.1
#K05-32-G57.1ic					173.6	8995	51	22		0.42	0.30	2640	6.1
K05-32-G58.1oc	6.3	6.2	735	568	185.0	9765	111	70	43	0.63	0.60		6.1
#K05-32-G58.3ic	3.2	3.1	675	408	75.3	13251	79	34	41	0.43	1.06		8.8
K05-32-G59.1c	6.0	5.9	730	1501	359.0	8752	154	314	37	2.03	0.43	2679	6.6
K05-32-G61.1c	5.3	5.4	720	577	165.1	9861	52	40	13	0.77	0.31	2671	6.5
K05-32-GX.1c					165.9	10117	104	41		0.39	0.63	2701	
#K05-32-G71.2c					162.3	9355	41	17		0.42	0.25	2728	6.6
K05-32-G73.2c					109.4	9968	83	54		0.64	0.76	2681	6.6
K05-32-G77.2c					175.3	9590	67	47		0.71	0.38	2671	6.5
K05-32-G78.1c					115.9	10292	100	44		0.44	0.87	2691	6.3
#K05-32-G79.1c					217.7	7985	56	36		0.64	0.26	2683	
#K05-32-G80.1c					164.2	9162	67	35		0.52	0.41	2655	
#K05-32-G81.1c					248.4	8745	112	53		0.47	0.45	2710	
****AVERAGE**	**4.8**	**4.9**	**710**	**479**	**159.8**	**9752**	**81**	**54**	**26**	**0.61**	**0.56**	**2713**	**6.1**
RIMS													
K05-32-G2.1ir	3.2	3.3	680	248	89.5	10994	641	60		0.09	7.17	2625	8.7
#K05-32-G3.3ir	7.1	6.8	745	186	62.0	10344	370	29		0.08	5.96	2608	8.9
K05-32-G3.4imr	4.8	4.8	710	209	79.4	10237	493	45		0.09	6.21		8.8
K05-32-G3.5or	3.2	3.6	675	194	70.4	10731	539	43		0.08	7.65	2626	9.2
K05-32-G3.1mor	3.9	3.8	695	188	78.5	11288	557	41	133	0.07	7.09	2611	8.8
K05-32-G3.7or	3.4	3.9	680	169	54.5	10621	355	31	188	0.09	6.52	2632	9.2
K05-32-G4.2ir	3.5	3.5	685	369	144.6	11030	532	55		0.10	3.68	2628	8.7
K05-32-G4.3mr	2.8	2.8	665	364	141.9	10549	524	56		0.11	3.69	2628	8.8
K05-32-G4.4or	4.7	4.9	710	151	28.7	12345	317	40		0.13	11.07	2623	9.0
K05-32-G4.5or	5.0	4.5	715	230	49.9	10683	402	45		0.11	8.06	2623	9.0
K05-32-G4.2mr	2.8	2.9	665	240	89.2	11023	539	50	164	0.09	6.05	2628	8.8
#K05-32-G5.2ir	3.5	3.7	685	120	26.3	11680	705	50		0.07	26.75	2639	9.8

TABLE 3
(continued)

*Sample No.	Ti(48) ppm	Ti(49) ppm	***T°C Ti (Zrc)	Y ppm	Yb ppm	Hf ppm	$U ppm	$Th ppm	Li ppm	Th/U	U/Yb	^Age (Ma)	^$\delta^{18}O$
RIMS													
K05-32-G5.3or	3.4	3.1	680	164	44.0	11091	582	69	169	0.12	13.21	2627	9.0
K05-32-G6.2ir	3.8	3.9	690	118	26.8	11797	539	14		0.03	20.07	2617	10.0
K05-32-G6.3or	3.1	2.9	675	264	96.0	10472	632	58		0.09	6.59	2622	8.8
K05-32-G6.4rtip	1.2	1.1	605	76	23.9	11769	451	4		0.01	18.83	2512	9.6
K05-32-G6.3mr	2.9	3.0	670	287	105.5	9932	533	50	143	0.09	5.05	2622	8.4
K05-32-G6.9ir	4.7	4.7	710	125	39.9	11052	512	35	86	0.07	12.86	2617	10.0
K05-32-G7.2ir	4.9	4.8	715	344	130.4	10490	557	54		0.10	4.27	2616	8.4
K05-32-G7.3or	2.8	2.9	670	229	82.9	10777	539	52		0.10	6.50		
K05-32-G8.2ir	3.2	3.3	680	353	124.7	10322	504	47		0.09	4.05	2627	8.6
K05-32-G8.3or	3.5	3.5	685	310	125.9	10589	555	54		0.10	4.41	2630	8.6
K05-32-G9.2or	4.1	3.9	700	91	20.2	11442	646	24		0.04	31.94	2601	10.0
K05-32-G9.6or	4.3	4.4	700	90	20.8	10962	802	30		0.04	38.57	2601	10.0
K05-32-G10.2or	3.8	3.8	690	78	21.4	11679	900	24	211	0.03	42.00	2594	10.0
K05-32-G13.2r	7.3	7.5	750	180	64.3	11726	651	8	219	0.01	10.12		10.4
K05-32-G15.2r	4.0	4.2	695	124	55.5	12031	1561	31	113	0.02	28.11	2640	10.1
#K05-32-G16.3r					79.9	11450	484	15		0.03	6.05	2615	10.4
K05-32-G22a.1r	2.7	2.9	665	254	105.2	11303	659	61		0.09	6.27		
K05-32-G27.2r	4.2	3.8	700	147	50.0	11617	642	14	194	0.02	12.84	2619	10.0
K05-32-G34.2r	4.2	3.9	700	308	122.3	10809	470	38	152	0.08	3.84	2615	9.3
K05-32-G35.2r	3.0	3.0	675	221	85.2	10240	520	44	229	0.08	6.11	2612	8.7
K05-32-G37.2r	3.9	4.3	695	101	33.0	11315	660	15	173	0.02	20.02	2631	10.1
K05-32-G39.2ir					125.2	10384	487	45		0.09	3.89	2620	9.1
K05-32-G39.3or					125.6	10078	521	45		0.09	4.15	2620	8.6
K05-32-G42.2r	3.6	3.5	685	232	49.5	12287	1427	62	223	0.04	28.82	2630	9.7
K05-32-G43.2r	3.8	3.3	690	81	12.2	15315	1833	25	209	0.01	150.70	2623	9.3
#K05-32-G44.2r					62.3	11140	854	12		0.01	13.71	2644	10.0
K05-32-G46.2r	10.0	9.9	780	191	102.7	11631	1034	14	252	0.01	10.07	2635	10.0
K05-32-G50.2or	3.5	3.7	685	264	97.7	10917	476	41	144	0.09	4.87		8.5
K05-32-G50.3ir					70.3	10671	456	36		0.08	6.49	2619	
K05-32-G53.2r	6.5	6.0	740	166	82.6	12231	730	12	207	0.02	8.83	2620	9.6
K05-32-G55.2r	3.8	3.7	690	75	18.2	11910	519	12	235	0.02	28.58		
K05-32-G57.2r	2.3	2.3	650	107	18.4	11795	641	15	210	0.02	34.85	2659	10.0
K05-32-G58.2r	4.1	4.0	700	211	90.7	11229	806	21	198	0.03	8.89		10.3
K05-32-G59.2r	3.3	3.3	680	94	36.3	11355	604	16	223	0.03	16.64	2606	10.2

TABLE 3
(continued)

*Sample No.	Ti(48) ppm	Ti(49) ppm	***T°C Ti (Zrc)	Y ppm	Yb ppm	Hf ppm	$U ppm	$Th ppm	Li ppm	Th/U	U/Yb	^Age (Ma)	^$\delta^{18}O$
RIMS													
K05-32-G61.2r	3.5	3.7	685	175	40.8	11079	553	70	217	0.13	13.53	2617	9.4
K05-32-G63.2r	5.1	5.0	715	215	83.1	10668	513	43	87	0.08	6.17	2620	9.9
#K05-32-G70.1r					86.4	10402	495	44		0.09	5.73	2630	
K05-32-G71.1r					121.0	10722	454	45		0.10	3.76	2618	8.7
K05-32-G72.1r					16.3	11400	611	19		0.03	37.61	2567	
K05-32-G73.1r					23.0	10981	620	25		0.04	26.93	2583	9.5
K05-32-G75.1rtip					26.3	11421	587	12		0.02	22.33	2526	
K05-32-G76.1r					13.0	11510	680	20		0.03	52.50	2596	
K05-32-G77.1or					25.8	11575	456	44		0.10	17.69	2585	9.0
K05-32-G78.2or					88.2	10256	545	50		0.09	6.17	2633	9.1
K05-32-G79.2r					34.9	11386	894	21		0.02	25.62		
K05-32-G80.2r					21.6	9443	424	16		0.04	19.66		
K05-32-G81.2r					102.0	10710	1161	22		0.02	11.38		
K05-32-G9.1ir	4.0	3.5	695	116	23.8	12841	346	46		0.13	14.53	2628	8.9
K05-32-G9.3mr	3.7	3.8	690	79	17.1	12263	178	25		0.14	10.39	2601	10.2
K05-32-G9.4ir	3.7	3.9	690	424	159.0	11373	652	73		0.11	4.10	2628	8.5
K05-32-G9.5mr	3.8	3.7	690	77	13.3	11479	172	23		0.13	12.87		
K05-32-G10.4ir	4.4	4.2	705	216	79.6	10570	377	30		0.08	4.73	2590	8.5
K05-32-G10.1mr	6.2	6.2	735	388	131.5	9928	576	65	217	0.11	4.38	2590	8.5
K05-32-G10.3mr	3.8	3.6	690	259	97.7	10057	585	52	184	0.09	5.99	2594	10.0
****AVERAGE**	**4.1**	**4.1**	**695**	**200**	**67.5**	**11158**	**614**	**36**	**184**	**0.07**	**15.70**	**2613**	**9.3**
DISTURBED CORES													
K05-32-G3.2ic	4.3	4.2	700	619	261.8	10132	178	120		0.68	0.68	2668	8.5
#K05-32-G3.6oc	5.8	5.5	730	540	221.4	9373	136	83	92	0.61	0.61	2694	6.6
K05-32-G3.5mc					138.8	10502	165	84		0.51	1.19	2644	8.7
K05-32-G3.6oc					206.3	8800	129	76		0.59	0.63	2694	6.6
K05-32-G5.1c	4.0	4.0	695	520	176.8	11459	121	54	6	0.44	0.69	2641	7.4
K05-32-G6.6mc	5.5	5.4	725	780	189.2	9137	350	278		0.80	1.85	2666	7.6
K05-32-G6.5moc	7.2	6.6	750	1045	267.5	9426	427	345		0.81	1.60	2661	8.1
K05-32-G6.1ic	6.5	6.1	740	1502	357.3	8959	438	325	30	0.74	1.23	2645	8.9
K05-32-G6.6oc					247.2	8735	337	239	42	0.71	1.36	2677	6.6
K05-32-G6.7oc					284.7	9589	369	269		0.73	1.30	2666	7.6
K05-32-G63.1c	3.5	3.7	685	645	244.2	10674	99	30	7	0.31	0.41	2671	9.0

TABLE 3
(continued)

*Sample No.	Ti(48) ppm	Ti(49) ppm	***T°C Ti (Zrc)	Y ppm	Yb ppm	Hf ppm	$U ppm	$Th ppm	Li ppm	Th/U	U/Yb	^Age (Ma)	^$\delta^{18}O$
DISTURBED CORES													
K05-32-G31.1ic					418.0	9562	213	117		0.55	0.51	2705	9.1
K05-32-G31.2oc					158.9	11600	155	75		0.48	0.97		
****AVERAGE**	**5.2**	**5.0**		**774**	**235.0**	**9881**	**262**	**160**	**21**	**0.58**	**1.27**	**2668**	**7.9**
GRAIN 16													
K05-32-G16.1ic1	3.1	3.3	675	574	188.6	10812	62	34		0.54	0.33	2678	7.2
K05-32-G16.2oc	3.7	3.6	690	362	123.3	12775	94	36		0.38	0.76	2696	5.3
K05-32-G16.1ic2	7.1	6.8	750	1376	430.1	10591	215	137	64	0.64	0.50	2679	7.6
#K05-32-G16.4moc					54.8	11389	49	9		0.19	0.90	2606	7.4
K05-32-G16.5mc					112.5	10145	38	13		0.36	0.33	2705	5.7
K05-32-G16.6moc					152.1	9844	49	16		0.33	0.33	2746	5.1
K05-32-G16.7mic					233.2	9878	83	45		0.54	0.36	2678	7.4
K05-32-G16.8mic					292.6	9816	110	58		0.53	0.38	2721	6.2
K05-14 RIM													
K05-14-G12r	1.2	1.2	605	172	40.5	12665	585	2	167	<0.01	14.43	2624	8.7
K05-21A RIMS													
K05-21A-1.2mor	2.4	2.4	655	123	28.4	12052	1128	13	195	0.01	39.68	2621	8.0
K05-21A-2.2mor	2.7	2.6	665	193	45.6	12555	768	10	194	0.01	16.84	2631	8.1
K05-21A-3.3ir	3.9	3.8	695	185	79.0	11816	673	13		0.02	8.52	2629	8.5
K05-21A-14.2r	3.2	3.2	675	97	28.2	12018	1009	37	181	0.04	35.73	2625	7.5
K05-21A-21.2r	2.6	2.5	660	73	13.0	10435	579	7	252	0.01	44.71	2625	7.7

These analytical spots overlie inclusions, core-rim boundaries, metamorphic veins (in cores) or are discordant ages, and are not plotted nor used to compute averages.

* Locations of analytical spots within grains denoted by: c=core, r=rim, i=inner, o=outer, m=middle.

** Averages do not include analyses with # (those that overlap inclusions, core-rim boundaries, etc.).

*** Temperature based on Ti concentration in zircon, computed with the calibration of Ferry and Watson (2007), and rounded to nearest 5 °C.

$ The U and Th (and the other trace element) values reported in this table were not analyzed at the same locations of the age analyses, but at locations next to the age analytical spots. Hence the U and Th concentrations reported in this table will not be identical to those from the age analyses reported in table 2.

^ Age and $\delta^{18}O$ values from table 2.

(Watson and Harrison, 2005; Ferry and Watson, 2007; Fu and others, 2008) and on pressure (Ferry and Watson, 2007; Ferriss and others, 2008). Ferriss and others (2008) suggest on the basis of quantum-mechanical calculations that the pressure correction

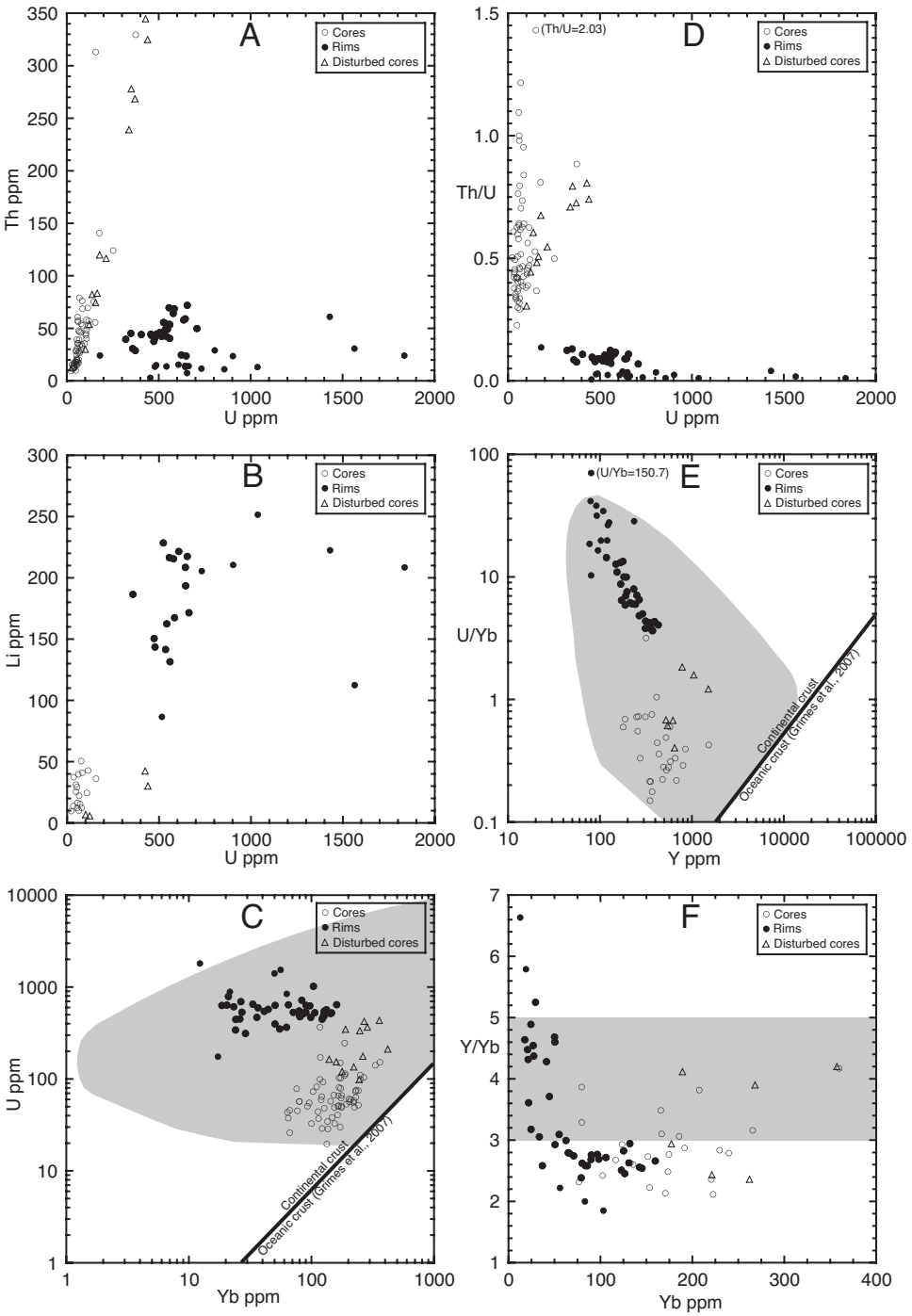

Fig. 12. Comparison of the concentrations (ppm) and concentration (ppm) ratios of selected trace elements in detrital (igneous) cores, disturbed cores, and metamorphic rims in zircons from the granulite grade site 32. (A) Th vs. U. (B) Li vs. U. (C) U vs. Yb. (D) Th/U vs. U. (E) U/Yb vs. Y. (F) Y/Yb vs. Yb. The shaded area in **C** and **E** is from Grimes and others (2007) and represents the field of compositions from >1500 analyses of continental crust zircons (Phanerozoic and Archean) measured at the U.S. Geological Survey–Stanford SHRIMP-RG facility. The solid line in **C** and **E** defines the approximate boundary between the continental crust zircon and oceanic crust zircon fields, also from Grimes and others (2007). The shaded area in **F** defines zircons with Y/Yb ratios from 3 to 5; Y/Yb ratios of 3 to 5 or higher likely reflect overlap of garnet and zircon growth (personal communication, Joe Wooden).

for the Ti (Zrc) geothermometer is double the preliminary estimate (−50 °C/GPa) of Ferry and Watson (2007). The Ti (Zrc) geothermometer is calibrated at pressures (~1.0 GPa: Watson and Harrison, 2005; Ferry and Watson, 2007) similar to those estimated for the amphibolite-granulite transition (0.7-0.8 GPa) and granulite (1.0-1.1 GPa) zones, and somewhat above that for the middle amphibolite facies site 14 (0.6 GPa) in the Kapuskasing (Mäder and others, 1994; Pattison, 2003). Therefore the pressure correction to our results would be minor for the two higher grade sites and relatively small (<40 °C) for the middle amphibolite facies site. An $a(TiO_2) = 0.7$ was assumed for the thermometry calculations, typical for the titanite-bearing, rutile-absent paragneiss rock compositions present at all three sites (Ghent and Stout, 1984). The paragneiss at all three sites contains quartz, so $a(SiO_2)=1.0$.

Only one zircon grain with a metamorphic rim of sufficient width to analyze for trace elements was available in sample K05-14 from the amphibolite facies site 14. Measured Ti concentration in this rim was 1.2 ppm (table 3), yielding a Ti (Zrc) temperature of 605 °C. At the amphibolite-granulite facies transition site 21A, Ti concentrations of five metamorphic rims ranged from 2.4 to 3.9 ppm (table 3), yielding Ti (Zrc) temperatures from 655 to 695 °C (ave. T=670 °C). At site 32, Ti-in-zircon geothermometry yields still higher apparent temperatures ranging from 650 C to 780 °C, averaging 695 °C (table 3). Ti content in the young (2512 Ma) outer tip of grain 6 records a lower apparent temperature of ~600 °C, the coolest and youngest growth phase in the record at site 32. Apparent temperatures from Ti (Zrc) geothermometry of the rims increase with increasing metamorphic grade of the three sites as shown by changes in phase petrology and independent geothermometry, indicating that these thermometry results as a whole reflect actual increases in temperature of zircon growth and metamorphic grade, with depth in this crustal section. The T range recorded by Ti (Zrc) at site 21A, 655 to 695 °C, is reasonable for upper amphibolite facies conditions, and equivalent to the geothermometry results (650-700 °C) of Mäder and others (1994) for the upper amphibolite facies in the Kapuskasing. However the average T (695 °C) recorded by Ti (Zrc) at site 32 is well below the range of T (750-800 °C) recorded in the granulite zone by grt-cpx-plg-hbd-qtz equilibria (Mäder and others, 1994; Pattison, 2003), although several of the highest Ti (Zrc) temperatures (up to 780 °C) overlap these regional geothermometry results.

Resetting of Ti contents of these zircon rims via diffusion is unlikely even at granulite facies conditions (Cherniak and Watson, 2007); therefore we interpret the Ti contents of the metamorphic rims to be primary. The Ti (Zrc) results may be undervaluing temperature at the granulite site because of complications from variable $a(TiO_2)$, uncalibrated activity-composition effects, and/or disequilibrium that may have also complicated earlier applications of the Ti (Zrc) thermometer to igneous zircons (Valley and others, 2006; Fu and others, 2008; Hofmann and others, 2009). For these reasons, we regard the Ti (Zrc) results as minimum estimates of temperature.

DISCUSSION

Nature of Metamorphic Zircon Growth

The mechanism(s) responsible for formation of metamorphic zircon rims may impact the mobility of Pb, O and trace elements in zircon (Harley and Kelly, 2007; Martin and others, 2008), and can affect the choice of boundary conditions for diffusion modeling of the multiple spot oxygen isotope data. Martin and others (2008) distinguish two endmember modes/mechanisms of formation for metamorphic zircon in the Naxos metamorphic complex by combining textural observations with *in situ* ion microprobe analyses of Pb, O and trace elements: 1) Replacement of preexisting zircon by coupled dissolution/reprecipitation; 2) Overgrowth of new zircon on pre-existing zircon grains. Metamorphic zircons formed by replacement would be

characterized by a wide, poorly-polished (porous) transition zone (TZ), often containing U-rich inclusions, between inherited (primary) cores and metamorphic rims, features that are indicative of replacement (Geisler and others; 2007). Martin and others (2008) argue that O and REE can be inherited from the pre-existing zircon and hence these elements exhibit closed system behavior during replacement. However with regard to the zircons exhibiting rim replacement textures (from metabasite) that they studied, they were not able to distinguish any significant difference in $\delta^{18}O$ values between primary zircon cores (6.2±0.8‰), zircon rims (7.8±1.8‰) and host rock garnet (5.8-8.0‰; 6.5‰ ave), given the analytical uncertainty of their ion microprobe analyses. Therefore it is not possible to determine unambiguously from their data whether the zircon replacement rims form in equilibrium with the rock matrix (open system) or inherit oxygen from the magmatic core (closed system). In contrast, zircon rims formed by overgrowth on pre-existing grains are non-porous, generally inclusion-free and in O isotope exchange equilibrium with the rock host. Martin and others (2008) propose that these overgrowths exhibit open system behavior with respect to O and REE (that is, rims grow in equilibrium with the host rock matrix). They find that U-Pb ratios are reset in the cores during both modes of rim formation. The dominant formation mechanisms of the metamorphic rims on the Kapuskasing zircons can be evaluated by combining observations of CL zoning and microstructure with *in situ* ion microprobe analyses of Pb, O and trace elements.

None of the approximately 375 grains imaged in CL and SE at all three sites studied, including the 104 grains analyzed for Pb and O isotope compositions on the ion microprobe, exhibit porous rims or transition zones at core-rim boundaries, nor do these rims contain abundant U-rich inclusions (fig. 3), features attributed to replacement (Geisler and others, 2007). Contacts between cores and rims are sharp, and metamorphic rims commonly exhibit CL banding ~concentric to the core-rim boundary (fig. 4) consistent with outward growth rather than *in situ* replacement. As described earlier, many of the core surfaces preserve features that suggest their mechanical abrasion during stream or wind transport as detrital grains eroded from the Abitibi-Wawa magmatic arc; the morphology of euhedral magmatic zircons with rounded tips and abraded edges, and irregular to curvilinear (conchoidal) boundaries that appear to be fracture surfaces cross-cutting primary oscillatory CL zoning within the core (figs. 2, 3, and 8). The overall width of zircon rims increases significantly with increasing metamorphic grade (fig. 2) with no decrease in the size of the detrital cores as would be expected in an overgrowth scenario.

The oxygen isotope compositions of the metamorphic rims also are consistent with their formation as overgrowths in isotopic equilibrium with their rock hosts. Oxygen isotope fractionation between zircon and garnet should be close to zero permil at granulite facies conditions (Valley and others, 2003) and the metamorphic rims have $\delta^{18}O$ values that are in or closely approach oxygen isotope exchange equilibrium with garnet—and by extension with the paragneiss rock host. This is true at all three metamorphic grades studied, despite differences in the $\delta^{18}O$ values of garnet at these three sites (figs. 5 and 6). Moreover, at site 32, the range in $\delta^{18}O$ of the zircon rims (8.4 to 10.4‰) and the significant difference in $\delta^{18}O$ values (0.7‰) of garnet from leucosome (9.2‰) and the surrounding rock matrix (9.9‰) indicate significant oxygen isotope heterogeneity in the paragneiss. The $\delta^{18}O$ value of garnet from the leucosome (9.2‰) coincides with the mode (the 9.0-9.5‰ interval) of the $\delta^{18}O$ values of the zircon rims, and the $\delta^{18}O$ value of garnet from the matrix (9.9‰) falls in the middle of the higher range (9.4-10.4‰) of $\delta^{18}O$ values of zircon rims (fig. 6C). These correlations suggest that there are two groups of zircon rims that are in oxygen isotope exchange equilibrium with garnet from two isotopically distinct domains within the paragneiss at site 32, leucosome and host rock matrix, respectively.

The oxygen isotope data indicate that the metamorphic rims in these three paragneiss samples from the Kapuskasing formed in communication (open system), and in O isotope exchange equilibrium, with their rock matrix hosts.

The only rims in which significant variation in $\delta^{18}O$ value has been documented are observed at Site 32 where they are zoned concentrically in $\delta^{18}O$ (grains 43, 64, 71, 78, fig. 9, table A1 http://earth.geology.yale.edu/~ajs/SupplementaryData/2011/08BowmanTableA1.xls; grain 6, fig. 11), consistent with observed CL banding and with outward radial/concentric growth. Overall, the metamorphic rims have trace element compositions quite distinct from those of the igneous cores (fig. 12). The O and Pb isotope data, concordant ages and trace element data from the metamorphic rims indicate that the zircon rims did not inherit their O, Pb and trace element characteristics from the igneous cores, regardless of the process by which the rims formed. Rather, the oxygen isotope data argue for formation of the rims in a close approach to oxygen isotope exchange equilibrium specifically—and predict chemical equilibrium generally (for example, open system)—with the paragneiss rock host at all three metamorphic grades, consistent with an overgrowth scenario.

Zircon Metamorphism at Granulite Facies Producing Rare "Disturbed" Cores

In rare cases at the granulite-grade site 32, the CL signal, U-Pb and $\delta^{18}O$ values of detrital cores (grains 3, 6; fig. 11) are modified with respect to normal cores. Anomalously young $^{207}Pb/^{206}Pb$ ages and anomalous enrichments in $^{18}O/^{16}O$ are correlated with disturbance (dimming and blurring) of the CL signal in the core, which provides a means to recognize these isotopically disturbed domains. The shifts in CL intensity, $\delta^{18}O$ and $^{207}Pb/^{206}Pb$ age within these "disturbed" cores are not correlated with proximity to the core-rim boundary (fig. 11) as would be expected if these values were reset by diffusion of Pb and O from the rim. Rather, these correlated shifts in age, $\delta^{18}O$ and CL signal suggest some type of replacement or recrystallization process in these "disturbed" cores, accompanied by Pb and O isotope exchange with the host rock matrix (open system), during or prior to metamorphic rim growth.

The behavior of the trace elements during $^{18}O/^{16}O$ modification of these "disturbed" igneous cores is variable. U and Th contents increase up to five-fold with respect to normal cores (fig. 12) in step with increases in $\delta^{18}O$ (fig. 13). The Th/U ratios, however, remain high even in the highest $\delta^{18}O$ and U-rich areas of these cores, much higher than Th/U ratios in the metamorphic rims. These high Th/U ratios suggest that rather than experiencing additions of Th and U from the paragneiss rock host (characterized by low Th/U), the disturbed zircon cores experienced a concentration of Th and U to a similar degree during their transformation (by removal/dissolution of other components from the zircon core?). Alternatively, they initially had higher Th and U values that perhaps increased their metastability relative to end-member zircon and predisposed them to recrystallization. The REE of the disturbed cores do not appear to have been modified in the domains of oxygen isotope modification; for example, there is no particular correlation of Yb concentration with $\delta^{18}O$ in the disturbed cores of grains 3 and 6 (fig. 13D). Disturbed cores (with one exception) are not enriched in Li with respect to normal cores (fig. 12B), nor is Li content well correlated with $\delta^{18}O$ or $^{207}Pb/^{206}Pb$ age (table 3) although the sample pool is limited (four paired analyses). It appears therefore that most trace elements in zircon (U and Th excepted) exhibit closed-system behavior while O and Pb undergo open-system exchange during formation of these disturbed cores. The lack of Li enrichment accompanying $^{18}O/^{16}O$ enrichment in disturbed cores suggests that these disturbed cores were altered prior to growth of the Li-enriched zircon rims. Such alteration would then have occurred relatively early along the metamorphic heating path before the paragneiss reached sufficient T and $a(ZrO_2)$ conditions necessary for zircon saturation and metamorphic zircon rim growth.

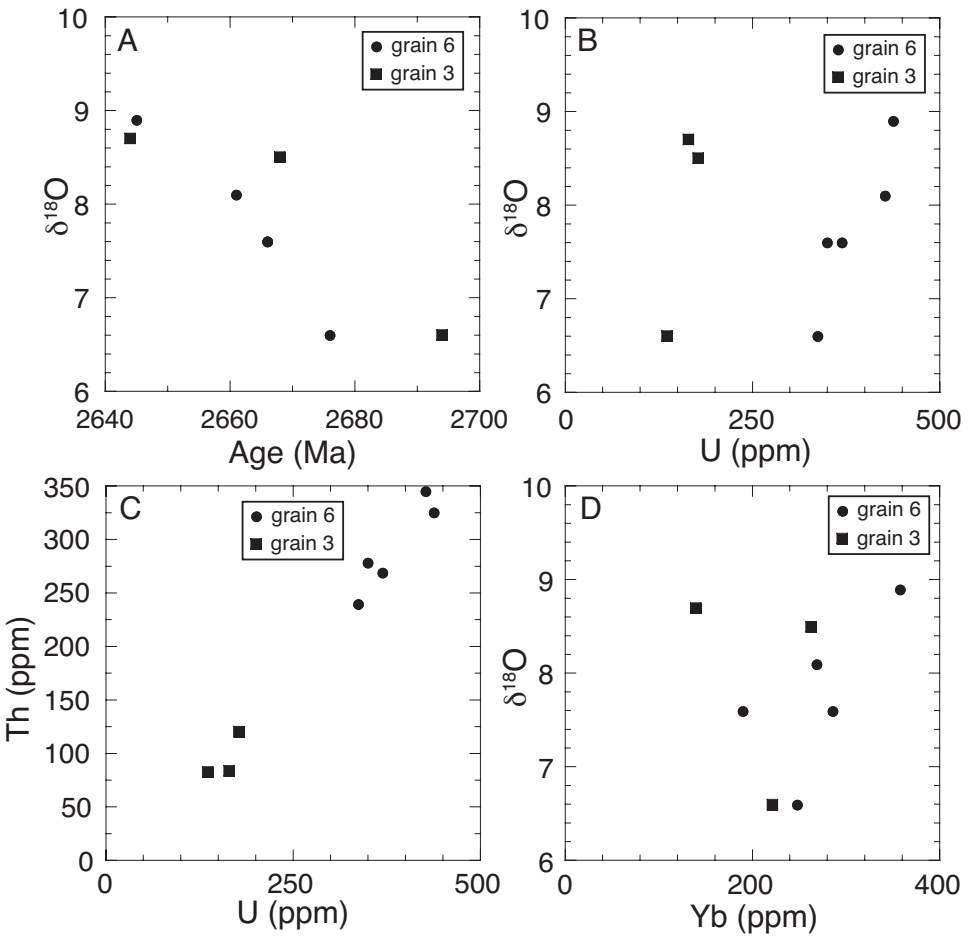

Fig. 13. Relationships among $^{207}Pb/^{206}Pb$ age, $\delta^{18}O$ values and selected trace element compositions from disturbed cores in grains 3 and 6, site 32. (A) $\delta^{18}O$ vs. $^{207}Pb/^{206}Pb$ age. (B) $\delta^{18}O$ vs. U. (C) Th vs U. (D) $\delta^{18}O$ vs. Yb.

Test of Fast ("Wet") vs. Slow ("Dry") Diffusion of Oxygen

The consistently low $\delta^{18}O$ values of the normal cores, the lack of correlation of these core $\delta^{18}O$ values with proximity to the core-rim boundary, and the close approach of oxygen isotope exchange equilibrium between $^{18}O/^{16}O$-enriched rims and host rock (garnet; fig. 6C) establish that the distinct $\delta^{18}O$ values of cores and rims are primary values, which allow for modeling of the volume diffusion history between the two domains. Based on the textural evidence for the formation of these rims as overgrowths, normal core-rim boundaries were immobile features during metamorphism and hence can be treated as fixed discontinuities to simplify diffusion modeling.

Experiments suggest that oxygen has significantly higher diffusivity in zircon under water-saturated (hydrous fluid present) conditions—fast "wet" diffusion—down to $P(H_2O)$ as low as 7 MPa (70 bars) compared to slow "dry" diffusion under water-absent conditions (Watson and Cherniak, 1997). Based on these experimental results, Cherniak and Watson (2003) conclude that fast, "wet" diffusion of oxygen in zircon will occur whenever $f(H_2O)$ exceeds 7 MPa regardless of whether or not a

hydrous fluid is present, provided that $f(H_2O)$ under fluid-absent conditions and $P(H_2O)$ under fluid-present conditions have the same effect on oxygen diffusion. This proviso has yet to be tested, and Peck and others (2003) have suggested that if the carrier species for oxygen within zircon is H_2O, then diffusion of oxygen might be significantly slower under fluid-absent conditions. One possible explanation for the difference between fast and slow diffusion in zircon is that the presence of a hydrous or at least H_2O-bearing fluid phase, rather than the absolute value of $f(H_2O)$, may be necessary to trigger/expedite fast "wet" diffusion of oxygen in zircon. This possibility can be tested using the ion microprobe analyzes of the Kapuskasing zircons, as these zircons are isotopically zoned and have been subjected to prolonged, high-T (granulite grade) metamorphism at significant $f(H_2O)$ but water-undersaturated conditions (that is, in the absence of a hydrous fluid phase).

There is abundant evidence in the Kapuskasing and many other granulite terranes for the presence of substantial values of $f(H_2O)$ (for example, ~1000's of bars) at or near peak metamorphic temperatures, but at water-undersaturated and fluid-absent $[p(H_2O) \leq P_{fl} < P_{lith}]$ conditions (Bohlen and others, 1980; Phillips, 1980; Valley and others, 1983, 1990; Edwards and Essene, 1988; Ghent, 1988; Lamb and Valley, 1988; Moecher and Essene, 1990; Mäder and others, 1994). Texturally-primary matrix biotite and hornblende (paragneiss) and hornblende (mafic gneiss) are present throughout the amphibolite-granulite transition and granulite zones in the Kapuskasing, including at our granulite study site 32. Both minerals, together with leucosome bands (in the granulite zone), define the main foliation. Assuming chemical equilibrium, the compositions of grt-cpx-plg-hbd-qtz assemblages in mafic gneiss from this region of the granulite zone in the Kapuskasing constrain P = 1.0 to 1.1 GPa, T = 750 to 800 °C and $a(H_2O)$ from 0.1 to 0.5 (Percival, 1983; Mäder and others, 1994; Pattison, 2003). The presence of hornblende at these high T and P conditions constrains the $a(H_2O)$ to 0.1 to 0.5 which in turn constrains $f(H_2O)$ to significant values (~1000-5000 bars) in at least the mafic gneisses in the granulite zone (Mäder and others, 1994). Chemical compositions of texturally-primary biotite (unpublished analyses, J. R. Bowman) in the paragneiss at site 32 would indicate a similar or higher range of values of $f(H_2O)$ assuming this biotite was in chemical equilibrium with its associated mineral assemblage (grt-plg-bio-qtz) at 750 to 800 °C, consistent with textural relationships. Further, ubiquitous leucosome bands (originally tonalitic melts) are present within both paragneiss and mafic gneiss at site 32. Thin section observations show that these leucosomes in the paragneiss contain abundant zircons, and rims are clearly visible on some of these grains. The presence of tonalitic melts in the paragneiss (whether generated *in situ* or by injection) at T as low as 750 to 800 °C would require that these melts—and by extension the surrounding gneiss matrix—had substantial $f(H_2O)$, 1000 to 5000 bars (Wyllie, 1977; Ellis and Thompson, 1986; Beard and Lofgren, 1991; Patino Douce and Beard, 1995, 1996). Formation and/or injection of such melts at lower T would require still higher $f(H_2O)$. While it is possible that the zircon rims at Site 32 experienced lower $f(H_2O)$ conditions for a portion of their history, the overall picture at and after the peak metamorphic conditions is one of metamorphism at substantial $f(H_2O)$—well above 7 MPa—under water-undersaturated (fluid-absent) conditions.

Watson and Cherniak (1997) estimate that "wet" diffusion of oxygen in zircon is sufficiently fast that the centers of zircon grains of ≤100 μm radius (typical size of these Kapuskasing zircon cores) will have their initial $\delta^{18}O$ values modified within $\sim 10^5$ yrs at T>700 °C. Diffusion profiles for 1 and 10 Ma resulting from "wet" diffusion at 700 °C are superimposed on the measured $\delta^{18}O$-distance profiles for six grains in figure 14. Even for a geologically short time period of 1 Ma, such rapid "wet" diffusion of oxygen would cause substantial broadening of all of the measured $\delta^{18}O$ discontinuities, and

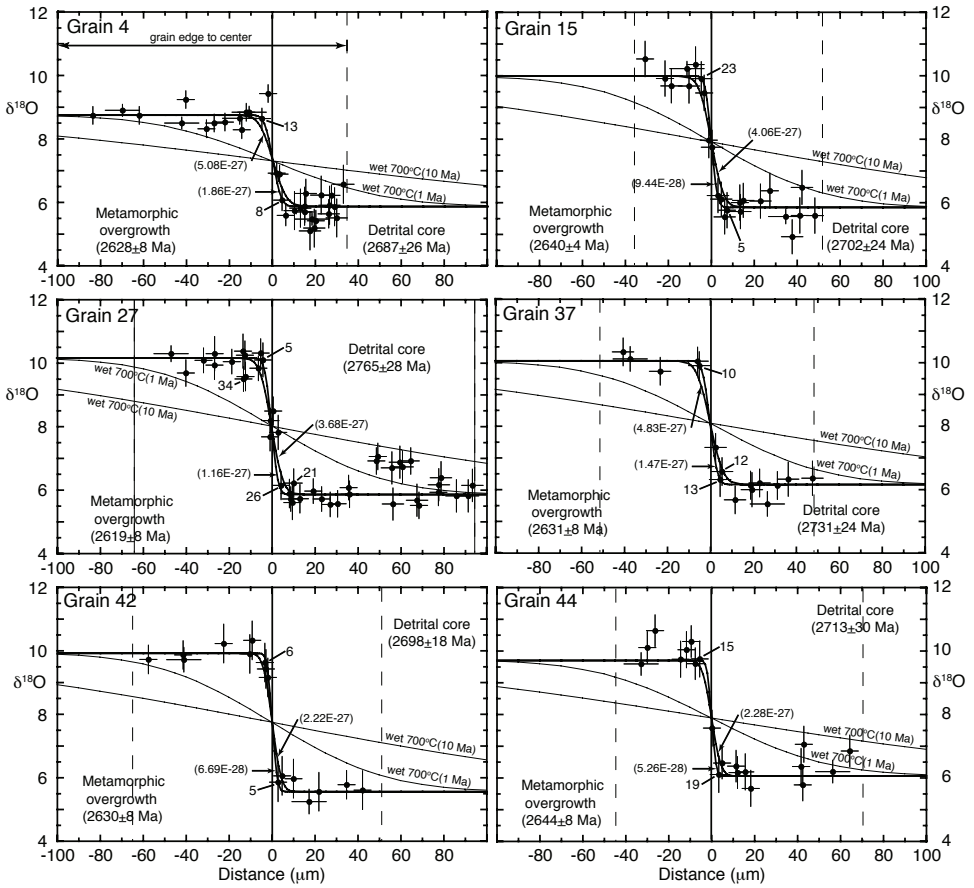

Fig. 14. Calculated diffusion profiles are superimposed on the $\delta^{18}O$-distance profiles for six zircon grains with normal CL cores from the granulite-grade site 32. The vertical solid line in each plot at 0 μm is the core-rim boundary defined in CL. Vertical dashed lines represent the locations of the center of the core (right) and outer edge of the grain (left) except in grain 4 where the plot ends at the outer edge of the grain. Diffusion profiles resulting from "wet" diffusion (Watson and Cherniak, 1997) for 1 and 10 Ma timescales at 700 °C are superimposed (thin lines, labeled) on each profile. Diffusion profiles (thicker black lines) are fitted to key analyses (numbered) near the core-rim boundary in each grain and to their 2 SD analytical errors as discussed in the text and Appendix D. Other numbered analyses (21 and 34 in grain 27; 12 in grain 37) are discussed in Appendix D. The diffusion profiles fitted to the analytical results for these and seven additional grains (table 4) constrain the diffusion coefficient for oxygen in zircon to log D^{Zrc}_{ox} values less than or equal to −27.5 to −26.4 (D in units of m^2/s).

the centers of four of the six zircon cores would lose their initial $\delta^{18}O$ values (including analytical uncertainty). The remaining two cores would lose their initial $\delta^{18}O$ values in well less than 10 Ma (fig. 14). Clearly, these composite zircons have not experienced such fast "wet" diffusion of oxygen for any geologically significant period of time in spite of water fugacities during high T metamorphism (~1000-5000 bars) sufficient for partial melting.

The measured $\delta^{18}O$-distance profiles can provide empirical constraints on the diffusivity of oxygen in zircon (D^{Zrc}_{ox}) for specific temperature (T) ranges if reasonable limits to the timescale and T history of metamorphic zircon rim growth are available. Spatially correlated SHRIMP U-Pb and Ti analyses of 24 metamorphic rims at the granulite site suggest that all but one of these zircon rims have grown at high T

[minimum of 660-780 °C; 695 °C ave.; Ti (Zrc results)] over a timespan of ~80 Ma from 2659 to 2580 Ma (table 2, 3; fig. 5). The common presence of zircons with metamorphic overgrowths within the leucosomes of the paragneiss (thin section observations) confirm the high T origin of these overgrowths, given the reasonable interpretation that the metamorphic overgrowths on these zircons formed in the presence of melt (which provided the source of ZrO_2). These geochronology results, the upper range of Ti (Zrc) temperatures and the presence of leucosome (melt) lenses within the paragneiss are consistent with regional geothermometry and geochronology in this part of the Kapuskasing indicating peak metamorphism in the range 750 to 800 °C with metamorphism starting from 2660 Ma (Krogh, 1993; Mäder and others, 1994; Pattison, 2003). Temperature may not have remained above 750 °C for the entire 80 Ma time period of zircon rim growth. We therefore opt to use 700 °C, essentially the average Ti (Zrc) temperature, as an estimate of the minimum T for the 80 Ma time period of zircon rim growth.

Model results using an 80 Ma timescale are compiled in table 4 for the thirteen grains from the granulite grade site analyzed in detail, and modeling results are superimposed on the $\delta^{18}O$-distance profiles for six of the grains in figure 14. These diffusion profiles are calculated using the one-dimensional (1-D) non-steady state solution for an infinite composite medium with fixed initial discontinuity in $\delta^{18}O$ (eq. 3.45 and 3.46, Crank, 1975). Details of the modeling procedures are presented in Appendix D. Calculated profiles are not "best-fits" to all of the data, but are calculated to fit the $\delta^{18}O$ values of key analyses (see Appendix D for further explanation) near the core-rim boundaries (fig. 14); results are listed for each grain in table 4.

For a timescale of 80 Ma, the measured profiles and the values of the key analyses can be reproduced in all thirteen grains with low values for the diffusivity of oxygen in zircon ($\log D^{Zrc}_{ox}$) ranging from -27.5 to -26.4 m^2/s (table 4; fig. 14). Recent studies of Barrovian terranes suggest that peak T can be driven by synmetamorphic magmatism or advective fluid flow, and may be maintained for only a few million years, a small portion of the 80 Ma growth period of metamorphic zircon rims at the Kapuskasing granulite zone site (Oliver and others, 2000; Baxter and others, 2002; Ague and Baxter, 2007; Lancaster and others, 2008; Lyubetskaya and Ague, 2010). At deeper crustal levels characteristic of the Kapuskasing granulite zone, the physics of heat conduction would argue that peak T could be maintained for longer timescales by synmetamorphic intrusions. If the timescale for modeling were shortened to 10 Ma, the calculated diffusivity values for peak metamorphic T conditions would increase by a factor of 8 (see results for grains 15, 44, 56, 58; table 4). However, regardless of the actual timescale for peak T in the granulite zone of the Kapuskasing, there is good geochronological control at this granulite grade site for 80 Ma of zircon rim growth at high temperature (>660 °C). These empirical results establish slow values for the diffusion coefficient of oxygen in zircon in the T range of 700 to 800 °C for an ~80 Ma timescale of high-grade metamorphism and zircon rim growth.

The key analyses used to constrain these modeled diffusion profiles (for example, #23 and #5 in grain 15; #19 and #15 in grain 44; fig. 14) are located between 4 to 8 μm from the core-rim boundary and have $\delta^{18}O$ values equal to or well within analytical uncertainty (<1 SD) of the initial $\delta^{18}O$ value of core or rim interiors. Therefore the diffusive broadening of the $\delta^{18}O$ discontinuity at the core-rim boundary is less than the scale of the diameter of the analytical spots, 7 μm, and the actual diffusion gradient is likely even steeper than modeled. This possibility is strengthened by the study of Page and others (2007) whose 1μm diameter analytical spots documented that measurable diffusive broadening was restricted to within ≤2 μm of the core-rim boundary in the grain they analyzed. Hence our model results should be regarded as maximum values for the diffusivity of oxygen in zircon ($\log D^{Zrc}_{ox}$) in the T range 700 to 800 °C and for

TABLE 4

Model constraints to the diffusion of oxygen in zircon (D^{Zrc}_{ox}) based on detailed $\delta^{18}O$ profiles measured in thirteen zircon grains from the granulite site 32

Grain #	Core $\delta^{18}O$	Rim $\delta^{18}O$	Time-scale (Ma)	Constraining key analyses[d,e] Core	Rim	D^{Zrc}_{ox}: Fit 1[f]	Log D^{Zrc}_{ox}: Fit 1	Max. D^{Zrc}_{ox}: Fit 2[g]	Log D^{Zrc}_{ox}: Fit 2
4	5.86[a]	8.74[a]	80	8 (6.08, 4.4)	13 (8.65, -5.0)	1.86E-27	-26.73	5.08E-27	-26.29
13	5.71[a]	10.42[a]	80	18 (6.40, 3.7)	13 (10.42, -9.1)	2.43E-27	-26.61	9.58E-27	-26.02
15	5.84[a]	9.98[a]	80	5 (5.77, 7.3)	23* (9.92, -4.8)	9.44E-28	-27.02	4.06E-27	-26.39
	5.84[a]	9.98[a]	10			7.52E-27	-26.12	3.23E-26	-25.49
27	5.85[b]	10.15[a]	80	26 (6.16, 4.0)	5 (10.11, -4.4)	1.16E-27	-26.94	3.68E-27	-26.43
37	6.14[a]	10.04[a]	80	13 (6.33, 4.4)	10 (9.92, -5.3)	1.47E-27	-26.83	4.83E-27	-26.32
42	5.56[a]	9.92[a]	80	5* (5.87, 3.5)	6 (9.64, -3.6)	6.69E-28	-27.18	2.22E-27	-26.65
44	6.06[b]	9.70[c]	80	19* (6.12, 3.2)	15 (9.76, -5.7)	5.26E-28	-27.28	2.28E-27	-26.64
	6.06[b]	9.70[c]	10			4.17E-27	-26.38	1.81E-26	-25.74
46	6.28[b]	10.08[c]	80	12 (6.87, 4.0)	13* (10.08, -5.6)	6.52E-28	-27.19	4.38E-27	-26.36
56	6.09[c]	9.60[c]	80	11* (6.27, 6.9)	13 (9.57, -5.3)	3.59E-27	-26.44	1.47E-26	-25.83
	6.09[c]	9.60[c]	10			2.87E-26	-25.54	1.17E-25	-24.93
58	6.17[b]	10.04[a]	80	17 (6.07, 6.9)	18* (10.16, -4.1)	3.41E-28	-27.47	2.73E-27	-26.56
	6.17[b]	10.04[a]	10			2.73E-27	-26.56	2.18E-26	-25.66
73	6.80[a]	9.11[a]	80	17 (7.19, 4.7)	18* (9.08, -4.1)	6.34E-28	-27.20	6.49E-27	-26.19
77	6.53[a]	9.15[c]	80	6 (6.57, 5.2)	25 (9.15, -4.2)	4.24E-28	-27.37	2.52E-27	-26.60
78	6.60[b]	10.46[c]	80	12 (6.63, 5.7)	14 (10.46, -4.3)	1.05E-27	-26.98	4.83E-27	-26.32

[a] Because the domain (core or rim) is isotopically homogeneous (all analyses in the domain were within analytical uncertainty, 2 SD, with few exceptions), the overall average of the analyses in that domain was used as its initial $\delta^{18}O$ value.

[b] Higher $\delta^{18}O$ analyses in localized areas of the interiors of cores that could represent xenocrysts (see Appendix D and text) are excluded from calculating the initial $\delta^{18}O$ value for the core (for example, in the cores of grains 27, 44, 46, and 58).

[c] If rims or cores (grains 56, 78) are zoned or heterogeneous isotopically, the average of locally homogeneous domains ($\delta^{18}O$ "plateaus") closest to the core-rim boundary within zoned rims was used as the initial $\delta^{18}O$ value [for example, analyses 13 and 14 in the zoned rim of grain 78 (fig. 9, http://earth.geology.yale.edu/~ajs/SupplementaryData/2011/08Bowman TableA1.xls) have the same $\delta^{18}O$ value and define a $\delta^{18}O$ "plateau" of ~10.4‰ within ~15 μm of the core-rim boundary that was used as the initial $\delta^{18}O$ of the rim of grain 78 for the diffusion modeling]. For the rim of grain 44, the average of the four lowest $\delta^{18}O$ values (fig. 9, http://earth.geology.yale.edu/~ajs/SupplementaryData/2011/08Bowman TableA1.xls) was taken as the initial value for the rim, as these four analyses define a similar $\delta^{18}O$ value throughout the rim.

[d] Constraints to the diffusivity of oxygen in these zircon grains are based on model fits to specific key analyses, not statistical "best-fits" to the entire data set. These key analyses are spot analyses that are closest to the core-rim boundary and that still have $\delta^{18}O$ values equal to that of the initial $\delta^{18}O$ value of the rim or core within 1 SD. The key analyses in the core and rim that are used to constrain model fits for each grain are identified by their analysis or spot number (see fig. 14, http://earth.geology.yale.edu/~ajs/SupplementaryData/2011/08Bowman TableA1.xls). The $\delta^{18}O$ value of the key analysis and its distance (in μm) from the core-rim boundary are provided in parentheses. Additional details on modeling constraints for selected grains are included in Appendix D.

[e] If one of the key analyses (core or rim) provides a significantly closer constraint than the other, the more constraining key analysis is labeled with an *.

[f] Fit 1: Diffusivity of oxygen in zircon modeled by matching the $\delta^{18}O$ value(s) of the key spot analyses. If one of the key analyses provides a significantly closer constraint, the value of D^{Zrc}_{ox} reported is that resulting from the more constraining key analysis.

[g] Fit 2: Upper limit to the model diffusivity from matching the 2 SD uncertainty to the $\delta^{18}O$ value(s) of the constraining or key analyses; that is, $\delta^{18}O$ core analysis + 2SD; $\delta^{18}O$ rim analysis − 2SD.

timescales of ~80 Ma. Thus, the lowest (slowest) of our calculated values, $\log D^{Zrc}_{ox} = -27.5\ m^2/s$, is the most restrictive constraint from this study to the diffusivity of oxygen in zircon for the T range 700 to 800 °C. Our calculated values overlap the diffusivity

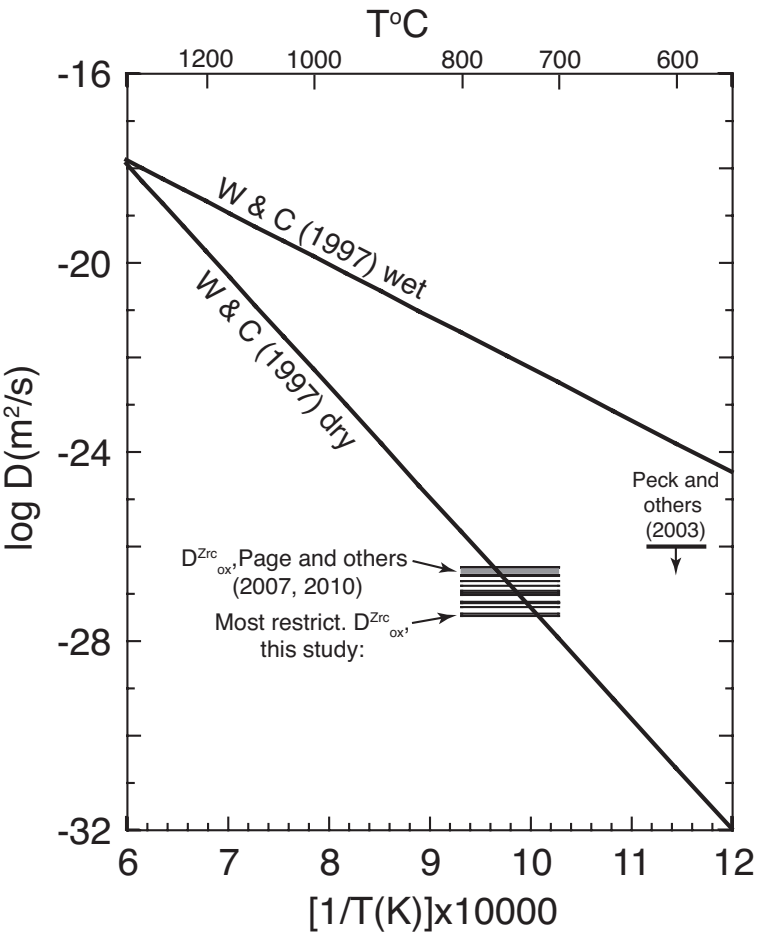

Fig. 15. Comparison of empirically-established limits to the diffusivity of oxygen in zircon (D^{Zrc}_{ox}) from Page and others (2007, 2010) (gray band) and this study (thin black lines) at estimated temperatures of granulite facies metamorphism and zircon rim growth to the experimentally-determined "wet" and "dry" diffusivities from Watson and Cherniak (1997). Estimates of D^{Zrc}_{ox} determined from modeling of the detailed $\delta^{18}O$-distance profiles measured in each of the thirteen zircon grains from this study are plotted as lines for an estimated temperature window of 700–800 °C based on regional geothermometry and Ti (Zrc) analyses. As the constraints on D^{Zrc}_{ox} generated in this study are upper limits, the slowest of our modeled values, log $D_{ox} = -27.5$, should be considered the most restrictive constraint on D^{Zrc}_{ox} for the T range 700–800 °C and for timescales of ~80 Ma (see text for further details). The range of our calculated values for D^{Zrc}_{ox} overlaps the D^{Zrc}_{ox} value determined by Page and others (2007, 2010). Both these empirical estimates overlap experimentally-determined "dry" D_{Zrc} (Watson and Cherniak, 1997) for the T range 700–800 °C, but are much slower than predicted by the "wet" diffusion experiments of Watson and Cherniak (1997). Also shown is the empirical estimate of maximum log $D^{Zrc}_{ox} = -26$ at 600 °C from Peck and others (2003) which is also much slower than that predicted by the "wet" diffusion experiments.

value of $\log D^{Zrc}_{ox} = -26.5 \pm 1$ m^2/sec determined by Page and others (2007, 2010) for oxygen diffusion at an estimated T=700 to 800 °C in a metamorphic zircon grain from a granulite site in the Adirondacks (fig. 15). For the estimated T range of 700 to 800 °C (fig. 15), both these constraints on D^{Zrc}_{ox} are much slower than values predicted by the experimentally-measured "wet" diffusion of oxygen but partly overlap the experimentally-determined dry diffusivity of oxygen in zircon (Watson and Cherniak, 1997). The slowest, most restrictive of our results ($\log D^{Zrc}_{ox} = -27.5$) would be ~one log unit

slower than predicted by the "dry" diffusion experiments (Watson and Cherniak, 1997) if T remained at 750 °C for the 80 Ma time period of rim growth. Alternatively, our most restrictive result would match the experimental, "dry" diffusivity if the time period at 750 °C was 16 Ma.

Regardless of assumptions regarding specific temperature, time and water fugacity, our tests indicate that oxygen diffusion is slow in unrecrystallized zircons (the great majority of zircons) from rocks that have experienced metamorphism (including partial melting) at high pressures and temperatures, and substantial $f(H_2O)$ but water-undersaturated conditions. Even in situations where discrete fractures have propagated through primary zircon there is no evidence of $\delta^{18}O$ gradients due to diffusion. The measured $\delta^{18}O$-distance profiles across the core-rim boundaries in all of the composite zircon grains analyzed in detail constrain maximum values of the diffusivity of oxygen in zircon (D^{Zrc}_{ox}) that are compatible with, or slower than values that would be predicted from the experimentally-determined slow diffusion of oxygen under "dry" conditions (Watson and Cherniak, 1997) during extended, high-grade metamorphism (700-800 °C, 80 Ma). These zircons record no evidence for the more rapid diffusion rates determined experimentally for "wet" oxygen diffusion (Watson and Cherniak, 1997) despite zircon rim growth of extended duration at high T and substantial values of $f(H_2O)$ in the range 1000 to 5000 bars. The H_2O-saturated conditions of the "wet" diffusion experiments (Watson and Cherniak, 1997) contrast with the H_2O-undersaturated conditions that characterize high-grade metamorphism in the Kapuskasing. Our results suggest that $f(H_2O)$ at fluid-absent conditions does not have the same effect on oxygen diffusion in zircon as $P(H_2O)$ at fluid-present conditions. Our results also suggest that the diffusion of oxygen in zircon is considerably slower in the absence of a hydrous fluid phase, even at substantial $f(H_2O)$. Fast diffusion of oxygen in zircon may require the presence of a hydrous fluid phase (water-saturated conditions) to produce molecular species (H_2O and/or OH^-; Zhang and others, 1991; Cherniak and Watson, 2003; Peck and others, 2003) that could transport oxygen more efficiently within zircon, rather than a threshold value of $f(H_2O)$.

T-Time and Fluid Evolution in the Archean Lower Crust Recorded by Zircon Zoning

Our diffusion tests also demonstrate that the O and Pb isotope compositions and trace element concentrations measured in these zircons—both igneous cores and high-grade metamorphic rims—are primary if two pitfalls are avoided by SEM imaging: disturbed (dimmed and blurred CL response) zircon domains and spot analysis of mixed (for example, different generations and composition of zircon) domains. Thus the age, $\delta^{18}O$ and trace element values—and any zoning of these values—within unrecrystallized high-grade zircons are robust micron-scale records of not only the time-T history of zircon growth but also the state of geochemical evolution of the crustal rock host in which the zircon grew. In particular, the $\delta^{18}O$ and trace element values will be sensitive tracers of geochemical evolution, including that resulting from fluid/melt metasomatism in the deep crust. This record is particularly valuable in high-grade rocks, because these events may not be preserved in less refractory minerals, and also valuable in detrital zircon suites that may have experienced prior metamorphic/sedimentary cycles.

The geochemically zoned zircons from the paragneiss at this granulite-grade site in the Kapuskasing (Moser and others, 2008; this study) document a micron-scale record of the early genesis and T-time evolution of Archean lithosphere. Detrital igneous zircon cores with $\delta^{18}O$ values of 5.1 to 7.1 permil record creation of primitive to increasingly evolved crust from 2.85 ± 0.02 Ga to 2.67 ± 0.02 Ga. Sharp geochemical unconformity between these igneous cores and higher $\delta^{18}O$ (8.4-10.4‰) metamorphic overgrowths as old as 2660 Ma dictates a rapid sequence of arc unroofing,

weathering and erosion, burial of detrital zircons in $^{18}O/^{16}O$-enriched (weathered) sediment, transport to lower crust and heating to granulite-grade temperatures late in upper plate assembly. The maximum age for deposition of the Borden Lake conglomerates and associated sediments is 2667 Ma (Krogh, 1993). Therefore heating and transport to the lower crust of the Borden Lake sequence did not begin until after 2667 Ma. Growth of metamorphic zircon rims started soon after as allowed by the age measurement of 2659 Ma (Grain 57, table 3) at temperature exceeding 650 °C as indicated by Ti (Zrc) thermometry. Temperature and pressure increased to at least 750 °C and 1.0 to 1.1 GPa (regional geothermobarometry, Mäder and others, 1994) in <8 Ma, defining a rapid heating rate in the vicinity of ~100 °C/10^6 yrs and rapid transport of this sedimentary/volcanic package to the lower crust at ~0.15 GPa/10^6 yrs in this region. Rapid convective overturn of the supracrustal sequence (for example, Collins and others, 1998), as opposed to tectonic underthrusting, is an attractive mechanism to account for these rates of burial and heating as this time interval occurs in the waning stages of the Kenoran orogeny.

U-Pb geochronology and geothermometry indicate growth of metamorphic zircon rims at both the amphibolite-granulite transition site 21A and the granulite site 32 over an extended ~80 Ma interval from 2660 to 2580 Ma at high temperatures. Tonalite melt pods emplaced in mafic gneiss throughout the granulite zone of the Kapuskasing have been dated at 2630 ± 4 Ma (Krogh, 1993). Anhydrous granulite facies assemblages (orthopyroxene + clinopyroxene) are hydrated (to hornblende) next to these melt pods, showing that the terrain reached granulite facies conditions prior to 2630 Ma. Regardless of the specific timing for the attainment of peak metamorphic T, a large number of zircon rims with minimum Ti (Zrc) temperatures from 670 to 730 °C formed in the paragneiss at site 32 from 2630 to as late as 2580 Ma (table 3). The youngest zircon rim analyzed for Ti (grain 10, 2594 Ma, Ti (Zrc) T = 690 °C; table 3) indicates that the terrain remained hot for over 35 Ma.

Our early results from this investigation are compelling particularly in the case of $\delta^{18}O$ zoning in metamorphic overgrowths and what they reveal about deep crustal fluid evolution. A longstanding paradox in the Kapuskasing Uplift granulites is the source and magnitude of the fluid flux that evidently hydrated peak granulite-facies assemblages, particularly along contacts between syn- to late tectonic tonalitic dikes and boudin in-fills. Puris and Wickham (1994) estimated fluid flux at lithologic contacts in the granulite domain based on m-scale gradients in the whole rock and mineral $\delta^{18}O$ values. The implicit assumption was that fluid flow was the result of high temperatures of prograde metamorphism, and their conclusion was that deep crustal fluid flux was small. Our zircon rim data indicate a more complicated history. Metamorphic rims of broadly equivalent age from the ~10kg paragneiss sample at the granulite site exhibit almost 2 permil variation in $\delta^{18}O$ value. This range (8.4-10.4‰) encompasses the smaller but still significant variation in $\delta^{18}O$ value of garnet from leucosome (9.2‰) and rock matrix (9.9‰) in this sample, suggesting that melt injection is the cause of the $\delta^{18}O$ variability. Presently these leucosomes are narrow and make up a small percentage of the rock volume. If this was the case during metamorphism then it follows that fluid flux must have locally been quite high in order to maintain a 1.5 permil difference in $\delta^{18}O$ composition and avoid buffering of the injected leucosomes by the country rock. More detailed study is under way to resolve the significance of $\delta^{18}O$ heterogeneity in the rims in the context of late stage craton formation processes. The combination of $\delta^{18}O$ values, ages, Ti thermometry and trace element information from metamorphic zircon offers a new approach to resolving longstanding questions relating the timing and source of fluid flow in the petrogenesis of lower crust.

CONCLUSIONS

Coordinated cathodoluminescence (CL) imaging and ion microprobe analyses document micron-scale U-Pb-O isotope and trace element zoning in zircons from amphibolite to granulite facies meta-sediments across a mid to lower crust transition in the Kapuskasing uplift of the Archean Superior province. Most zircons have bright CL (detrital) cores with oscillatory zoning surrounded by darker CL (metamorphic) rims. Despite 80 m.y. of high temperature metamorphism at the lower crustal (granulite) site, igneous (detrital) zircon cores generally retain primary composition, range from 2.85 to 2.67 Ga in age, have $\delta^{18}O$ values of 5.1 to 7.0 permil, and U (20-372 ppm), Yb (66-359), Y (176-1501), Th/U (0.23-2.0) and U/Yb (0.15-3.2) values similar to magmatic arc sources worldwide (Grimes and others, 2007). Metamorphic rims record nearly continuous overgrowth events for ~80 Ma from 2.66 to 2.58 Ga during regional metamorphism that reached granulite facies (≥700 °C). Across this crustal cross-section (and the amphibolite to granulite facies transition), rims form with significantly higher $\delta^{18}O$ values (8.4-0.4‰) in ~exchange equilibrium with the paragneiss rock host. The rims also have significantly higher U (178-1833 ppm) and U/Yb (3.7-150.7) values, and lower Th/U (0.01-0.14), Yb (12-159) and Y (75-424), similar to continental reservoirs (Grimes and others, 2007). We note that Li concentrations in the rims are sometimes two orders of magnitude higher than values in the cores, a first order indication that any Li diffusion between rims and cores has been extremely sluggish as also reported by Ushikubo and others (2008).

The textural characteristics of the dark CL rims, the sharp core-rim boundaries defined in CL, consistent differences in age, $\delta^{18}O$ and trace element compositions between cores and rims, coupled with oxygen isotope zoning within some rims, prove that the dark CL rims are overgrowths rather than replacements of pre-existing detrital (igneous) zircon. Metamorphic rims grew after relatively rapid transport of these arc-derived sediments, possibly by convective overturn, to the lower crust and high temperatures. Metamorphic zircon rims formed in oxygen isotope exchange equilibrium with their paragneiss rock host at all three metamorphic grades sampled; hence during formation of these rims, oxygen exchanged with the paragneiss rock host. However once formed, the zircon rims remained chemically isolated (closed system) and did not exchange oxygen isotopes or trace elements with the rock matrix. The great majority of detrital (igneous) cores also preserve their primary isotopic and trace element signals. Thus both zircon cores and rims remain isolated chemically (that is, closed systems) from the paragneiss rock host during the entire episode of prolonged high-T metamorphism.

A small number of cores (5 of 51 grains analyzed) from the highest temperature (granulite) site have experienced patchy and variable age, $^{18}O/^{16}O$, U-Pb and Th alteration that is spatially correlated with dimming and blurring of the CL signal. Spatial patterns of these changes within these "disturbed" cores are inconsistent with the process of diffusion, and are more likely the result of high temperature recrystallization or replacement. This alteration caused Pb-loss at ~2.64 Ga, elevation of $\delta^{18}O$ values close to those of the host paragneiss, and a five-fold increase in Th and U concentrations. These disturbed cores have partially exchanged oxygen isotopes with the paragneiss rock host (partially open system with respect to O during this replacement/recrystallization), but have largely retained the trace element characteristics of their detrital (igneous) core precursors (behaved as closed systems with respect to trace elements).

Multiple spot traverses reveal steep oxygen isotope discontinuities (4‰ over <10μm) at core-rim boundaries that confirm the extremely sluggish rates of volume diffusion of O in non-metamict zircon during extended (~80 Ma) granulite-grade metamorphism (T>700 °C) at substantial $f(H_2O)$ but water-undersaturated (fluid-

absent) conditions. Application of simple diffusion models to detailed $\delta^{18}O$ profiles measured in 13 grains constrains maximum values of the diffusivity of oxygen in zircon ($\log D^{Zrc}_{ox}$) to the range -27.5 to -26.4 m^2/sec. The slowest of our calculated values is the most restrictive constraint to the diffusivity of oxygen in zircon for the T range 700 to 800 °C. This range of diffusivity is similar to, or somewhat slower than that inferred by Page and others (2007, 2010) and the experimentally-determined "dry" [water-absent] diffusivity of oxygen (Watson and Cherniak, 1997) for the estimated 80 Ma and 700 to 800 °C time-T window of rim formation. The more rapid diffusion rates determined experimentally for "wet" oxygen diffusion (Watson and Cherniak, 1997) are not applicable to the Kapuskasing metamorphic environment in spite of metamorphic water fugacities in the range of 1000 to 5000 bars during high T zircon rim growth, and in the vicinity of deformation microstructures. Our test suggests that the diffusion of O in zircon is considerably slower in the absence of a hydrous fluid phase, even at substantial $f(H_2O)$. Fast diffusion of O in zircon may require the presence of a hydrous fluid. Thus, the "dry" experimental data from Watson and Cherniak (1997) may apply to fluid-absent (water-undersaturated) conditions to substantial values (100-500 MPa) of $f(H_2O)$ and may be generally applicable in many rocks formed in the deep crust.

The diffusion tests presented here indicate that the age, oxygen isotope and trace element zoning preserved in these single crystals of zircon are primary. Hence, this zoning provides a robust microcrystalline record of the T-time-geochemical/fluid conditions of the middle to lower crust during the early genesis and evolution of North American lithosphere. Isotopically and chemically zoned zircons offer a potential new micron-scale record for the T-time-fluid flow history of deep crustal rocks; a record that will not be preserved in less refractory phases.

ACKNOWLEDGEMENTS

National Science Foundation grant EAR-0510280 to Moser and Bowman is gratefully acknowledged, as is a Natural Sciences and Engineering Research Council (NSERC) grant to Moser. The WiscSIMS lab (Wisconsin Secondary Ion Mass Spectrometer Laboratory) was supported by NSF grants EAR-0516725 and EAR-0509639, and the University of Wisconsin Department of Geoscience Weeks Fund during this study. John Fournelle (University of Wisconsin) and Brad Ito (USGS-Stanford Ion Microprobe Facility) provided significant assistance with SEM imaging and Mike Spicuzza (University of Wisconsin) assisted in laser fluorination analysis. We thank Daniele Cherniak, John Percival and Zachary Sharp for thoughtful and constructive reviews.

Appendix A

Sample site descriptions and optical characteristics of the zircon populations

Geology and Petrology of the Sample Sites

Site 14 is a large exposure of garnet-biotite metagraywacke intermixed with metaconglomerates metamorphosed to middle amphibolite facies. Site 21A is located at the amphibolite-granulite facies transition (fig. 1), and consists of garnet-biotite paragneiss in contact with mafic (garnet-hornblende) gneiss. Site 32 consists of a well-exposed outcrop of homogeneous garnet-biotite-hornblende paragneiss in contact with mafic gneiss within the granulite zone, located near the eastern termination of the Borden Lake Belt (fig. 1). The paragneiss at site 32 contains ~2 to 5 percent by volume of cm-thick, discontinuous garnet-quartz plagioclase biotite leucosome. The paragneiss units sampled (~15 kg) at these three sites within the belt all occur in a ~1 km wide zone of the southern limb of the synform along strike over a distance of 25 km.

Optical Characteristics of the Zircon Populations

Paragneiss samples (~15 Kg) at all three sites yielded a large number of high quality, non paramagnetic zircon grains. Zircons from the lower grade site 14 are primarily small, light pink, rounded to elongate

grains. In CL, these grains have rounded edges that often cut across primary CL zoning (see below), consistent with a detrital origin. A few grains are larger and have narrow brown zircon overgrowths. The majority of zircons from the amphibolite/granulite transition site 21A also consist of small pink detrital grains but there are a greater number of large brown prisms with pink/colorless cores. Zircons from the granulite grade site 32 consist of small, light pink, rounded to elongate detrital grains and numerous large, transparent brown prisms often containing pink to colorless cores. Detrital grains are rounded at Site 14 as are the surfaces between cores and metamorphic overgrowths at the two higher grade sites; therefore some component of rounding of the cores is presumed to be due to mechanical erosion prior to metamorphism.

Appendix B

analytical methods

Laser Fluorination for Oxygen Isotope Analysis

Garnet separates for oxygen isotope analysis were prepared with standard magnetic and heavy liquid separation techniques, and then purified to >99 percent by hand-picking. Garnet separates were analyzed with the laser-aided fluorination system (Valley and others, 1995) at the University of Wisconsin. Analytical precision is evaluated through replicate analysis of UWG-2, an internal lab garnet standard ($\delta^{18}O = 5.80‰$, Valley and others, 1995) and is ±0.05 permil. Results are reported in standard delta notation relative to VSMOW.

Ion Microprobe Methods

U-Pb age and trace element analysis.—U-Pb isotopic age dating and trace element analysis were conducted on the SHRIMP-RG (reverse geometry) ion microprobe co-operated by U.S. Geological Survey and Stanford University in the SUMAC facility at Stanford University. Mounted zircon grains were washed with a saturated EDTA solution or a 1N HCl solution and thoroughly rinsed in distilled water to minimize Pb contamination, then dried in a vacuum oven and coated with Au. For U-Pb age analyses, secondary ions were generated from an ~20 μm diameter, ~1 μm deep target spot with an O_2^- primary ion beam varying from 4–6 nA. The basic acquisition routine began with $^{90}Zr_2{}^{16}O^+$ as a high mass normalizing species, followed by $^{204}Pb^+$, a background measured at 0.050 mass units above $^{204}Pb^+$, then $^{206}Pb^+$, $^{207}Pb^+$, $^{208}Pb^+$, $^{238}U^+$, $^{232}Th^{16}O^+$ and $^{238}U^{16}O^+$ and $^{232}Th^+$. In addition, 9 or 10 REE, Y and Hf were measured briefly (typically 1 sec/mass) immediately following the geochronology peaks. The analytical routine also included ^{30}Si, ^{48}Ti, ^{49}Ti, and ^{56}Fe to provide data for calculating Ti in zircon temperatures. Peak centering both on ubiquitous species and on guide peaks adjacent to low-abundance or interference-prone species was used to eliminate any potential effects of magnet drift or peak wandering. Analysis times were ~12 minutes, involving 4 to 5 scan cycles through the mass sequence. Measurements were made at mass resolutions of $M/\Delta M = 7500–8500$ (10% peak height), which eliminates all interfering molecular species, particularly for the REE. Concentration data for U, Th and all measured trace elements were standardized against well-characterized, homogeneous zircon standards MAD-green (4196 ppm U) or CZ3 (550 ppm U) (Mazdab and Wooden, 2006). Age data were standardized against VP10 (1200 Ma, monzonite, southern California; A. P. Barth and J. L. Wooden, unpublished), which was analyzed repeatedly throughout the duration of the analytical session. Data reduction for geochronology follows the methods described by Williams (1997), and Ireland and Williams (2003), and uses the MS Excel add-in Squid and Isoplot programs of Ken Ludwig (Ludwig, 2001, 2003). The SHRIMP-RG spot locations were then documented with SEM imaging.

After U-Pb age analysis and SEM imaging, samples were re-coated with gold and measurements of the abundances of a suite of trace elements [Li (except in the 2006 session), F, Al, S, P, Ca, Sc, Ti, Fe, Y, Nb, Zr, La, Ce, Pr, Nd, Sm, Eu, Ho, Gd, Tb, Dy, Er, Tm, Yb, Lu, Hf, Th and U] were made adjacent to U-Pb spots. Operating and analytical conditions for trace element analyses are described in detail in Mazdab and Wooden (2006) and Mazdab (2009). Secondary ions were generated from a ~15 μm diameter, ~1 μm deep target spot with a 1.5 nA O_2^- primary ion beam directed through a 50 μm Kohler aperture. Analysis times were ~15 minutes, involving two scan cycles through the mass sequence. Measurements were made at mass resolution ($M/\Delta M$) of ~11000 (10% peak height). To determine trace element concentrations, average count rates of each element of interest were ratioed to the high mass normalizing species ($^{90}Zr_2{}^{16}O^+$, $^{30}Si^+$) to account for any primary current drift, and the derived ratios for the unknowns were compared to an average of those for the standards to determine concentrations. Concentration data for all measured trace elements were standardized against well-characterized, homogeneous zircon standards MAD-green or CZ3 (Mazdab and Wooden, 2006). Spot to spot precisions (as measured on the standards) vary according to elemental ionization efficiency and concentration. For the MAD-green zircon, precisions generally range from about ±3% for Hf, ±5% for the HREE, ±10% for Ti, ±10–15% for P, Sc, Y and the MREE, and up to ±40% for La (all values at 2 SD).

Oxygen isotope analysis.—After polishing to remove the SHRIMP U-Pb and trace element pits (~1 μm deep), oxygen isotope analysis was then performed with the CAMECA ims-1280 ion microprobe at the

WiscSIMS facility at University of Wisconsin–Madison. WiscSIMS spots were placed in the same geographic location/CL domain as the pre-existing U-Pb spots using both 15 micron and 7 micron spot diameters. All measurement uncertainties are 2 SD unless otherwise stated. Operating and analytical conditions for the University of Wisconsin CAMECA ims-1280 used in the oxygen isotope analysis of zircons in this study are described in detail by Kita and others (2009) and Page and others (2007). The Cs^+ primary ion beam (20 keV total acceleration voltage) was focused to a diameter of 15 and 7 μm on the sample surface with the primary ion intensities of ~2 nA and ~1nA, respectively. Two Faraday cup (FC) detectors were used to simultaneously measure ^{16}O and ^{18}O at the secondary ion intensity for ^{16}O of $\sim 2\times10^9$ cps and $\sim 1 \times 10^9$ cps for 15μm and 7μm spots, respectively. The analytical time per spot was about 4 minutes. Data were corrected for the instrumental bias (instrumental mass fractionation, IMF) using the UW KIM-5 zircon standard (5.09‰, VSMOW, Valley, 2003) that was cast and polished in the center of sample mounts within 5 mm of all analyzed grains. Standards were measured four times every 10 to 20 sample analyses. The instrumental bias correction is based on the average of the standard analyses (normally N=8) bracketing each group of the sample analyses. A total of 1,103 spot analyses including standards were made in two separate analytical sessions, which are reported in table A1 http://earth.geology.yale.edu/~ajs/SupplementaryData/2011/08BowmanTableA1.xls. The external errors of the sets of 8 bracketing standard analyses (2 SD on separate spots) are assigned as uncertainty of individual data (table A1 http://earth.geology.yale.edu/~ajs/SupplementaryData/2011/08BowmanTableA1.xls), averaging 0.34 permil for 15μm and 0.49 permil for 7μm spot analyses, respectively, which represent the spot to spot reproducibility or precision. Oxygen isotope ratios are normalized relative to VSMOW and reported in standard $\delta^{18}O$ notation.

Appendix C

trace element compositions of zircons

The trace element composition of the igneous cores is quite distinct from that of the metamorphic rims (fig. 12, table 3, table A2 http://earth.geology.yale.edu/~ajs/SupplementaryData/2011/09BowmanTableA2.xls). Igneous cores have lower U (20-372 ppm; 81 ave.), Th (10-330 ppm; 54 ave.) and Li contents (10-51 pm; 26 ave.); U and Th contents are in the lower part of the range for typical Phanerozoic and Archean magmatic values (Grimes and others, 2007, 2009; unpublished SUMAC SHRIMP-RG data library). Li contents are much higher than typical of Phanerozoic oceanic crustal zircons that are generally <1 ppm but are in line with those of zircons from continental sources and Archean rocks (Ushikubo and others, 2008; Bouvier and others, 2009; Grimes and others, 2011; unpublished SUMAC SHRIMP-RG data library). Cores have Th/U ratios from 0.23 to 2.0 (0.61 ave.), U/Yb ratios from 0.15 to 3.2 (0.56 ave.), and Y and Yb contents of 176–1501 ppm (479 ave.) and 66–359 (160 ave.) ppm, respectively (figs. 12C, 12D, and 12E), similar to values for magmatic arc sources (Grimes and others, 2007, 2009).

Compared to the cores, metamorphic rims (fig. 12) have significantly higher U (178-1833 ppm; 614 ave.) and Li (86-252 ppm; 184 ave.) contents, have somewhat lower Th contents (8-73 ppm, 36 ave.), and consequently have significantly lower Th/U ratios (0.01-0.14; 0.07 ave.) that are typically characteristic of metamorphic zircons (for example, Hoskin and Black, 2000; Rubatto, 2002; Hoskin and Schaltegger, 2003). The Ce contents of rims are only somewhat lower than those in cores (table A2 http://earth.geology.yale.edu/~ajs/SupplementaryData/2011/09BowmanTableA2.xls) whereas the zircon rims have significantly higher U/Yb ratios (3.7-150.7; 15.5 ave.), lower Y (75-424 ppm; 200 ave.) and lower Yb (12-159 ppm; 68 ave.) values than the cores (fig. 12). Metamorphic rims define trends of increasing U/Yb with decreasing Y and increasing Y/Yb with decreasing Yb (figs. 12E and 12F). These trends suggest that some garnet grew contemporaneously with the growth of the zircon rims, preferentially taking up Yb relative to Y (Bea and Montero, 1999; Schaltegger and others, 1999; Rubatto, 2002; Rubatto and Herman, 2007). Despite the low Yb values of the rims, however, rims do not have high Y/Yb ratios (≥5) also thought to be diagnostic of coeval garnet and zircon growth (Rubatto, 2002; Rubatto and Herman, 2007); less than half of the rims have Y/Yb ratios > 4 with only a few having Y/Yb ratios > 5.

The trace element compositions of the disturbed cores are similar to, to somewhat higher than those of normal detrital cores (for example, Th, U, Yb, Y, Y/Yb, U/Yb and U/Ce; fig. 12, table 3, table A2 http://earth.geology.yale.edu/~ajs/SupplementaryData/2011/09BowmanTableA2.xls). Y/Yb ratios of both types of cores overlap those of rims, but the Y/Yb ratios of rims extend to higher values. U/Ce ratios in both types of cores are much lower than U/Ce ratios in rims (table A2 http://earth.geology.yale.edu/~ajs/SupplementaryData/2011/09BowmanTableA2.xls). Disturbed cores tend to have higher U contents than, but similar Th/U ratios to normal cores (fig. 12D), which indicates that disturbed cores tend to be enriched in both U and Th by up to five-fold compared to normal cores (figs. 12A and 12D). Other trace element differences between disturbed and normal cores are the result largely of the enrichment in U. For example, compositions of disturbed cores only partly overlap the fields for normal cores in U vs. Yb and U/Yb vs. Y

plots (figs. 12C and 12E), yet Y and Yb contents in disturbed cores are within the upper range of measured Y and Yb concentrations in normal cores.

Appendix D

diffusion profile modeling

The diffusion profiles are calculated using the one-dimensional (1-D) non-steady state solution for an infinite composite medium with fixed initial discontinuity in $\delta^{18}O$ (eq. 3.45 and 3.46, Crank, 1975). Because the ion microprobe data restrict any diffusive broadening too close to the core-rim boundary, model comparisons to measured $\delta^{18}O$ values are done for a narrow zone at the core-rim boundary that is small in comparison to the sizes of these zircon grains (fig. 14). In this situation, 1-D diffusive transport and the use of boundary conditions of fixed initial $\delta^{18}O$ values at the center and outer edge of the grain are good approximations.

The calculated diffusion profiles are not "best-fits" to all of the data. Instead, model profiles are fitted to the "key" analyses that are located closest to the core-rim boundary, and which still have $\delta^{18}O$ values equal to or within 1 SD analytical uncertainty of the initial core or rim $\delta^{18}O$ values. These key analyses (numbered in each plot of fig. 14 and listed for each grain in table 4) constrain the locations closest to the core-rim boundary that have $\delta^{18}O$ values unaffected (or minimally affected) by diffusion, and therefore place upper limits on the diffusion coefficient. In six of the 13 grains evaluated, the modeling can simultaneously reproduce the $\delta^{18}O$ values of the key analysis in both core and rim (table 4); that is, the same model value for the diffusivity of oxygen in zircon (D^{Zrc}_{ox}) can reproduce the $\delta^{18}O$ value of the key analysis in both core and rim. In the other seven grains, one of the key analyses provides a somewhat closer constraint than the other. Alternative approaches, such as statistical "best fits" to all of the analyses defining the $\delta^{18}O$-distance profiles in these zircon grains, are possible. Such approaches can yield somewhat higher limits to D^{Zrc}_{ox} because analyses farther from the core-rim boundary than the key analyses, and which may have $\delta^{18}O$ values substantially lower or higher than those of the key analyses (depending on whether these are in the rim or core), will influence the solution (for example, analyses 21 and 34 in grain 27; fig. 14). The statistical best-fit approach therefore ignores to some degree the critical constraints for the absence of diffusion that the key analyses provide. A "best-fit" to the entire profile for grain 27 can be reasonably approximated by calculating a solution that passes midway between the $\delta^{18}O$-distance values of spots 5 and 34 (fig. 14). The resulting solution increases the limit to D^{Zrc}_{ox} from grain 27 by 0.8 log unit.

Modest to minor differences in the values of D^{Zrc}_{ox} generated by the modeling will result from: 1) alternate choices of key analyses for constraints; or 2) use of the closest analyses in both core and rim simultaneously—and "splitting the difference" in duplicating their $\delta^{18}O$-distance values—in cases where one of these analyses is closer to the core-rim boundary (or has a $\delta^{18}O$ value closer to the initial $\delta^{18}O$ chosen for that domain) than the other. For example, a model solution for grain 37 that matches spot 12 instead of spot 13 in the core (fig. 14) would increase the value of the D^{Zrc}_{ox} defined by the modeling from 1.47E-27 (table 4) to 3.77E-27 m^2/sec. A model solution for grain 42 that matches spot 5 in the core almost reproduces the $\delta^{18}O$ value of spot 6 in the rim (fig. 14). A model fit to spot 6 alone increases the value of D^{Zrc}_{ox} from 6.69E-28 to 1.32E-27 m^2/sec. A model fit that splits the difference or mismatch between spots 5 and 6 yields a value between, 9.96E-28 m^2/sec.

Different choices for the initial $\delta^{18}O$ values of the core and rim will also produce modest to negligible differences in the value of D^{Zrc}_{ox} generated by the modeling. Detailed ion microprobe analyzes within core and rim interiors define large areas of homogeneous $\delta^{18}O$, allowing good definition of the initial $\delta^{18}O$ values of cores and rims. Results from analytical spots, identified in post-analysis inspection via SEM, that fall on inclusions, metamorphic micro-veins (within cores), or that overlap cracks and have low ^{16}O yields, are not plotted in the $\delta^{18}O$-distance profiles (figs. 9 and 14). Neither these mixed analyses nor analyses that overlap core-rim boundaries (and physically mix two isotopic domains) are used in calculating the initial $\delta^{18}O$ values of the cores and rims for modeling. The initial $\delta^{18}O$ values of both cores and rims can be well-defined by one or more of the following methods.

Method A. If all analyses (with no more than one to three exceptions, depending on the total number of analyses in the domain) in a domain are within analytical uncertainty (2 SD), that is, the domain is isotopically homogeneous, the overall average of these analyses was used as the initial $\delta^{18}O$ value of that domain (for example, both core and rim of grain 42, fig. 14).

Method B. If there are localized areas of higher $\delta^{18}O$ in the interiors of cores that could represent xenocrysts, these higher $\delta^{18}O$ analyses were excluded from calculating the initial $\delta^{18}O$ value for the core nearer the boundary with the rim (for example, the cores of grains 27 and 44).

Method C. If rims are zoned or heterogeneous isotopically, the average of locally homogeneous domains ($\delta^{18}O$ "plateaus") closest to the core-rim boundary within these zoned rims was used as

the initial $\delta^{18}O$ value (for example, analyses 13 and 14 in the zoned rim of grain 78 (fig. 9, table A1 http://earth.geology.yale.edu/~ajs/SupplementaryData/2011/08BowmanTableA1.xls) define a $\delta^{18}O$ "plateau" of ~10.4‰ within ~15 mm of the core-rim boundary).

Because the core and rim domains in these grains have been analyzed in some detail, the differences between logical choices for initial values for core and rim are small, and the impact of these changes on the calculated $D^{Zrc}{}_{ox}$ are modest to small. For example in grain 27, use of the overall average for both core and rim (6.07 and 10.04‰, respectively), instead of the values (5.85, 10.15‰) resulting from factoring out $\delta^{18}O$ outliers (the high $\delta^{18}O$ xenocryst domain in the core and the two analyses in the rim that differ by >2 SD from the average), results in an increase in the calculated value of $D^{Zrc}{}_{ox}$ from 1.16×10^{-27} to 2.65×10^{-27} m^2/sec. If the $\delta^{18}O$ value for the core of grain 15 is adjusted down from the overall average of 5.84‰ to 5.56‰ by removal of the two analyses (spots 9 and 13, table A1 http://earth.geology.yale.edu/~ajs/SupplementaryData/2011/08BowmanTableA1.xls) in the core interior with significantly (>2 SD difference from the average) higher $\delta^{18}O$ values, the calculated value of $D^{Zrc}{}_{ox}$ would decrease from 9.44×10^{-28} to 8.06×10^{-28} m^2/sec.

Given the extensive textural, isotopic and trace element evidence for the origin of the zircon rims as metamorphic overgrowths rather than replacement of preexisting zircon, we conclude that it is reasonable to treat the core-rim boundaries defined in CL as fixed discontinuities for modeling. Therefore we have not applied mathematically more complex moving-boundary solutions to our measured zircon profiles. Bickle and Baker (1990) used both fixed- and moving-boundary solutions to model measured $\delta^{18}O$ gradients at marble-schist boundaries in the Naxos metamorphic complex. At least in that application, both approaches yielded equivalent results.

Modest (<0.5 to 1.0 log unit) differences in the values of $D^{Zrc}{}_{ox}$ may arise from different modeling approaches ("best-fits" to all of the analyses vs. use of "key" analyses), different choices for initial $\delta^{18}O$ values for core and rim, and from the use of different key analyses for model constraints. However all such approaches yield values of $D^{Zrc}{}_{ox}$ that are much slower than values predicted by the experimentally-measured "wet" diffusion of oxygen in zircon (Watson and Cherniak, 1997) (fig. 15).

References

Ague, J. J., and Baxter, E. F., 2007, Brief thermal pulses during mountain building recorded by Sr diffusion in apatite and multi-component diffusion in garnet: Earth and Planetary Science Letters, v. 261, n. 3–4, p. 500–516, http://dx.doi.org/10.1016/j.epsl.2007.07.017

Baxter, E. F., Ague, J. J., and DePaolo, D. J., 2002, Prograde temperature-time evolution in the Barrovian type-locality constrained by Sm/Nd garnet ages from Glen Clova, Scotland: Journal of the Geological Society, London, v. 159, n. 1, p. 71–82, http://dx.doi.org/10.1144/0016-76901013

Bea, F., and Montero, P., 1999, Behavior of accessory phases and redistribution of Zr, REE, Y, Th, and U during metamorphism and partial melting of metapelites in the lower crust: an example from the Kinzigite Formation of Ivrea-Verbano, NW Italy: Geochimica et Cosmochimica Acta, v. 63, n. 7–8, p. 1133–1153, http://dx.doi.org/10.1016/S0016-7037(98)00292-0

Beard, J. S., and Lofgren, G. E., 1991, Dehydration melting and water-saturated melting of basaltic and andesitic greenstones and amphibolites at 1, 3, and 6–9 kb: Journal of Petrology, v. 32, p. 365–401, http://dx.doi.org/10.1093/petrology/32.2.365

Benn, K., and Kamber, B. S., 2009, In situ U/Pb granulite-hosted zircon dates, Kapuskasing structural zone, Ontario: A Late Archean large igneous province (LIP) as a substrate for juvenile crust: Journal of Geology, v. 117, n. 5, p. 519–541, http://www.jstor.org/stable/10.1086/600864

Bickle, M. J., and Baker, J., 1990, Advective-diffusive transport of isotopic fronts—an example from Naxos, Greece: Earth and Planetary Science Letters, v. 97, n. 1–2, p. 78–93, http://dx.doi.org/10.1016/0012-821X(90)90100-C

Bohlen, S. R., Peacor, D. R., and Essene, E. J., 1980, Crystal chemistry of a metamorphic biotite and its significnce in water barometry: American Mineralogist, v. 65, p. 55–62.

Bouvier, A., Ushikubo, T., Kita, N., Cavosie, A. J., Kozdon, R., and Valley, J. W., 2009, Li isotopes in Archean zircons: EOS, Transactions, American Geophysical Union, v. 90, n. 52, p. V14B–07.

Bursnall, J. T., Leclair, A. L., Moser, D. E., and Percival, J. A., 1994, Structural correlation within the Kapuskasing uplift: Canadian Journal of Earth Sciences, v. 31, p. 1096–1103, http://dx.doi.org/10.1139/e94-097

Calvert, A. J., Sawyer, E. W., Davis, W. J., and Ludden, J. N., 1995, Archaean subduction inferred from seismic images of a mantle suture in the Superior Province: Nature (London), v. 375, n. 6533, p. 670–674, http://dx.doi.org/10.1038/375670a0

Cavosie, A. J., Valley, J. W., Wilde, S. A., and EIMF, 2006, Correlated microanalysis of zircon: Trace element, $\delta^{18}O$, and U-Th-Pb isotopic constraints on the igneous origin of complex >3900 Ma detrital grains: Geochimica et Cosmochimica Acta, v. 70, n. 22, p. 5601–5616, http://dx.doi.org/10.1016/j.gca.2006.08.011

Cavosie, A. J., Valley, J. W., and Wilde, S. A., 2007, The oldest terrestrial mineral record: A review of 4400 to 4000 Ma detrital zircons from the Jack Hills, Western Australia: Developments in Precambrian Geology, v. 15, p. 91–111, http://dx.doi.org/10.1016/S0166-2635%2807%2915025-8

Cherniak, D. J., and Watson, E. B., 2003, Diffusion in zircon, *in* Hanchar, J. M., and Hoskin, P. W. O., editors, Zircon: Reviews in Mineralogy and Geochemistry, v. 53, p. 113–144, http://dx.doi.org/10.2113/0530113

——— 2007, Ti diffusion in zircon: Chemical Geology, v. 242, n. 3–4, p. 470–483, http://dx.doi.org/10.1016/j.chemgeo.2007.05.005

Chiarenzelli, J. R., and McLelland, J. M., 1993, Granulite facies metamorphism, palaeo-isotherms and disturbance of the U-Pb systematics of zircon in anorogenic plutonic rocks from the Adirondack Highlands: Journal of Metamorphic Geology, v. 11, n. 1, p. 59–70, http://dx.doi.org/10.1111/j.1525-1314.1993.tb00131.x

Collins, W. J., Van Kranendonk, M. J., and Teyssier, C., 1998, Partial convective overturn of Archaean crust in the east Pilbara Craton, Western Australia: driving mechanisms and tectonic implications: Journal of Structural Geology, v. 20, n. 9/10, p. 1405–1424, http://dx.doi.org/10.1016/S0191-8141(98)00073-X

Corfu, F., and Davis, D. W., 1992, A U-Pb geochronology framework for the western Superior Province, *in* Thurston, P. C., Sutcliffe, R. H., Stott, G. N., and Williams, H. R., editors, The Geology of Ontario: Ontario Geological Survey Special Volume 4, pt. 2, p. 1335–1346.

Crank, J., 1975, The mathematics of diffusion (2nd edition): London, Oxford University Press, 414 p.

Crowe, D. E., Valley, J. W., and Baker, K. L., 1990, Micro-analysis of sulfur-isotope ratios and zonation by laser microprobe: Geochimica et Cosmochimica Acta, v. 54, n. 7, p. 2075–2092, http://dx.doi.org/10.1016/0016-7037(90)90272-M

Davis, D. W., 2002, U-Pb geochronology of Archean metasedimentary rocks in the Pontiac and Abitibi subprovinces, Quebec, constraints on timing, provenance and regional tectonics: Precambrian Research, v. 115, n. 1–4, p. 97–117, http://dx.doi.org/10.1016/S0301-9268(02)00007-4

Edwards, R. L., and Essene, E. J., 1988, Pressure, temperature and C-O-H fluid fugacities across the amphibolite-granulite transition, Northwest Adirondack Mountains, New York: Journal of Petrology, v. 29, p. 39–72, http://dx.doi.org/10.1093/petrology/29.1.39

Ellis, D. J., and Thompson, A. B., 1986, Subsolidus and partial melting reaction in the quartz-excess $CaO+MgO+Al_2O_3+SiO_2+H_2O$ system under water-excess and water-deficient conditions to 10 kb: some implications for the origin of peraluminous melts from mafic rocks: Journal of Petrology, v. 27, p. 91–121, http://dx.doi.org/10.1093/petrology/27.1.91

Ferriss, E. D. A., Essene, E. J., and Becker U., 2008, Computational study of the effect of pressure on the Ti-in-zircon geothermometer: European Journal of Mineralogy, v. 20, p. 745–755, http://dx.doi.org/10.1127/0935-1221/2008/0020-1860

Ferry, J. M., and Watson, E. B., 2007, New thermodynamic models and revised calibrations for the Ti-in-zircon and Zr-in-rutile thermometers: Contributions to Mineralogy and Petrology, v. 154, n. 4, p. 429–437, http://dx.doi.org/10.1007/s00410-007-0201-0

Fu, B., Page, F. Z., Cavosie, A. C., Fournelle, J., Kita, N. T., Lackey, J. S., Wilde, S. A., and Valley, J. W., 2008, Ti-in-Zircon thermometry: applications and limitations: Contributions to Mineralogy and Petrology, v. 156, n. 2, p. 197–215, http://dx.doi.org/10.1007/s00410-008-0281-5

Geisler, T., Schaltegger, U., and Tomaschek, F., 2007, Re-equilibration of zircon in aqueous fluids and melts: Elements, v. 3, p. 43–50, http://dx.doi.org/10.2113/gselements.3.1.43

Ghent, E. D., 1988, Tremolite and H_2O activity attending metamorphism of hornblende-plagioclase-garnet assemblages: Contributions to Mineralogy and Petrology, v. 98, n. 2, p. 163–168, http://dx.doi.org/10.1007/BF00402109

Ghent, E. D., and Stout, M. Z., 1984, TiO_2 activity in metamorphosed pelitic and basic rocks: principles and applications to metamorphism in southeastern Canadian Cordillera: Contributions to Mineralogy and Petrology, v. 86, n. 3, p. 248–255, http://dx.doi.org/10.1007/BF00373670

Grimes, C. B., John, B. E., Kelemen, P. B., Mazdab, F. K., Wooden, J. L., Cheadle, M. J., Hanghoj, K., and Schwartz, J. J., 2007, Trace element chemistry of zircons from oceanic crust: A method for distinguishing detrital zircon provenance: Geology, v. 35, n. 7, p. 643–646, http://dx.doi.org/10.1130/G23603A.1

Grimes, C. B., John, B. E., Cheadle, M. J., Mazdab, F. K., Wooden, J. L., Swapp, S., and Schwartz, J., 2009, On the occurrence, trace element geochemistry, and crystallization history of zircon from in situ ocean lithosphere: Contributions to Mineralogy and Petrology, v. 158, p. 757–783, http://dx.doi.org/10.1007/s00410-009-0409-2

Grimes, C. B., Ushikubo, T., John, B. E., and Valley, J. W., 2011, Uniformly mantle-like $\delta^{18}O$ in zircons from oceanic plagiogranites and gabbros: Contributions to Mineralogy and Petrology, v. 161, n. 1, p. 13–33, http://dx.doi.org/10.1007/s00410-010-0519-x

Harley, S. L., and Kelly, N. M., 2007, The impact of zircon-garnet REE distribution data on the interpretation of zircon U-Pb ages in complex high-grade terrains: An example from the Rauer Islands, East Antarctica: Chemical Geology, v. 241, n. 1–2, p. 62–87, http://dx.doi.org/10.1016/j.chemgeo.2007.02.011

Harrison, T. M., 2009, The Hadean crust: Evidence from >4 Ga zircons: Annual Reviews in Earth and Planetary Sciences, v. 37, p. 479–505, http://dx.doi.org/10.1146/annurev.earth.031208.100151

Harrison, T. M., Schmitt, A. K., McCulloch, M. T., and Lovera, O. M., 2008, Early (≥4.5 Ga) formation of terrestrial crust: Lu-Hf, $\delta^{18}O$, and Ti thermometry results for Hadean zircons: Earth and Planetary Science Letters, v. 268, n. 3–4, p. 476–486, http://dx.doi.org/10.1016/j.epsl.2008.02.011

Hawkesworth, C. J., and Kemp, A. I. S., 2006, Using hafnium and oxygen isotopes in zircons to unravel the record of crustal evolution: Chemical Geology, v. 226, n. 3–4, p. 144–162, http://dx.doi.org/doi:10.1016/j.chemgeo.2005.09.018

Hofmann, A. E., Valley, J. W., Watson, E. B., Cavosie, A. J., and Eiler, J. M., 2009, Sub-micron scale distributions of trace elements in zircon: Contributions to Mineralogy and Petrology, v. 158, n. 3, p. 317–335. http://dx.doi.org/10.1007/s00410-009-0385-6

Hoskin, P. W. O., and Black, L. P., 2000, Metamorphic zircon formation by solid state recrystallization of protolith igneous zircon: Journal of Metamorphic Geology, v. 18, p. 423–439.

Hoskin, P. W. O., and Schaltegger, U., 2003, The composition of zircon and igneous and metamorphic petrogenesis, *in* Hanchar, J. M., and Hoskin, P. W. O., editors, Zircon: Reviews in Mineralogy and Geochemistry, v. 53, p. 27–62, http://dx.doi.org/doi:10.2113/0530027

Ireland, T. R., and Williams, I. S., 2003, Considerations in zircon geochronology by SIMS, *in* Hanchar, J. M., and Hoskin, P. W. O., editors, Zircon: Reviews in Mineralogy and Geochemistry, v. 53, p. 215–242, http://dx.doi.org/10.2113/0530215

King, E. M., Valley, J. W., Davis, D. W., and Edwards, G. R., 1998, Oxygen isotope ratios of Archean plutonic zircons from granite-greenstone belts of the Superior Province: Indicator of magmatic source: Precambrian Research, v. 92, n. 4, p. 365–387, http://dx.doi.org/10.1016/S0301-9268(98)00082-5

Kita, N. T., Ushikubo, T., Fu, B., and Valley, J. W., 2009, High precision SIMS oxygen isotope analysis and the effect of sample topography: Chemical Geology, v. 264, n. 1–4, p. 43–57, http://dx.doi.org/10.1016/j.chemgeo.2009.02.012

Krogh, T. E., 1993, High precision U-Pb ages for granulite metamorphism and deformation in the Archean Kapuskasing structural zone, Ontario; implications for structure and development of the lower crust: Earth and Planetary Science Letters, v. 119, n. 1–2, p. 1–18, http://dx.doi.org/10.1016/0012-821X(93)90002-Q

Krogh, T. E., and Moser, D. E., 1994, U-Pb zircon and monazite ages from the Kapuskasing uplift: age constraints on deformation within the Ivanhoe Lake fault zone: Canadian Journal of Earth Sciences, v. 31, p. 1096–1103, http://dx.doi.org/10.1139/e94-098

Lamb, W. M., and Valley, J. W., 1988, Granulite facies amphibole and biotite equilibria, and calculated peak-metamorphic water activities: Contributions to Mineralogy and Petrology, v. 100, n. 3, p. 349–360, http://dx.doi.org/10.1007/BF00379744

Lancaster, P. J., Baxter, E. F., Ague, J. J., Breeding, C. M., and Owens, T. L., 2008, Synchronous peak Barrovian metamorphism driven by syn-orogenic magmatism and fluid flow in southern Connecticut, USA: Journal of Metamorphic Geology, v. 26, n. 5, p. 527–538, http://dx.doi.org/10.1111/j.1525-1314.2008.00773.x

Lancaster, P. J., Fu, B., Page, F. Z., Kita, N. T., Bickford, M. E., Hill, B. M., McLelland, J. M., and Valley, J. W., 2009, Genesis of metapelitic migmatites in the Adirondack Mts., New York: Journal of Metamorphic Geology, v. 27, n. 1, p. 41–54, http://dx.doi.org/10.1111/j.1525-1314.2008.00802.x

Li, H., Schwarcz, H. P., and Shaw, D. M., 1991, Deep crustal oxygen isotope variations; the Wawa-Kapuskasing crustal transect, Ontario: Contributions to Mineralogy and Petrology, v. 107, n. 4, p. 448–458, http://dx.doi.org/10.1007/BF00310679

Longstaffe, F. J., and Schwarcz, H. P., 1977, $^{18}O/^{16}O$ of Archean clastic metasedimentary rocks: a petrogenetic indicator for Archean gneisses?: Geochemica et Cosmochimica Acta, v. 41, n. 9, p. 1303–1312, http://dx.doi.org/10.1016/0016-7037(77)90074-6

Ludwig, K. R., 2001, Squid (1.13b), A users manual: Berkeley Geochronology Center Special Publication No. 2.

——— 2003, Isoplot (3.41d), A geochronological toolkit for Excel: Berkeley Geochronology Center Special Publication No. 4.

Lyubetskaya, T., and Ague, J. J., 2010, Modeling metamorphism in collisional orogens intruded by magmas: I. Thermal evolution: American Journal of Science, v. 310, p. 427–458, http://dx.doi.org/10.2475/06.2010.01

Mäder, U. K., Percival, J. A., and Berman, R. G., 1994, Thermobarometry of garnet-clinopyroxene-hornblende granulites from the Kapuskasing structural zone: Canadian Journal of Earth Sciences, v. 31, n. 7, p. 1134–1145, http://dx.doi.org/10.1139/e94-101

Martin, L., Duchêne, S., Deloule, E., and Vanderhaeghe, O., 2006, The isotopic composition of zircon and garnet: A record of the metamorphic history of Naxos, Greece: Lithos, v. 87, n. 3–4, p. 174–192, http://dx.doi.org/10.1016/j.lithos.2005.06.016

——— 2008, Mobility of trace elements and oxygen in zircon during metamorphism: Consequences for geochemical tracing: Earth and Planetary Science Letters, v. 267, n. 1–2, p. 161–174, http://dx.doi.org/10.1016/j.epsl.2007.11.029

Mazdab, F. K., 2009, Characterization of flux-grown trace-element-doped titanite using the high-mass-resolution ion microprobe (SHRIMP-RG): Canadian Mineralogist, v. 47, n. 4, p. 813–831, http://dx.doi.org/10.3749/canmin.47.4.813

Mazdab, F. K., and Wooden, J. L., 2006, Trace element analysis in zircon by ion microprobe (SHRIMP-RG): technique and applications: Geochimica et Cosmochimica Acta, v. 70, n. 18, Supplement 1, p. A405, http://dx.doi.org/10.1016/j.gca.2006.06.817

Moecher, D. P., and Essene, E. J., 1990, Scapolite phase equilibria: additional constraints on the role of CO_2 in granulite genesis, *in* Vielzeuf, D., and Vidal, P., editors, Granulites and Crustal Evolution: Amsterdam, The Netherlands, Kluwer Academic Publishers, p. 385–396.

Mojzsis, S. J., Harrison, T. M., and Pidgeon, R. T., 2001, Oxygen-isotope evidence from ancient zircons for liquid water at the Earth's surface 4,300 Myr ago: Nature, v. 409, p. 178–181, http://dx.doi.org/10.1038/35051557

Moser, ms, D. E., 1993, A geological, structural and geochronological study of the mid-crustal Wawa gneiss domain, Chapleau, Ontario: Kingston, Ontario, Canada, Queen's University, Ph. D. thesis, 165 p.

——— 1994, The geology and structure of the mid-crustal Wawa gneiss domain—a key to understanding tectonic variation with depth and time in the late Archean Abitibi–Wawa orogen: Canadian Journal of Earth Sciences, v. 31, n. 7, p. 1064–1080, http://dx.doi.org/10.1139/e94-096

Moser, D. E., Heaman, L. M., Krogh, T. E., and Hanes, J. A., 1996, Intracrustal extension of an Archean orogen revealed using single-grain U-Pb zircon geochronology: Tectonics, v. 15, n. 5, p. 1093–1109, http://dx.doi.org/10.1029/96TC00130

Moser, D. E., Bowman, J. R., Wooden, J. L., Valley, J. W., Mazdab, F. K., and Kita, N. T., 2008, Creation of a

continent recorded in zircon zoning: Geology, v. 36, n. 3, p. 239–242, http://dx.doi.org/10.1130/G24416A.1

Oliver, G. J. H., Chen, F., Buchwaldt, R., and Hegner, E., 2000, Fast tectonometamorphism and exhumation in the type area of the Barrovian and Buchan zones: Geology, v. 28, n. 5, p. 459–462, http://dx.doi.org/10.1130/0091-7613(2000)28⟨459:FTAEIT⟩2.0.CO;2

Page, F. Z., Ushikubo, T., Kita, N. T., Riciputi, L. R., and Valley, J. W., 2007, High precision oxygen isotope analysis of picogram samples reveals 2-μm gradients and slow diffusion in zircon: American Mineralogist, v. 92, n. 10, p. 1772–1775, http://dx.doi.org/10.2138/am.2007.2697

Page, F. Z., Kita, N. T., and Valley, J. W., 2010, Ion microprobe analysis of oxygen isotopes in garnets of complex chemistry: Chemical Geology, v. 270, n. 1–4, p. 9–19, http://dx.doi.org/10.1016/j.chemgeo.2009.11.001

Patino Douce, A. E., and Beard, J. S., 1995, Dehydration melting of biotite gneiss and quartz amphibolite from 3 to 15 kbar: Journal of Petrology, v. 36, n. 3, p. 707–738, http://dx.doi.org/10.1093/petrology/36.3.707

——— 1996, Effects of P, $f(O_2)$ and Mg/Fe ratio on dehydration melting of model metagreywackes: Journal of Petrology, v. 37, p. 999–1024.

Pattison, D. R. M., 2003, Petrogenetic significance of orthopyroxene-free garnet+clinopyroxene+plagioclase + quartz-bearing metabasites with respect to the amphibolite and granulite facies: Journal of Metamorphic Geology, v. 21, n. 1, p. 21–34, http://dx.doi.org/10.1046/j.1525-1314.2003.00415.x

Pattison, D. R. M., Chacko, T., Farquhar, J., and McFarlane, C. R. M., 2003, Temperatures of granulite facies metamorphism: constraints from experimental phase equilibria and thermobarometry corrected for retrograde exchange: Journal of Petrology, v. 44, n. 5, p. 867–900, http://dx.doi.org/10.1093/petrology/44.5.867

Peck, W. H., King, E. M., and Valley, J. W., 2000, Oxygen isotope perspective on Precambrian crustal growth and maturation: Geology, v. 28, n. 4, p. 363–366, http://dx.doi.org/10.1130/0091-7613(2000)28⟨363:OIPOPC⟩2.0.CO;2

Peck, W. H., Valley, J. W., and Graham, C. M., 2003, Slow oxygen diffusion rates in igneous zircons from metamorphic rocks: American Mineralogist, v. 88, n. 7, p. 1003–1014.

Percival, J. A., 1983, High-grade metamorphism in the Chapleau-Foleyet area, Ontario: American Mineralogist, v. 68, n. 7–8, p. 667–686.

——— 1990, A field guide to the Kapuskasing uplift, a cross section through the Archean Superior Province, *in* Salisbury, M. H., and Fountain, D. M., editors, Exposed Cross Sections of the Continental Crust: Dordrecht, Kluwer, p. 171–193.

——— 2007a, Geology and metallogeny of the Superior Province, Canada, *in* Goodfellow, W. D., editor, Mineral Resources of Canada: A Synthesis of Major Deposit-types, District Metallogeny, the Evolution of Geological Provinces, and Exploration Methods: Geological Association of Canada Mineral Deposits Division Special Publication No. 5, p. 903–928.

——— 2007b, Eo- to Mesoarchean terranes of the Superior Province and their tectonic context, *in* Van Kranendonk, M. J., Smithies, R. H., and Bennett, V. C., editors, Earth's Oldest Rocks: Developments in Precambrian Geology, v. 15, p. 1065–1085.

Percival, J. A., and Card, K. D., 1985, Structure and Evolution of Archean crust in central Superior Province, Canada, *in* Ayres, L. D., Thurston, P. C., and Weber, W., editors, Evolution of Archean Supracrustal Sequences: Geological Association of Canada Special Paper 28, p. 179–192.

Percival, J. A., and West, G. F., 1994, The Kapuskasing Uplift; a geological and geophysical synthesis: Canadian Journal of Earth Sciences, v. 31, n. 7, p. 1256–1286, http://dx.doi.org/10.1139/e94-110

Percival, J. A., Sanborn-Barrie, M., Skulski, T., Stott, G., Helmstaedt, H., and White, D. J., 2006a, Tectonic evolution of the Western Superior Province from NATMAP and Lithoprobe studies: Canadian Journal of Earth Sciences, v. 43, n. 7, p. 1085–1117, http://dx.doi.org/10.1139/e06-062

Phillips, G. N., 1980, Water activity changes across an amphibolite-granulite facies transition, Broken Hill, Australia: Contributions to Mineralogy and Petrology, v. 75, n. 4, p. 377–386, http://dx.doi.org/10.1007/BF00374721

Puris, E. M., and Wickham, S. M., 1994, Quantification of lower crustal synmetamorphic fluid fluxes in the Kapuskasing structural zone based on oxygen-isotope profiles across two paragneiss-mafic gneiss contacts: Canadian Journal of Earth Sciences, v. 31, n. 7, p. 1122–1145, http://dx.doi.org/10.1139/e94-100

Rubatto, D., 2002, Zircon trace element geochemistry: partitioning with garnet and the link between U-Pb ages and metamorphism: Chemical Geology, v. 184, n. 1–2, p. 123–138, http://dx.doi.org/10.1016/S0009-2541(01)00355-2

Rubatto, D., and Hermann, J., 2007, Experimental zircon/melt and zircon/garnet trace element partitioning and implications for the geochronology of crustal rocks: Chemical Geology, v. 241, n. 1–2, p. 38–61, http://dx.doi.org/10.1016/j.chemgeo.2007.01.027

Rumble, D., Giorgis, D., Ireland, T., Zhang, Z., Xu, H., Yui, T. F., Yang, J., Xu, Z., and Liou, J. G., 2002, Low $\delta^{18}O$ zircons, U-Pb dating, and the age of the Qinglongshan oxygen and hydrogen isotope anomaly near Donghai in Jiangsu Province, China: Geochimica et Cosmochimica Acta, v. 66, n. 12, p. 2299–2306, http://dx.doi.org/10.1016/S0016-7037(02)00844-X

Schaltegger, U., Fanning, C. M., Günther, D., Maurin, J.-C., Schulmann, K., and Gebauer, D., 1999, Growth, annealing and recrystallization of zircon and preservation of monazite in high-grade metamorphism: conventional and in-situ U-Pb isotope, cathodoluminescence and microchemical evidence: Contributions to Mineralogy and Petrology, v. 134, n. 2–3, p. 186–201, http://dx.doi.org/10.1007/s004100050478

Sharp, Z. D., 1990, A laser-based microanalytical method for the *in-situ* determination of oxygen isotope

ratios of silicates and oxides: Geochimica et Cosmochimica Acta, v. 54, n. 5, p. 1353–1357, http://dx.doi.org/10.1016/0016-7037(90)90160-M
Ushikubo, T., Kita, N. T., Cavosie, A. J., Wilde, S. A., Rudnick, R. L., and Valley, J. W., 2008, Lithium in Jack Hills zircons: Evidence for extensive weathering of Earth's earliest crust: Earth and Planetary Science Letters, v. 272, n. 3–4, p. 666–676, http://dx.doi.org/10.1016/j.epsl.2008.05.032
Valley, J. W., 2003, Oxygen isotopes in zircon, *in* Hanchar, J. M., and Hoskin, P. W. O., editors, Zircon: Reviews in Mineralogy and Geochemistry, v. 53, p. 343–386, http://dx.doi.org/10.2113/0530343
Valley, J. W., and Kita, N. T., 2009, In situ Oxygen Isotope Geochemistry by Ion Microprobe, *in* Fayek, M., editor, Secondary Ion Mass Spectrometry in the Earth Sciences: Mineralogical Association of Canada Short Course 41, p. 19–63.
Valley, J. W., McLelland, J., Essene, E. J., and Lamb, W. M., 1983, Metamorphic fluids in the deep crust: evidence from the Adirondacks: Nature, v. 301, p. 226–228, http://dx.doi.org/10.1038/301226a0
Valley, J. W., Bohlen, S. R., Essene, E. J., and Lamb, W. M., 1990, Metamorphism in the Adirondacks: II. The role of fluids: Journal of Petrology, v. 31, n. 3, p. 555–596, http://dx.doi.org/10.1093/petrology/31.3.555
Valley, J. W., Chiarenzelli, J. R., and McLelland, J. M., 1994, Oxygen Isotope Geochemistry of Zircon: Earth and Planetary Science Letters, v. 126, n. 4, p. 187–206, http://dx.doi.org/10.1016/0012-821X(94)90106-6
Valley, J. W., Kitchen, N., Kohn, M. J., Niendorf, C. R., and Spicuzza, M. J., 1995, UWG-2, A garnet standard for oxygen isotope ratio—Strategies for high precision and accuracy with laser heating: Geochimica et Cosmochimica Acta, v. 59, n. 24, p. 5223–5231, http://dx.doi.org/10.1016/0016-7037(95)00386-X
Valley, J. W., Bindeman, I. N., and Peck, W. H., 2003, Empirical calibration of oxygen isotope fractionation in zircon: Geochimica et Cosmochimica Acta, v. 67, n. 17, p. 3257–3266, http://dx.doi.org/10.1016/S0016-7037(03)00090-5
Valley, J. W., Lackey, J. S., Cavosie, A. J., Clechenko, C. C., Spicuzza, M. J., Basei, M. A. S., Bindeman, I. N., Ferreira, V. P., Sial, A. N., King, E. M., Peck, W. H., Sinha, A. K., and Wei, C. S., 2005, 4.4 billion years of crustal maturation: Oxygen isotopes in magmatic zircon: Contributions to Mineralogy and Petrology, v. 150, n. 6, p. 561–580, http://dx.doi.org/10.1007/s00410-005-0025-8
Valley, J. W., Cavosie, A. J., Fu, B., Peck, W. H., and Wilde S. A., 2006, Comment on "Heterogeneous Hadean Hafnium: Evidence of continental growth at 4.4 to 4.5 Ga": Science, v. 312, p. 1139a, http://dx.doi.org/10.1126/science.1125301
Watson, E. B., and Cherniak, D. J., 1997, Oxygen diffusion in zircon: Earth and Planetary Science Letters, v. 148, n. 3–4, p. 527–544, http://dx.doi.org/10.1016/S0012-821X(97)00057-5
Watson, E. B., and Harrison, T. M., 2005, Zircon thermometer reveals minimum melting conditions on earliest Earth: Science, v. 308, p. 841–844, http://dx.doi.org/10.1126/science.1110873
Wilde, S. A., Valley, J. W., Peck, W. H., and Graham, C. M., 2001, Evidence from detrital zircons for the existence of continental crust and oceans on the Earth 4.4 Gyr ago: Nature, v. 409, p. 175–178, http://dx.doi.org/10.1038/35051550
Williams, I. S., 1997, U-Th-Pb geochronology by ion microprobe: not just ages but histories: Society of Economic Geologists Reviews in Economic Geology, v. 7, p. 1–35.
Wyllie, P. J., 1977, Crustal anatexis: An experimental review: Tectonophysics, v. 43, n. 1–2, p. 41–71, http://dx.doi.org/10.1016/0040-1951(77)90005-1
Zhang, Y., Stolper, E. M., and Wasserburg, G. J., 1991, Diffusion of a multi-species component and its role in oxygen and water transport in silicates: Earth and Planetary Science Letters, v. 103, n. 1–4, p. 228–240, http://dx.doi.org/10.1016/0012-821X(91)90163-C